Technical Report

Model Identification and Seismic Analysis of Meloland Road Overcrossing

by

S.D. Werner
C.B. Crouse
L. Katafygiotis
J.L. Beck

Prepared for

California Department of Transportation
Division of Structures
Sacramento, California

May 1993

DAMES & MOORE

2101 Webster Street
Suite 300
Oakland, California 94612

500 Market Place Tower
2025 First Avenue
Seattle WA 98121

FORWARD

The investigation described in this report has been supported under two closely-related projects funded by the California Department of Transportation. One project is entitled "Assessment of Bridge Seismic Design and Instrumentation Requirements using Full Scale Testing and Dynamic Analysis of the Meloland Road Overcrossing." It has been implemented under Contract Number 59G454 by the University of Nevada at Reno (prime contractor) and Dames & Moore (subcontractor). The project is being directed by B. M. Douglas of the University of Nevada at Reno and by S. D. Werner and C. B. Crouse of Dames & Moore. Mr. J. Gates of Caltrans is technical monitor for this project. The other project is entitled "Study of Caltrans' Seismic Evaluation Procedures for Short Bridge Overcrossing Structures," which is being implemented under Contract Number 59Q122 to Dames & Moore. S. D. Werner of Dames & Moore is directing this project, and J. -S. Hwang of Caltrans is technical monitor.

This report has been authored by S. D. Werner and C. B. Crouse of Dames & Moore, L. Katafygiotis of the University of Akron, and J. L. Beck of the California Institute of Technology. The seismic analyses of the bridge structure and foundation elements that are documented in the report were performed by A. Nisar, H. Sedarat, and T. Price of Dames & Moore. Helpful review comments on the report were provided by S. A. Mahin of the University of California at Berkeley.

CONTENTS

Chapter			Page
1	INTRODUCTION		
	1.1	Background Information	1-1
	1.2	Objective and Scope	1-3
	1.3	Report Organization	1-4
2	ANALYSIS PROCEDURE		
	2.1	Finite Element Model Configuration	2-1
	2.2	Engineering Estimates of Model Parameters	2-2
	2.3	System Identification	2-4
	2.4	Seismic Analysis	2-7
	2.5	Foundation Evaluation	2-8
	2.6	Structural Demand vs. Capacity Evaluations	2-9
3	ANALYSIS RESULTS		
	3.1	Model Parameters	3-1
	3.2	Structural Response	3-6
	3.3	Pile Foundation Analysis	3-9
	3.4	Assessment of Seismic Design Procedures	3-12
4	CONCLUDING COMMENTS		
	4.1	Evaluation and Applicability of Procedures and Results	4-1
	4.2	Assessment of Original Design	4-1
	4.3	Assessment of Current Seismic Evaluation Procedures	4-2
	4.4	Strong Motion Instrumentation of Bridges	4-3
REFERENCES			R-1
APPENDIX A			
SELECTED STRUCTURAL DRAWINGS FOR MELOLAND ROAD OVERCROSSING			A-1
APPENDIX B			
PROCEDURE FOR NONLINEAR STATIC ANALYSIS OF PILE-FOUNDATION SYSTEMS			B-1

CHAPTER 1
INTRODUCTION

1.1 Background Information

1.1.1 Bridge Description and Seismic Response

The Meloland Road Overcrossing (MRO) is a two-span, unskewed, reinforced concrete box girder bridge structure that is located about 5 miles east of El Centro and about ¼ mile west of the Imperial Fault in the Imperial Valley of southeastern California (Fig. 1-1a). The bridge was designed by the California Department of Transportation (Caltrans) in 1968 using procedures that, at that time, included only minimal consideration of the potential effects of seismic excitations. The deck of the bridge is supported by monolithic diaphragm abutments and by a single circular column central pier at its midlength (Fig. 1-1b). The pier and abutments are supported on timber piles. The MRO's approach embankments consist of stiff clay materials, and the native soils beneath the embankments and the central pier consist of alternating layers of clayey sand, silty sand, silty clay, and silty sand (Fig. 1-2). Dimensions and structural details for the bridge are shown in the drawings contained in Appendix A.

Because of its close proximity to the Imperial Fault, the MRO was instrumented in 1978 with an array of 26 strong motion accelerometers whose locations are shown in Fig. 1-3. All of these instruments were triggered during the Imperial Valley Earthquake of October 1979 (M_S = 6.4) and the resulting array of strong motion records at the MRO is the largest yet obtained at a bridge in the United States during a single earthquake event. The motions that were recorded at the bridge were quite strong, with peak accelerations of over 0.3 g at a free field instrument 200 ft. west of the bridge and over 0.5 g on the bridge deck. No structural damage to the bridge was observed despite these strong levels of seismic excitation. The accelerograph traces recorded at the MRO during the Imperial Valley Earthquake are shown in Figure 1-4.

1.1.2 Past Studies of Seismic Response

The strong motion records measured at the MRO have been studied by several investigators. For example, Werner et. al. (1987) and Douglas et. al. (1984 and 1990) studied the records in order to assess of the MRO's structural response and normal modes of vibration excited by the earthquake shaking. Although these studies provided important insights into the bridge's dynamic response characteristics during the earthquake, it was found that the single accelerometer location at the MRO's abutments and at the central pier footing were insufficient to characterize the translational and rotational response characteristics at these supports. Because of this, we could not fully evaluate the bridge's soil-structure interaction (SSI) effects, the internal forces and moments developed in the bridge's structural and foundation elements during the earthquake shaking, and the resulting adequacy of the MRO's seismic design. This issue is particularly important because short bridge overcrossing (SBO) structures that are typified by the MRO represent the largest single class of bridges in California, with many thousands located

throughout the state. Therefore, it is particularly important that Caltrans' seismic design and evaluation procedures for new and existing SBOs be calibrated against the invaluable seismic response data represented by the MRO's array of strong motion records.

1.1.3 University of Nevada-Reno/Dames & Moore Research Program

In order to address the above unresolved aspects of the MRO's seismic response, Caltrans awarded a research contract in 1988 to a team comprised of the University of Nevada at Reno (UNR) and Dames & Moore (D & M). This project has consisted of the following tasks:

(1) In situ static and dynamic testing of the soil materials at the site of the MRO, together with the reassessment of index properties of the soils and the installation of piezometers to record the location of the water table (as described in Douglas et. al., 1993).

(2) Full scale dynamic testing of the MRO. In this test program, dynamic excitation of the bridge was induced by quick release of a static load applied by a pressurized inclined strut that was attached to the MRO near the midlength of its deck and was supported at its base by a reaction foundation. The resulting free vibrations of the MRO's structure and surrounding soil materials were recorded by a dense array of accelerometers that were located along the deck, abutments, embankments, central pier footing, and adjacent soil materials. Details of this test program are provided in Douglas et. al. (1993).

(3) Analysis of the dynamic test data from Task 2 in order to: (i) evaluate the bridge-soil system's equivalent modes of vibration, and to compare these modal parameters to those previously estimated from the recorded earthquake motions in order to assess how nonlinear behavior affects the MRO's dynamic response over different excitation levels (Werner et. al., 1990); (ii) estimate equivalent spring stiffnesses at the MRO's abutments and central pier footing from the recorded test motions and the dynamic soil properties from Task 1 (Crouse, 1992); and (iii) estimate the bridge's structural and foundation stiffness characteristics through system identification of the recorded test motions (Douglas et. al., 1991; Vrontinos et. al., 1993).

(4) Use of the information from Tasks 1 through 3 to guide the development of a finite element model for detailed analysis of the MRO's seismic response during the 1979 Imperial Valley Earthquake.

(5) Implementation of a detailed seismic analysis of the MRO, and use of the results of the analysis to evaluate the procedures used by Caltrans for seismic design of short bridge overcrossing structures and foundation elements.

(6) Recommendation of an expanded strong motion instrumentation array at the MRO to more fully characterize its seismic response during future earthquakes (Crouse et. al. 1991). Phase 1 of these recommendations has been implemented by the California Division of Mines and Geology.

1.1.4 Dames & Moore Short Bridge Research Program

In addition to the above project, D & M is also implementing another closely-related Caltrans-sponsored research project that is addressing general seismic evaluation procedures for short bridge overcrossing (SBO) structures. The particular objectives of this project are to: (a) carry out a detailed review of Caltrans' current seismic evaluation procedures for SBOs; (b) develop improved evaluation procedures based on relevant analytical and experimental research programs, calibrations against strong motion records in SBOs, and the observed performance of SBOs during past earthquakes; and (c) document these improved procedures in a Memo-to Designers format to facilitate their future use under Caltrans' seismic retrofit program. D & M's development of improved evaluation procedures is focusing on the representation of column deformation capacities, the development of improved modeling procedures for seismic analysis of SBO soil-structure systems, and the assessment of bridge damping characteristics.

1.2 Objective and Scope

This report presents the results of research directed toward model identification and seismic analysis of the MRO. This research has been implemented to meet the requirements of Tasks 4 and 5 of the UNR-D&M research program (Sec. 1.1.3) and also to provide a basis for developing improved bridge modeling procedures as required under the D & M research program on SBOs (Sec. 1.1.4).

The scope of this research effort consisted of our development of a finite element model of the MRO whose parameters were estimated through the application of state-of-the-art system identification methods to the MRO's recorded motions from the Imperial Valley Earthquake. These estimated model parameters were also checked for consistency with an overall range of model parameter values computed using established engineering procedures. This model was then used in a series of parametric dynamic analyses of the seismic response of the MRO which enabled us to evaluate the effects of uncertainties in the various model parameters on the demand forces and moments in the structural members and the foundation springs. Maximum foundation spring forces and moments obtained from these analyses were used as input to nonlinear static analyses of the MRO's pile foundations in order to compute the demand forces and moments within the piles. The demand forces and moments within the MRO's structural and pile elements were then compared against the capacities of these elements. These analysis results have been interpreted to assess the seismic performance and design of the MRO, and also to provide an important basis for our development of improved modeling and seismic evaluation procedures for short bridge overcrossing structures.

The above efforts have focused on the modeling and analysis of the MRO's translational and rotational response to transverse horizontal input motions; i.e., the bridge's response to vertical and longitudinal input motions was not included in this research. This focus on the MRO's response to transverse horizontal input motions was adopted because: (a) this response will lead to more severe earthquake-induced internal forces and moments, particularly in the central pier which is the element of an SBO that is typically most vulnerable to seismic

excitation; and (b) our past evaluations of the MRO's recorded motions have shown that its response to transverse horizontal input motions is strongly affected by SSI, whereas SSI has only a negligible effect of the MRO's response to vertical and longitudinal input motions (Werner, et. al., 1987).

1.3 Report Organization

The remainder of this report is organized into three chapters and two appendices. Chapter 2 describes our model development and our procedures for analysis of the seismic response of the MRO, and Chapter 3 contains the results of this seismic analysis. Our conclusions and recommendations based on these analysis procedures and results are provided in Chapter 4. Appendix A contains relevant structural drawings of the MRO, and Appendix B provides a detailed description of our nonlinear foundation analysis procedure.

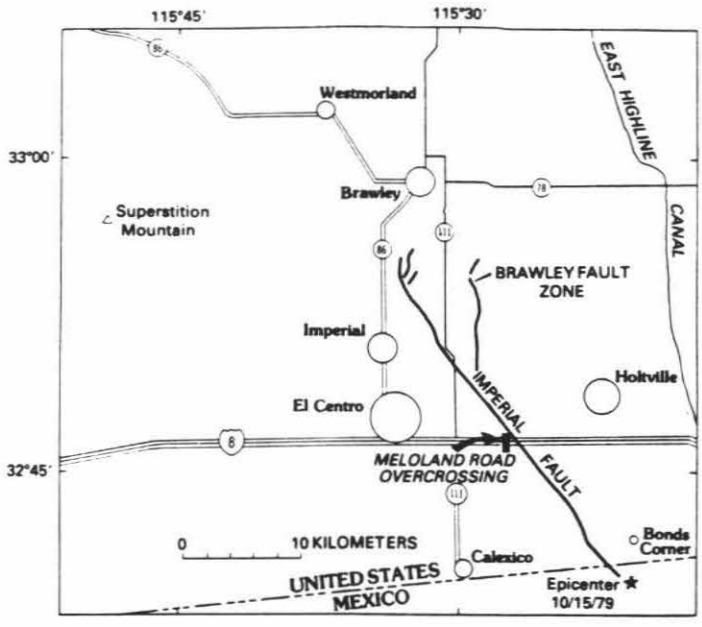

a) Proximity to Imperial Fault

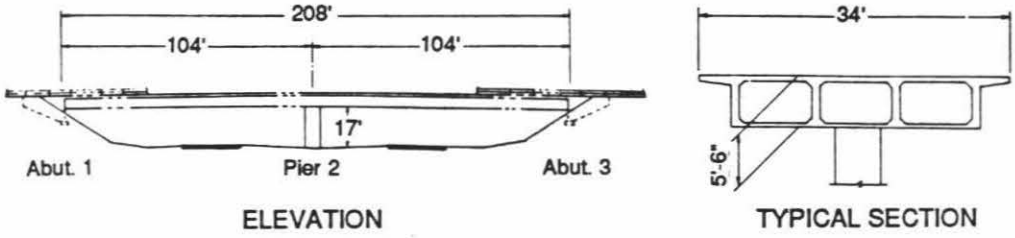

b) Bridge Dimensions

FIGURE 1-1

MELOLAND ROAD OVERCROSSING LOCATION AND CONFIGURATION (Werner et al, 1987)

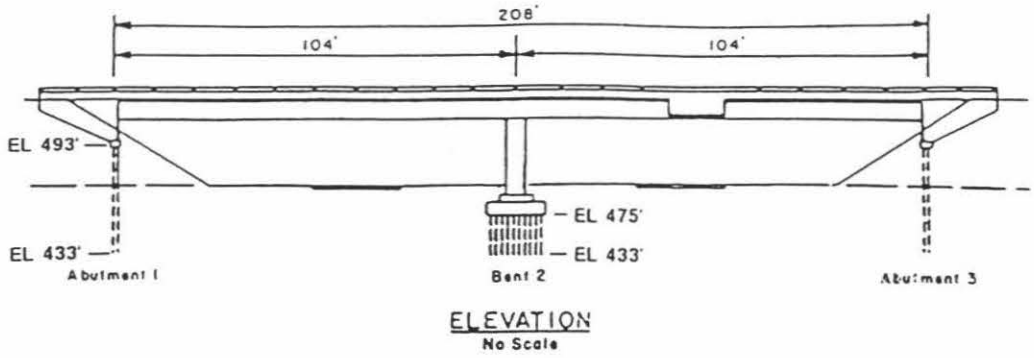

ELEVATION
No Scale

Abutment Soil Profile

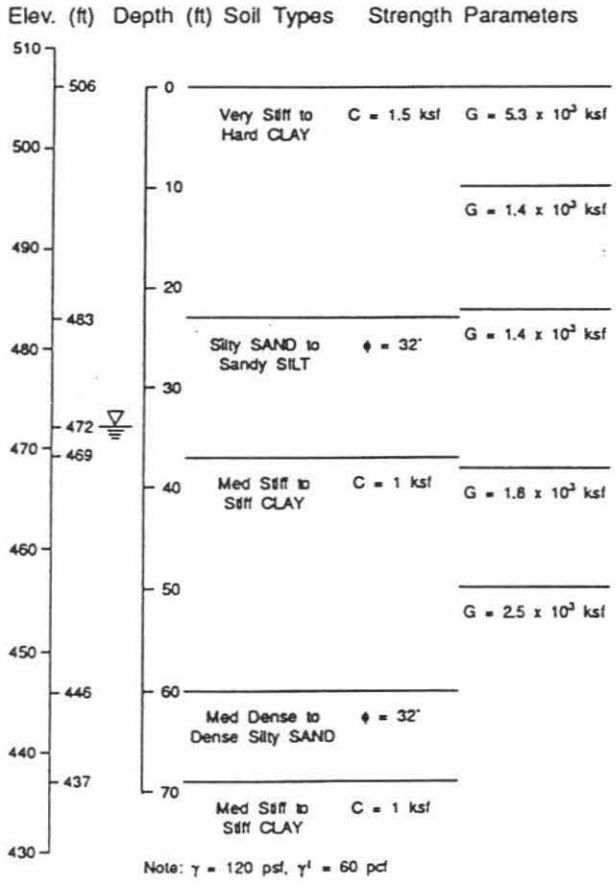

Pier Soil Profile

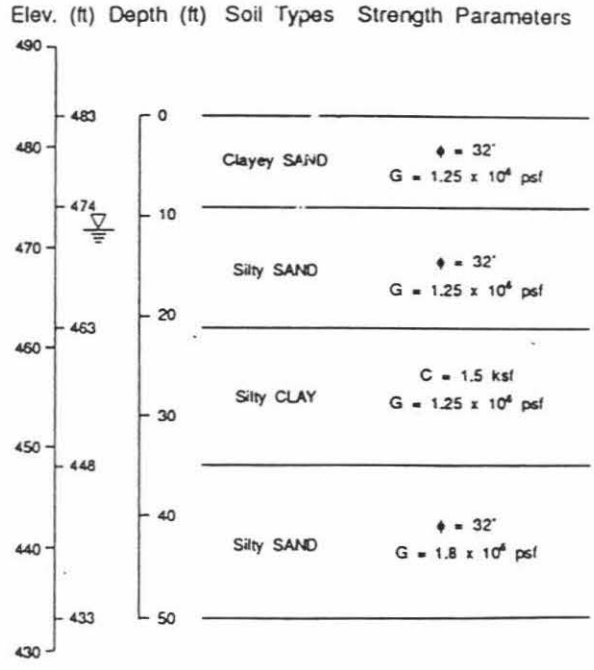

Symbols: γ = total unit weight, γ' = submerged unit weight,
ϕ = internal friction angle, c = cohesion,
G = low-strain shear modulus

FIGURE 1-2

SOIL CONDITIONS AT MELOLAND ROAD OVERCROSSING (DOUGLAS ET. AL., 1993)

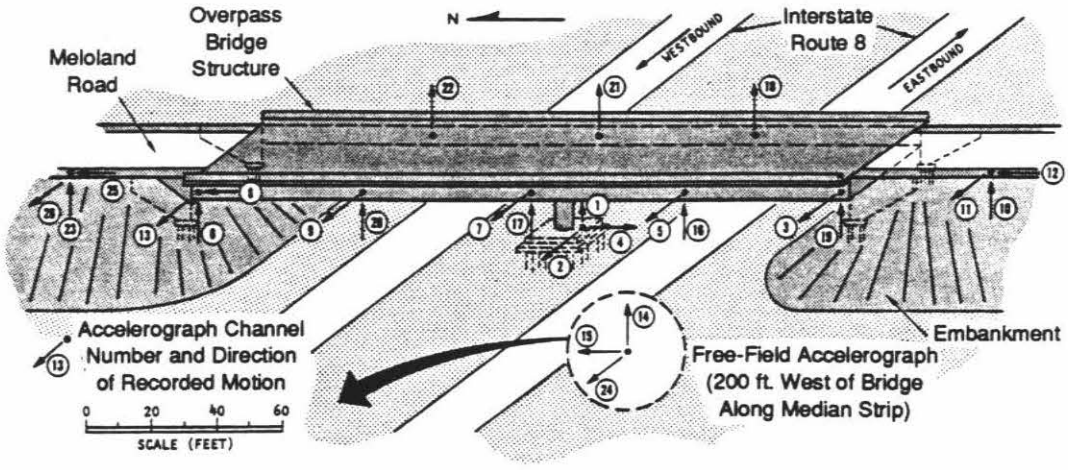

FIGURE 1-3

STRONG MOTION INSTRUMENTATION OF MELOLAND ROAD OVERCROSSING (Werner et al, 1987)

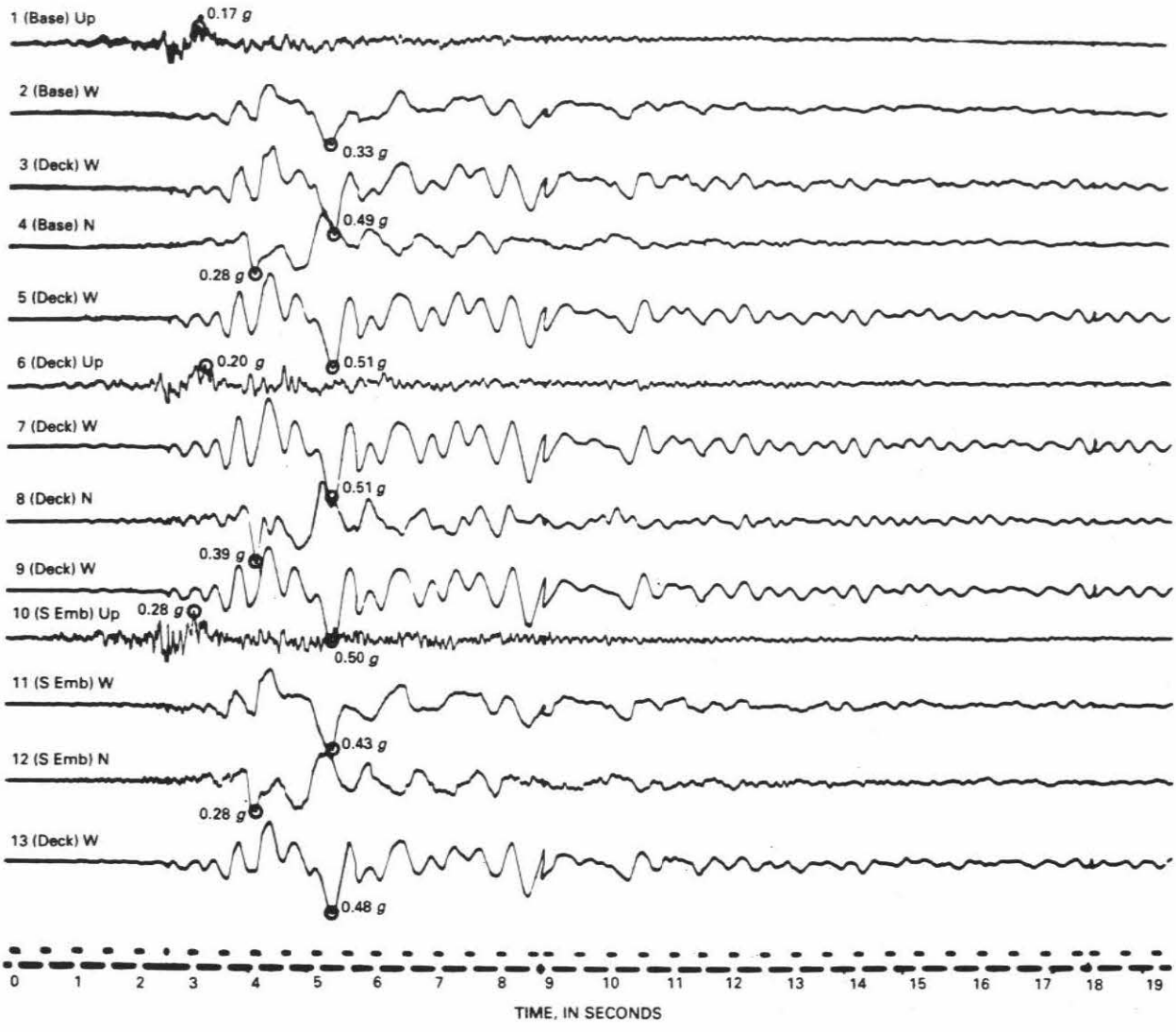

a) Channels 1 - 13

FIGURE 1-4

MRO STRONG MOTION RECORDS FROM 1979 IMPERIAL VALLEY EARTHQUAKE

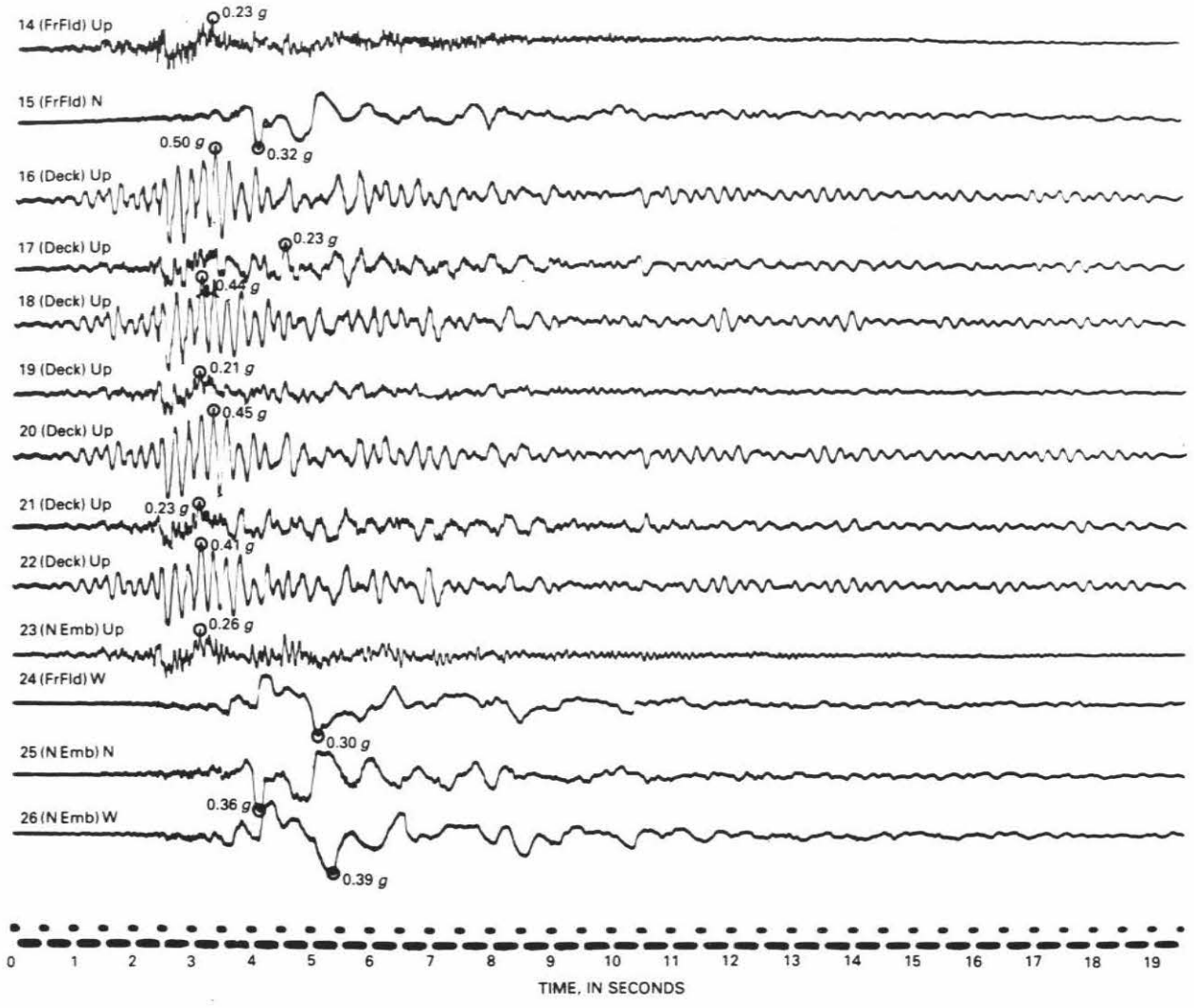

b) Channels 14 - 26

FIGURE 1-4 (continued)

MRO STRONG MOTION RECORDS FROM 1979 IMPERIAL VALLEY EARTHQUAKE

CHAPTER 2
ANALYSIS PROCEDURES

This chapter describes the following basic elements of our procedure for seismic analysis of the MRO's response to transverse horizontal input motions: (a) finite element model configuration; (b) engineering estimates of plausible ranges of model parameter values; (c) system identification methodology; (d) dynamic analysis procedure; (e) foundation analysis procedure; and (f) structural demand vs. capacity evaluations.

2.1 Finite Element Model Configuration

Examination of the strong motion records at the MRO shows that its transverse response is characterized by strong embankment motions that are amplified relative to the free field motions along the base of the pier due to the transverse response characteristics of the embankment (Fig. 1-4). These amplified embankment motions then drive the bridge abutments and the relatively stiff deck, whose motions are further amplified because of soil-structure interaction (SSI) at the abutment and the deck's inertia and stiffness characteristics. The seismic performance of the central pier (which is typically the most vulnerable structural element of an SBO) will depend on its strength and displacement ductility, and whether these are sufficient to accommodate the demand loading and relative displacements imposed by the deck motions and the motions at the base of the pier.

To represent these seismic response characteristics in our seismic analysis of the MRO, we developed the model shown in Figure 2-1. In this model, the bridge deck and central pier are represented by conventional beam elements. The stiffness and mass properties of these elements vary over the length of each deck span to account for the following variations in the deck's cross section: (a) a uniform box girder zone that extends over a length of 73 ft. from each abutment over the span length; (b) a 28 ft. long flared box girder zone in which the web thicknesses of the box girder increase uniformly from the end of the uniform zone to a maximum value at the junction with the solid zone of the deck; and (c) a 3 ft. long solid zone along the segment of each deck span that is above the central pier. The abutments are modeled by a transverse translational spring of stiffness k_y that extends from the end of the bridge deck to an embankment mass m_e, and by rotational spring stiffnesses $k_{x\theta}$ and $k_{z\theta}$. These spring stiffnesses model the effects of interaction between the abutment walls. pile cap, and pile elements and the surrounding soil material in the embankments. The transverse shear stiffness of the embankments is modeled by a translational spring k_{ye} that extends from the embankment mass to the inertial frame of the model.

Seismic input motions for this model were the transverse horizontal motions recorded at the base of the pier, and rocking-induced SSI at the base of the pier is represented by the rotational spring stiffness $k_{x\theta}$' that is shown in Figure 2-1. In this, we had originally planned to use the transverse horizontal free field motions recorded 200 ft. to the west of the MRO as input motions for the seismic analysis, and had planned to include a transverse translational spring stiffness as well as a rotational stiffness in our modeling of the SSI at the base of the pier.

However, we found that these free field motions did not exhibit strong coherence over the 200 ft. distance between the free field instrument and the bridge. This contributed to poor comparisons that were initially obtained between the MRO's recorded earthquake motions and its computed model motions based on model parameters estimated by our system identification procedure (see Sec. 2.3). Therefore, we instead used the transverse horizontal motions recorded at the base of the pier as input motions to our model. As shown in Chapter 3, these input motions led to much improved comparisons between the computed model motions and the recorded motions, even though this amounted to our neglecting translational (but not rotational) SSI effects at the base of the pier. This experience underscores the need for considering possible incoherence effects when locating free field instruments within a strong motion instrumentation array for bridges.

2.2 Engineering Estimates of Model Parameters

The second step of our analysis procedure was to develop engineering estimates of the various model parameters using a range of established engineering procedures. The objectives of these engineering estimates were: (a) to obtain plausible fixed values of those model parameters that were not estimated using the system identification procedures summarized in Section 2.3; and (b) to develop initial values and verify the plausibility of the final values of those model parameters that were estimated by the system identification. Our procedures for developing these engineering estimates are summarized in the following paragraphs.

2.2.1 Structural Elements

Our engineering evaluations of the model parameters for the MRO's structural elements focused on the estimation of gross-section and cracked-section EI values for the central pier and deck. The cracked-section EI values were obtained from nonlinear moment-curvature relationships that were computed using the BIAX Program (Wallace and Moehle, 1989) (Fig. 2-2). These moment-curvature relationships as well as the gross-section EI values were based on concrete strengths (f'_c) that were measured during Caltrans' tests of cores extracted from the MRO's central pier in 1992 (Klein, 1992). Concrete aging data from Wood (1991) were used to modify these measured strengths and estimate the corresponding strengths at the time of the Imperial Valley Earthquake in 1979. These measured and modified concrete strengths and the resulting EI and GJ values that were computed for the deck and central pier are provided in Tables 2-1 and 2-2 respectively.

2.2.2 Abutment and Central Pier Foundation Elements

Initial values of the abutment foundation stiffnesses, k_y, $k_{x\theta}$, and $k_{z\theta}$, and central pier foundation stiffness, $k_{x\theta}'$, were estimated based on: (a) stiffnesses computed from the motions recorded during the forced vibrations tests of the MRO conducted by UNR and D&M (Crouse, 1992); (b) stiffnesses computed from nonlinear models of the foundation-pile-soil system for the abutment and central pier foundations; and (c) modified values of the stiffnesses in (b) that produced estimates of the natural frequency and mode shape of the MRO's fundamental

symmetric transverse mode of vibration that were similar to those estimated by Werner et. al. (1987). The models of the foundation-pile-soil system were developed from modifications of the FHWA (1986) methodology that were recommended under a D & M project for the Washington State Department of Transportation (Crouse et. al., 1992). The soil properties used for these models were taken from Crouse et. al. (1992), and are based on in situ tests of the soils at the MRO that were conducted under Task 1 of the UNR-D&M research program (Sec. 1.1.3). The low-strain shear moduli reported in that publication were reduced by 50 percent to account for the reduction in shear modulus during strong ground motion. This 50 percent reduction was inferred from ground motions recorded at the nearby El Centro differential array during the 1979 Imperial Valley Earthquake (Crouse and Hushmand, 1990). The resulting initial values of the abutment and central pier foundation spring stiffnesses are reported later in Table 3-2 of Chapter 3.

2.2.3 Embankment Elements

The effective mass, m_e, of each embankment of the MRO was computed in terms of the embankment's mass density, ρ_s, and trapezoidal cross section by using the following expression:

$$m_e = \frac{\rho_s(W + SH)Hd}{4} \qquad (2\text{-}1)$$

where W, H, and S are the embankment's top width, height, and side slope (measured relative to the vertical) respectively, and d is the effective length of the segment of the embankment that is vibrating in phase with the bridge during its first transverse mode of vibration. Equation 2-1 was derived by first computing the kinetic energy of the embankment segment of length d, in which d was estimated from the embankment's mode shape amplitudes for the MRO's first symmetric transverse mode that was part of a classical mode model identified from the recorded earthquake motions by the MODE-ID system identification methodology (summarized in Sec. 2.3.3). On this basis, d was computed to be about 48 ft., which is about ¼ of the total length of the bridge. We then defined m_e to be that soil mass lumped alongside the abutment that has the same kinetic energy as that of the above embankment segment. It is noted that this approach assumes that the motions recorded at the embankment instrument 40 ft. from the bridge represent free field motions all along the length of the embankment.

The effective transverse horizontal spring stiffness of the embankment, k_{ye}, was computed from the following expression:

$$k_{ye} = \frac{\frac{4}{\pi}SGd}{\ln(1 + 2S\frac{H}{W})} \qquad (2\text{-}2)$$

Equation 2-2 is based on a derivation by Wilson and Tan (1990) of the shear stiffness of an embankment with a shear modulus G, a trapezoidal cross section with dimensions W, H, and S

as defined above, and an effective length d which is the same length as was used in the above effective mass calculation.

2.3 System Identification

2.3.1 Methodology

A key element of our development of the MRO's model parameters was a new system identification algorithm named MODEL-ID, which is an extension of a methodology developed by Katafygiotis (1991). This procedure is based on an assumed linear model with classical normal modes and N degrees of freedom, whose equations of motion can be expressed as follows:

$$M\ddot{\underline{x}} + C\dot{\underline{x}} + K\underline{x} = \underline{F}(t) \qquad \textbf{(2-3)}$$

where M, C, and K are the N x N mass, damping, and stiffness matrices, $\underline{x}$ is the displacement response vector, $\underline{F}(t)$ is the forcing vector, and a dot denotes differentiation with respect to time. In this, MODEL-ID represents C as a Rayleigh damping matrix with the following form:

$$C = \alpha M + \beta K \qquad \textbf{(2-4)}$$

where α and β are the Rayleigh damping coefficients which control the damping ratios of the model's normal modes of vibration (Clough and Penzien, 1975). For the case of earthquake excitation, the forcing vector $\underline{F}(t)$ is expressed in terms of the "input" acceleration time histories recorded at the supports of the subsystem of the structural system to be modeled. If the entire structural system is to be modeled, these "input"acceleration histories would consist of the recorded free field motions whereas, if only a subsystem of the total system is to be modeled, the "input" motions would consist of the array of motions recorded at the boundaries of the subsystem. The corresponding "output" motions designated by the vector $\underline{\ddot{x}}$ in Equation 2-3 are the acceleration histories recorded within the system or subsystem being modeled. It is noted that MODEL-ID can now accommodate only a single input acceleration history (together with multiple "output" motions). In the near future, this algorithm will be extended to accommodate multiple input motions.

The first step in the identification procedure is to select the subsystem to be modeled, together with the corresponding arrays of recorded "input" and "output" motions. For this subsystem, a set of model parameters is then defined whose values are uncertain and need to be identified (eg. SSI spring stiffnesses, and/or soil masses, bending and/or torsional rigidities of structural elements, etc.), and "first estimate" values of these parameters are computed. The total subsystem mass matrix M and stiffness matrix K are then expressed as a linear combination of these uncertain mass and stiffness parameters, i.e:

$$M = M_0 + \sum_{i=1}^{N_M} \theta_i^{(M)} M_i$$

$$K = K_0 + \sum_{i=1}^{N_K} \theta_i^{(K)} K_i \qquad \textbf{(2-5)}$$

In Equation 2-5, M_i (i=0,1,---N_M) and K_i (i=0,1,---N_K) are known N x N mass and stiffness matrices that are obtained from the specified (i.e., assumed known) mass and stiffness parameters (i=0) and from the "first estimate" values of the uncertain parameters (i≠0) as described in Section 2.2. The quantities $\theta_i^{(M)}$ and $\theta_i^{(K)}$ are nondimensional scaling factors associated with each uncertain model parameter. It is these factors, together with the Rayleigh damping coefficients α and β, that are identified by MODEL-ID.

The identification procedure used by MODEL-ID estimates the values of the above factors so as to minimize the difference between the recorded motions at each "output" location and the computed model motions. The procedure is based on the minimization of the following measure-of-fit function $J(\underline{\theta})$:

$$J(\underline{\theta}) = \left[\prod_{i=1}^{N_0} J_i(\underline{\theta}) \right]^{1/N_0} \qquad \textbf{(2-6)}$$

where $\underline{\theta}$ is a vector of order $N_\theta = N_M+N_K+2$ that contains the uncertain substructure scaling factors $\theta_i^{(M)}$ and, $\theta_i^{(K)}$ and the uncertain Rayleigh damping coefficients α and β, and N_0 is the number of degrees of freedom for which measurements are available. The quantity $J_i(\underline{\theta})$ is the following measure-of-fit function for the i^{th} "output" location and direction:

$$J_i(\underline{\theta}) = \left[\frac{\sum_{n=1}^{N_T} \left[\ddot{x}_i(n,\underline{\theta}) - \ddot{y}_i(n) \right]^2}{\sum_{n=1}^{N_T} \ddot{y}_i(n)^2} \right]^{1/2} \qquad \textbf{(2-7)}$$

In Equation 2-7, $\ddot{y}_i$ is the recorded acceleration at the i^{th} output location (with digitized values at N_T equally spaced time steps) and $\ddot{x}_i$ is the computed model acceleration for the corresponding degree of freedom in the model.

2.3.2 Application

The MODEL-ID methodology outlined above has been applied to the MRO's recorded earthquake motions to estimate model parameters. In these applications, the target response motions to be fitted by the computed model motions were the transverse horizontal motions at the embankments and abutments, and the transverse and rotational motions (corresponding to rotations about the long axis of the bridge deck) that were recorded at the midlength of each span and at the midlength of the bridge. The target rotational motions at each of the above deck locations were computed as the time-dependent difference between the vertical motion time histories recorded on each side of the deck divided by the distance between the instruments (26.5 ft.). The stiffness scaling factors $\theta_i^{(K)}$ that correspond to the uncertain model parameters discussed below were identified by MODEL-ID, together with the Rayleigh damping coefficients α and β. The masses within the model's structural elements were assumed to be fixed and known quantities, and were not identified by MODEL-ID.

The model parameters that were the focus of our system identification of the MRO's transverse response model were the bending rigidity EI_{zz} and torsional rigidity GJ of the various segments of the deck, the bending rigidity EI_{xx} of the central pier, the abutment spring stiffnesses k_y, $k_{x\theta}$, and $k_{z\theta}$, the spring stiffness at the base of the pier $k_{x\theta}'$, and the embankment mass m_e and spring stiffness k_{ye} (Fig. 2-1). However, before starting our system identification, we first evaluated how many of these parameters we could identify "uniquely" so that, no matter what initial values of the model parameters are assumed, the system identification process will converge to the same final values. These uniqueness requirements (which depend on the nature of the model and the number and location of the target recorded motions) dictated that no more than five model parameters plus the Rayleigh damping coefficients could be identified, and the rest would have to be fixed.

In view of this, we decided to fix the all of the structural parameters for the deck and central pier as well as the embankment mass m_e, and to identify the five spring stiffnesses listed above for appropriate combinations of the fixed parameters. Three different sets of fixed structural parameters for the deck and central pier were selected, corresponding to gross section properties everywhere, cracked section properties everywhere, and the parameters recommended in the ATC-32 Interim Report (ATC, 1992). (The ATC-32 recommendations are to use 0.5 x the gross EI value for the central pier, and 0.75 x the gross EI value together with the full gross GJ value for the deck.) In addition, two fixed values of the embankment mass were chosen. The first corresponded to our best estimate value that was computed using Equation 2-1 of Section 2.2.3, and the second corresponded to twice this best estimate value. This latter value of the embankment mass was used with the ATC-32 structural parameters only.

For each combination of these fixed parameter values, the MODEL-ID system identification methodology was used to estimate values of the Rayleigh damping coefficients and the soil spring stiffnesses at the abutments, central pier base, and embankments that led to a best fit between the recorded motions and the computed model motions. In addition, the methodology was used to carry out sensitivity studies to evaluate the relative influence of each of the identified

soil spring stiffnesses on the fit between the recorded motions and the computed model motions. To accomplish this, we first assumed a value of $J(\underline{\theta})$ that was slightly larger than the optimum value. Then, we used MODEL-ID to evaluate how much each of the soil spring stiffness values could be changed from their optimum value without exceeding this slightly larger value of $J(\underline{\theta})$. These sensitivity studies enabled us to judge how much we can change each of the identified spring stiffness values (e.g., if needed to provide values that are consistent with established engineering procedures) without significantly affecting the fit between the MRO's recorded earthquake motions and the computed model motions. They were carried out for two sets of values for the fixed parameters, corresponding to the ATC-32 structural parameters and the two embankment mass values indicated in the preceding paragraph.

2.3.3 Modal Identification

Although the MODEL-ID methodology and application procedure formed the primary basis of our model development for the MRO, a second system identification procedure named MODE-ID also played an important role. MODE-ID is a modal identification procedure for a system with any arbitrary configuration and classical normal modes (Beck, 1978; Werner et. al., 1987). For each significant normal mode excited by multiple support motions or force-time histories, MODE-ID estimates the natural frequency, damping ratio, participation factors, and mode shape components at the locations of the response measurements. For multiple support motion excitations, MODE-ID also estimates the pseudostatic matrix for the system. Within a Bayesian probability framework, the parameters estimated by MODE-ID can be viewed as the most probable values based on the given data (Beck, 1989). The MODE-ID methodology has been successfully applied to recorded motions from a variety of structure types including offshore platforms, bridges, and buildings (e.g., Mason et. al., 1989; Werner et. al., 1987 and 1990; and Werner et. al. 1992).

In this research, MODE-ID has been applied to the MRO's recorded earthquake motions in order to provide an independent basis for interpreting the finite element model parameters estimated by MODEL-ID, as well as the MRO's overall seismic response characteristics.

2.4 Seismic Analysis

The seismic analysis of the MRO was carried out by applying the SAP-90 program (Wilson and Habibullah, 1989) to models comprised of each set of fixed parameter values together with the associated soil spring stiffness values identified by MODEL-ID for the optimum case and for the sensitivity studies. For each set of model parameters, we computed earthquake demand values of the MRO's bending moments, shear forces, and central pier deformations, and compared these demand values to the capacities of the MRO's structural elements (as discussed in Sec. 2.6). In addition, peak values of demand spring forces and moments at the abutments and the base of the central pier that were computed for selected parametric cases were used in more detailed analyses of the pile foundations (as described in the following section).

2.5 Foundation Evaluation

2.5.1 Input Loads from Dynamic Analysis

The foundation loads computed from the above-indicated parametric seismic analyses were used as input to a separate analysis of the pile foundations at the abutments and at the base of the central pier. The particular loads that were used for the abutment foundation analysis were the foundation's transverse shear force, overturning moment (about the x-axis), and torsional moment (about the z-axis). For the analysis of the pile foundation at the base of the central pier, the loads that were used were the transverse shear force at the base of the pier and the overturning moment (about the x-axis).

During the dynamic analysis, the overturning moment at the abutment was computed at the location along the abutment end wall that corresponds to the neutral axis of the deck. This moment, together with the transverse shear force which was also computed at this location, was used to compute the corresponding overturning moment at the top of the abutment's pile cap using principles of static equilibrium.

In addition to the above loads, the vertical forces from the dead weight and the earthquake response of the MRO were imposed on the abutment and central pier foundations. These loads were estimated from simplified SAP-90 analyses of the vertical response of the MRO (see Sec. 3.3.1).

2.5.2 Methodology

A nonlinear static load-deflection model was developed to estimate the response of the MRO's abutment and central pier foundations. The model, which is summarized in Section 3.3.2 and presented in detail in Appendix B, consists of a rigid pile cap subjected to the loads described in Section 2.5.1. The resistance to the axial and transverse forces and an overturning moment about the longitudinal axis is supplied by (1) the piles and adjacent soil, 2) the shear resistance of the soils bearing against the bottom of the pile cap, (3) and the passive resistance of the soils against the side of the pile cap. The shearing resistance of the abutment-backfill system and the passive resistance of the wing wall-backfill system is neglected. The former condition is not generally considered, and the latter condition, although considered in Caltrans' current seismic evaluation procedures, was not included because the load transfer to the wing wall was not believed to be significant. However, it should be noted that the interaction behavior of the abutment foundation is complex, and the current experimental data base on the transverse force-deflection behavior for abutments is too limited to estimate with confidence how the loads are distributed among the various elements comprising the abutment foundation system. Nevertheless, the observed performance of the MRO during the 1979 Imperial Valley Earthquake and the results of analyses presented in this report indicated limits on the load-carrying capacity of certain elements.

2.6 Structural Demand vs. Capacity Evaluations

Our procedures for estimating the bending moment and shear capacities for the MRO's central pier and deck together with the displacement capacity for the pier are summarized in the following paragraphs. The numerical values of the bending moment and shear capacities for the deck and pier are shown in Table 2-3.

2.6.1 Moment Capacities

For both the central pier and the deck, we obtained moment capacities from nonlinear moment curvature relationships computed using the BIAX program (Section 2.2.1) and shown in Figure 2-2. Moments corresponding to first yield of the steel and to the development of an ultimate concrete strain of 0.003 in/in in the extreme fiber of the cross section were computed (see Table 2-3). For the central pier, the modified Kent and Park stress-strain relationship for concrete was used to model the confinement of the concrete by the pier's spiral steel transverse reinforcement (Scott et. al., 1982). For the deck, the concrete was considered to be unconfined.

2.6.2 Displacement and Shear Capacities of Central Pier

Our interim procedure for evaluating the central pier's demands and capacities is shown in Figure 2-3. It focuses on the estimation of the displacement capacity of the pier and is based on calibrations with extensive column test data. The steps of the procedure are as follows (Moehle and Aschheim, 1993):

(1) Carry out elastic dynamic analysis of the transverse seismic response of the SBO, and compute the elastic demand bending moments, shear forces, and relative displacement of the central pier, and the rotation of the base of the pier.

(2) Evaluate whether the pier yields by comparing its elastic demand moments to its plastic moment. If no yielding is indicated, the demand shear forces from the seismic analysis should be checked against the ultimate shear capacity of the pier. If the shear demand falls below the ultimate capacity, the pier is judged to be acceptable. The remaining steps outlined below apply to the condition where yielding of the central pier occurs.

(3) If yielding of the central pier is indicated, compute the displacement capacity of the pier. This involves: (a) the computation of the pier's plastic shear force; (b) the use of this plastic shear force in a concrete shear strength vs. ductility relationship, in order to compute the pier's ductility capacity and check the pier's shear capacity; (c) computation of the pier's yield displacement including the effects of flexure, shear deformations, and slippage of the longitudinal steel that ties the central pier to the footing; and (d) computation of the pier's relative displacement capacity by calculating the product of the above-indicated ductility capacity and yield displacement, and then adding this product to the rigid body displacement at the top of the pier due to earthquake-induced rotations of the footing. In this process, the effects of the restraint of the ends of the pier by the

deck and the foundation must be included.

(4) Compare this relative displacement capacity to the relative displacement demand computed from the seismic analysis. Use this comparison as a basis for assessing the seismic performance of the pier.

In Steps 2 and 3 above, our computation of the shear capacity of the central pier, V_u, is based on the following expression:

$$V_u = V_c + V_s \tag{2-8}$$

where V_c and V_s are the contributions of the concrete and the steel respectively to the pier's shear capacity. The steel contribution, V_s, is calculated as:

$$V_s = \frac{\pi}{2}\frac{A_{sp} f_y D}{s \tan\alpha} \tag{2-9}$$

where A_{sp} and f_y are the area and the yield strength respectively of the spiral steel, D is the diameter of the concrete core encased by the spiral steel, s is the spacing of the spirals, and α is the shear crack orientation (assumed = 30 deg). The concrete contribution, V_c, to the pier's shear capacity (lb) is computed as:

$$V_c = 3.5(k + \frac{N}{2000A_g})\sqrt{f'_c}\,0.8A_g \tag{2-10}$$

where N is the axial load on the pier (lb), f'_c is the concrete compressive strength (psi), A_g is the pier's gross cross sectional area (in^2), and k is a parameter that depends on whether or not the pier yields. If the central pier does not yield, k is set equal to 1.0. If yielding of the central pier does occur, k is obtained as the solution to Equation 2-10, in which V_c is first computed as the difference between the demand shear force from the dynamic analysis and the transverse steel's shear capacity contribution, V_s. This value of k is then used to obtain the pier's ductility capacity, as described by Moehle and Ascheim (1993).

2.6.3 Shear Capacity of Deck

We have estimated the shear capacity corresponding to the deck's transverse response as the sum of concrete and steel contributions as indicated above in Equation 2-8. The contribution of the concrete to the deck's shear capacity (lb) has been computed as:

$$V_c = 2\sqrt{f'_c}A_e \tag{2-11}$$

where A_e is the effective shear area of the deck (in^2). For this transverse response case, we have assumed that this effective area is equal to 80 percent of the total gross area of the top and bottom slabs of the deck. The contribution of the steel to the total shear capacity has been obtained from the following equation:

$$V_s = \frac{A_v f_y d}{s} \qquad (2\text{-}12)$$

where A_v and s are the area and spacing respectively of the transverse horizontal steel in the top and bottom slabs of the box girder deck, and d is the effective depth of the deck in the transverse direction. In this, we have assumed that this effective depth is equal to 80 percent of the width of the top and bottom slabs within the box girder. Also, we have included the contribution of the steel to the deck's overall shear capacity in the transverse direction even though the ends of the transverse horizontal steel bars in the top and bottom slabs are not hooked or anchored. However, we anticipate that the transverse shear demands for the deck will be low and that, even though the total length of the bars will not be developed, the segment of the bars that is developed should be sufficient to resist the low shear demands that are anticipated.

TABLE 2-1
CONCRETE STRENGTHS AT MELOLAND ROAD OVERCROSSING (Klein, 1992)

Specimen No.	Diameter (in)	Average Capped Length (in)	Compressive Strength, psi		
			(L/D = 2 per ASTM C 42)	Equivalent 6 in. × 12 in. Cylinder Strength (Oct. 1992)	Estimated 6 in. × 12 in. Cylinder Strength (Oct. 1979)(*)
1	3.96	6.18	5710	5520	5364
2	2.78	4.17	5160	4800	4665
3	3.95	7.65	5550	5360	5209
4A	3.96	3.48	5330	5150	5005
4B	2.78	5.95	5950	5750	5588
			Average Values	5316	5166

Note: * Estimated 6 in. × 12 in. cylinder strength in October 1979 (at time of 1979 Imperial Valley Earthquake) was based on use of concrete aging data by Wood (1991) in conjunction with: a) year of construction of MRO (1971); (b) age of concrete at time of Caltrans' tests in 1992 (21 years); and (c) age of concrete at time of 1979 Imperial Valley Earthquake (8 years).

TABLE 2-2
TRANSVERSE BENDING AND TORSIONAL RIGIDITIES
OF MELOLAND ROAD OVERCROSSING[1]

Element	Transverse Bending Rigidity (EI) (kip-ft^2)		Torsional Rigidity (GJ) (kip-ft^2)	
	Gross Section	Cracked Section	Gross Section	Cracked Section[2]
Central Pier (Axial Load = 1210 kips)[3]	1.81×10^7	8.15×10^6	1.55×10^7	3.10×10^6
Deck: At Mid-length of Each Span	2.45×10^9	6.22×10^8	1.53×10^8	3.06×10^7
Deck: Average for Flared Segment	2.84×10^9	8.62×10^8	1.60×10^8	3.2×10^7
Deck: Adjacent to Abutment	2.45×10^9	3.68×10^8	1.53×10^8	3.06×10^7

Note: (1) Section property computations based on following material properties:
Ultimate concrete compressive strength (f'_c) = 5166 psi
Yield stress in steel (f_y) = 45300 psi
Maximum strain in concrete (ε_u) = 0.003 in/in
Poissons ratio in concrete (υ_c) = 0.17

(2) Cracked section GJ values assumed to be 0.2 × gross section GJ values.

(3) Axial load of 1210 kips corresponds to computed dead load reaction at central pier.

TABLE 2-3
BENDING MOMENT AND SHEAR CAPACITIES
OF MELOLAND ROAD OVERCROSSING

Element	Bending Moment (kip - ft)[1]		Shear Capacity (kips)[2]
	At First Yield	At Extreme Fiber Concrete Strain = 0.003 in/in	
Central Pier (Axial Load = 1210 kips)[3]	5827	7881	924.5
Deck: Adjacent to Abutment	30195	42277	1823
Deck: At Mid-length of Span	46664	73345	1823
Deck: Above Central Pier	71600	102436	1823

Note:

(1) Bending moment capacities shown for central pier and deck correspond to bending about longitudinal (x-) axis and vertical (z-) axis respectively (see Fig. 2-1 for model axis orientations). Capacities obtained from results of moment-curvature calculations using BIAX program that are summarized in Section 2.2.1. and are shown in Figure 2-3.

(2) Shear capacities shown for central pier and deck correspond to shear in transverse horizontal (y-) direction. They have been computed using procedures summarized in Section 2.6.1. and 2.6.2.

(3) Axial load of 1210 kips for which bending moment and shear capacities of central pier were computed corresponds to dead load reaction at central pier.

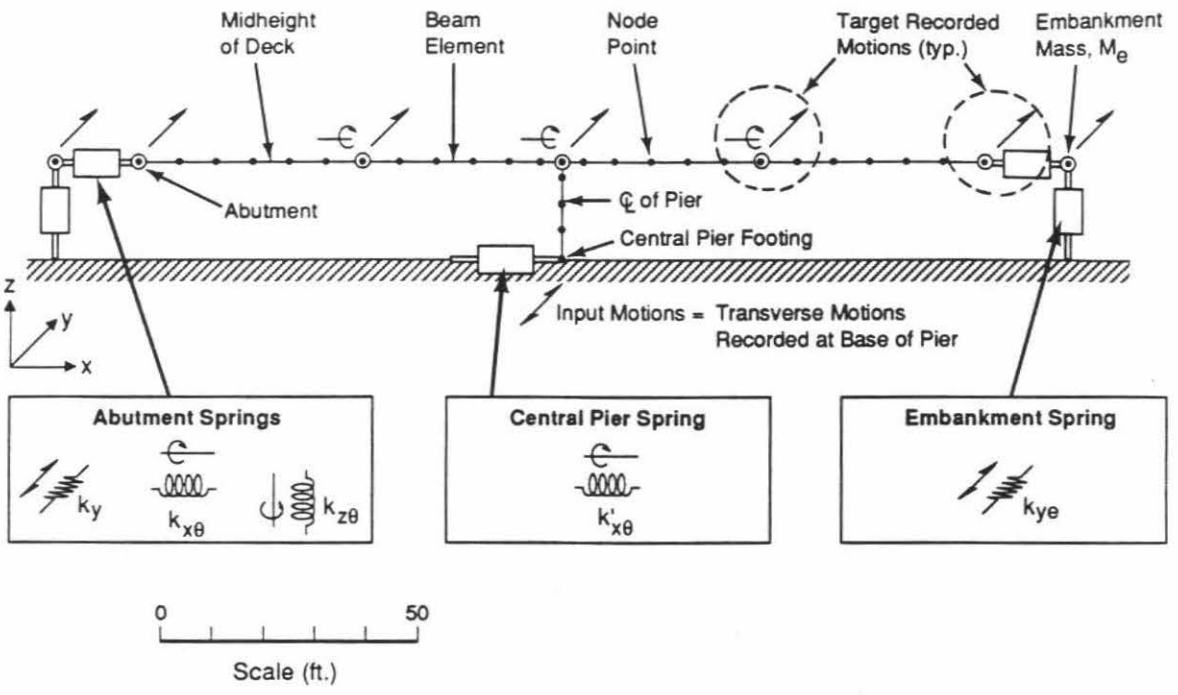

FIGURE 2-1

FINITE ELEMENT MODEL

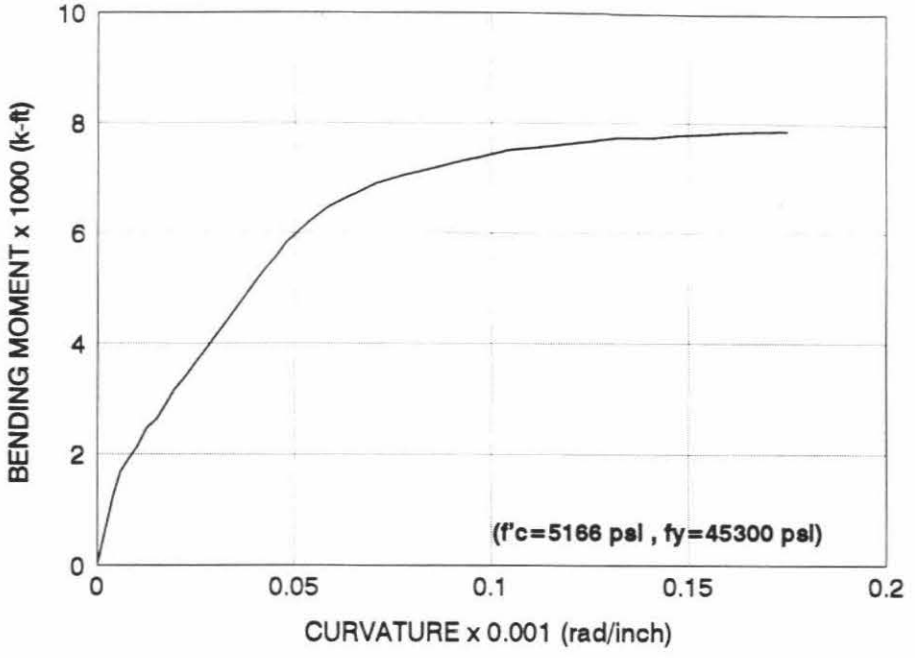

a) Central Pier (Axial Load = 1210 kips)

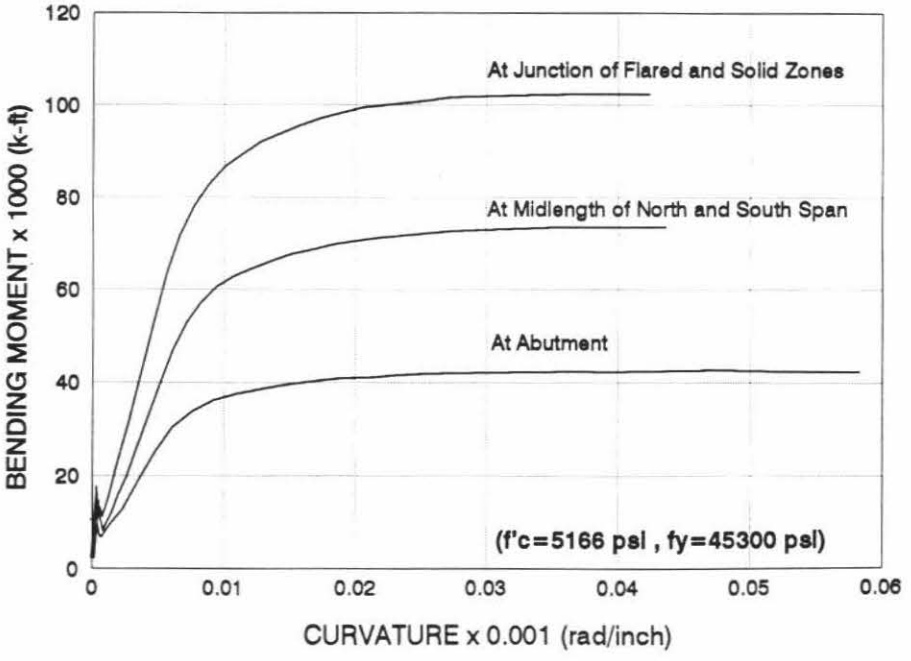

b) Deck

FIGURE 2-2

MOMENT CURVATURE RELATIONSHIPS FOR MELOLAND ROAD OVERCROSSING

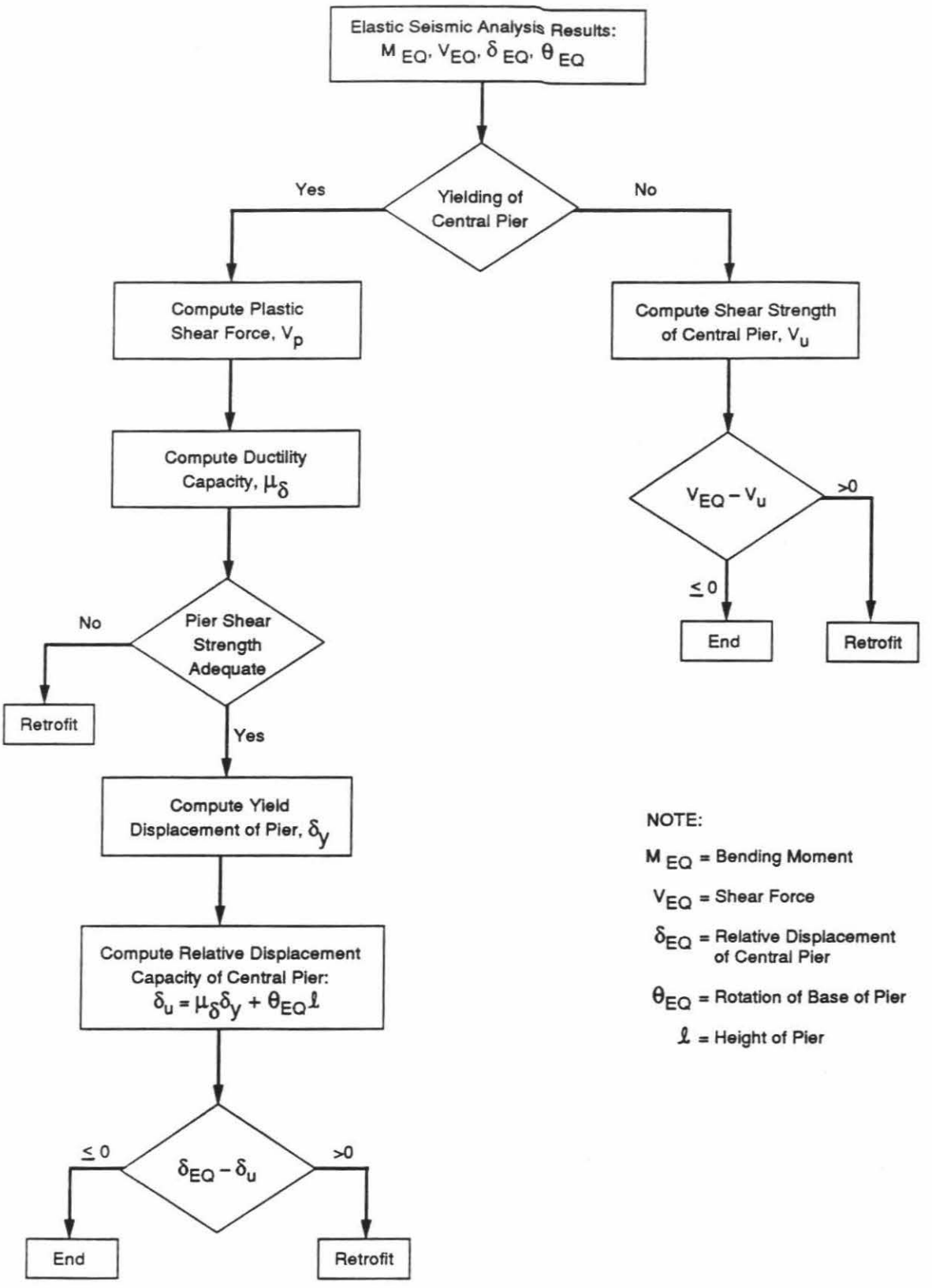

FIGURE 2-3

PROCEDURE FOR SEISMIC EVALUATION OF CENTRAL PIER

CHAPTER 3
ANALYSIS RESULTS

This chapter presents the results of our estimation of the finite element model parameters for the MRO's seismic analysis, our use of the parameters in seismic analyses of the MRO to compute its structural and foundation response, and our use of these analysis results to assess Caltrans' seismic design procedures.

3.1 Model Parameters

The MODEL-ID methodology was used to estimate the various soil spring stiffnesses discussed in Section 2.3.2 for the four basic combinations of fixed structural and embankment mass parameters that are listed in Table 3-1. In this table, Case 5-1 (which consists of the use of the ATC-32 recommended structural parameters and the embankment mass computed using Equation 2-1 represents our preferred combination of fixed parameters, and the remaining cases (5-2 through 5-4) encompass various modifications of these parameters that enable us to assess the sensitivity of the computed bridge response to these modifications. In addition, the MODEL-ID methodology was used to carry out sensitivity studies of each identified value of each soil spring stiffness on the fit between the MRO's recorded motions and computed model motions, as described in Section 2.3.2. These sensitivity studies were implemented for the Case 5-1 and 5-4 fixed parameter values only.

3.1.1 Tabulations of Identified Parameters $\theta_i^{(K)}$

The results of the application of MODEL-ID for these four cases are provided in Table 3-2. This table contains the optimum values of the stiffness scaling parameters $\theta_i^{(K)}$ corresponding to the abutment springs k_y, $k_{x\theta}$, and $k_{z\theta}$, the central pier foundation spring $k_{x\theta}$', and the embankment spring k_{ye} that were identified by MODEL-ID. Also shown in Table 3-2 is the value of the measure-of-fit parameter $J(\underline{\theta})$ associated with each set of optimum model parameters. The comparable values of $J(\underline{\theta})$ for each case indicates that each set of model parameters has led to comparable comparisons between the recorded earthquake motions and the computed model motions.

As discussed in Section 2.3.2, we also used MODEL-ID to perform sensitivity studies to assess the degree of confidence that can be associated with the optimum stiffness value that was identified for each soil spring. These studies, which were carried out for Cases 5-1 and 5-4 only, involved our assuming a value of the measure-of-fit-parameter $J(\underline{\theta})$ (as defined in Eq. 2-6 and 2-7) that was slightly larger than the optimum value obtained from our system identification. Then we used MODEL-ID to evaluate how much each of how much each spring stiffness could be changed from its optimum value without exceeding this slightly increased value of $J(\underline{\theta})$. This enabled us to assess how well each of each spring stiffness value was constrained by our model identification process as applied to the array of motions recorded at the MRO during the Imperial Valley Earthquake. The ranges of $\theta_i^{(K)}$ values obtained for each spring stiffness from these sensitivity evaluations are shown in parentheses in Table 3-2. These ranges show that: (a) the

transverse spring stiffness at the abutment, k_y, is particularly well constrained by the model and recorded earthquake motions, and is not strongly sensitive to the variations in embankment mass between Cases 5-1 and 5-4; (b) the transverse spring stiffness at the embankment, k_{ye}, is also well constrained by the model and recorded earthquake motions, but is more sensitive to variations in the embankment mass than is k_y; (c) the spring stiffness associated with rotations about the longitudinal axis at the abutment, $k_{x\theta}$, is reasonably well constrained (although somewhat less constrained than k_y and k_{ye}) but is sensitive to the variations in embankment mass between Cases 5-1 and 5-4; and (d) the spring stiffnesses associated with rotations about the z-axis at the abutment, $k_{z\theta}$, and rotations about the x-axis at the base of the central pier, $k_{x\theta}'$, are not well constrained by the model and recorded earthquake motions.

We have examined the range of soil spring stiffnesses that were obtained from the above sensitivity studies for Cases 5-1 and 5-4, and have used these ranges to define different sets of spring stiffness values that, together with the corresponding structural parameters and embankment masses, led to a value of $J(\underline{\theta})$ that was within the slightly increased value noted above. The models associated with each set of soil spring stiffnesses was used in parametric dynamic analyses of the seismic response of the MRO, in order to examine how the MRO's computed response may have been affected by these assumed soil stiffness variations. In addition, we carried out parametric dynamic analyses in which we assumed that the abutment rotations about the x-axis were first fixed and then pinned, in order to assess how closely the optimum value identified for this spring stiffness approached these idealized conditions. In this, we have designated the models with the optimum spring stiffness values from our system identification as Cases 5-1A and 5-4A, and have designated the models with the other sets of stiffness values using subsequent letters of the alphabet (e.g., Cases 5-1B, 5-1C, ... etc., and 5-4B, 5-4C,....., etc.). The various sets of spring stiffnesses that were assumed for these parametric dynamic analyses and the results of these analyses are described in Section 3.2.

In addition to the above parametric analyses, we also carried out dynamic analyses of the MRO using current Caltrans procedures to develop the model. The objective of these additional analyses was to compare bridge responses computed using Caltrans modeling procedures to those computed using models that were identified from the MRO's strong motion records. These comparisons will provide an important basis for our assessment of Caltrans' current seismic evaluation procedures under our short bridge research program (Sec. 1.1.4). The results of these particular comparisons are described in Section 3.4.

3.1.2 Comparison between Computed Model Motions and Recorded Motions

Typical comparisons between the earthquake motions recorded along the bridge deck and the computed motions at the corresponding degree-of-freedom in the finite element model are shown in Figures 3-1 and 3-2 for the Case 5-1A model parameters (i.e., the model parameters for Case 5-1 that led to the lowest value of $J(\underline{\theta})$) . Figure 3-1 shows that the recorded transverse translational components of the earthquake motions are very well fitted by the computed model motions. However, as shown in Figure 3-2, the rotational components of the recorded earthquake motions (which correspond to rotations about the longitudinal axis of the bridge) are not well

represented by the rotational motions computed from the finite element model. As noted in Section 2.3.2, these rotational components have been computed as the difference between the vertical motions recorded at the two sides of the deck (at the midlength of each span and above the central pier) divided by the distance between these accelerometer locations (26.5 ft.). This assumes that the bridge is vibrating as a beam and that vertical slab bending deformations of the deck are negligible.

To evaluate this poor fit between the recorded and computed model rotations, we applied the MODE-ID modal identification methodology to these recorded motions in order to assess how well the model identified by MODE-ID represented the recorded rotational motions. As noted in Section 2.3.3, the MODE-ID methodology differs from the MODEL-ID procedure in that it fits a classical mode model (i.e., consisting of natural frequencies, mode shapes, damping ratios, and participation factors of the significant modes excited by the shaking) rather than a finite element model to the recorded motions. Therefore, the objective of this independent application of MODE-ID was to enable us to assess whether or not the poor fit between the recorded and computed model rotations was a consequence of the finite element model's fixed and/or identified parameters.

The results of this application of MODE-ID to the recorded motions were similar to those obtained from MODEL-ID; i.e., the recorded transverse translational components of motion were well fitted by the computed model motions whereas the rotational components of motion were not (Fig. 3-3). This has led us to conclude that our poor fit to the rotational motions is not due to the finite element model that was identified. Rather, it is most likely a consequence of such factors as: (a) the lack of recorded rotational motions at the abutments, which correspond to rotational input motions to the deck structure itself and therefore are important for modeling the bridge's rotational response characteristics; and (b) the possible presence of slab bending deformations of the deck, which would lead to inaccuracies in our above-indicated approach for computing rotations by neglecting the presence of these deformations.

3.1.3 Normal Mode Characteristics of Model

Inspection of the results of our seismic analysis of the MRO using the above finite element models has shown that the response of the model in its first transverse mode of vibration is particularly important. Accordingly, we have tabulated and compared the natural frequencies, mode shapes, and damping ratios for this mode that were computed from the identified model parameters for Cases 5-1A through 5-4A. These modal parameters are provided in Table 3-3, which shows the following general trends:

- The natural frequency of the MRO's first transverse mode of vibration is not sensitive to the differences in model parameters for Cases 5-1A through 5-4A, and is seen to range from 2.5-2.6 Hz. for the four cases. This natural frequency is very similar to that indicated by the Fourier amplitude spectra of the recorded earthquake motions at the MRO (Werner, et. al., 1987).

- The modal damping ratios identified for the first transverse mode of vibration range from 0.19 to 0.26 for the various models. These damping ratios are much larger than the damping ratio of 0.05 that is used by Caltrans in their current seismic evaluation procedure for SBOs.

- The mode shape amplitudes at the abutments of the various models are large fractions (about 0.5 to 0.9) of the maximum mode shape amplitude at the top of the central pier. This clearly indicates that soil-structure interaction at the abutment is significant and has an important effect on the MRO's response to transverse input motions.

The following additional observations can be made from comparisons of the individual modal parameters shown in Table 3-3.

- The natural frequency, mode shape, and damping ratio are all nearly identical for Cases 5-1A (ATC-32 structural properties) and 5-2 (gross section properties). For these cases, the mode shape amplitude at the embankment is relatively small (about 7 percent of the maximum translational amplitude above the central pier).

- For Case 5-3, which corresponds to the use of cracked section properties throughout the bridge structure, the natural frequency is slightly lower (about 2.5 hz.) and the damping ratio is about 25 percent lower (0.19) than the values obtained for the other three cases. As expected, the mode shape for Case 5-3 exhibits larger deformations along the length of the deck than do the other cases, and a very small amplitude at the embankment.

- The effects of the embankment mass on the modal parameters is seen by comparing the parameters for Cases 5-1A and 5-4A. These comparisons show that the increased embankment mass in Case 5-4A does not have a significant effect on the natural frequency or damping ratio but does lead to a mode shape with smaller deformations along the deck and smaller displacements at the embankment.

3.1.4 Assessment of Engineering Estimates of Spring Stiffnesses

To further assess the identified abutment and central pier foundation spring stiffness values, we have performed separate calculations of k_y, $k_{x\theta}$, $k_{z\theta}$, and $k_{x\theta}$' using engineering procedures developed by FHWA (1986) and by Novak et. al. (1991). These particular procedures were selected because they were judged to be the most plausible of a variety of different methods that were reviewed and evaluated in a prior study of SSI analysis procedures for bridges that was carried out by Dames & Moore for the Washington State Department of Transportation (D & M, 1992). The engineering estimates of these various soil springs were compared to: (a) the optimum values and ranges established for each spring from our system identification of the recorded earthquake motions; and (b) the range of values previously estimated from the forced vibration tests of the MRO (Crouse, 1992). These comparisons were intended to provide a basis for assessing the applicability of the alternative engineering procedures on the basis of this calibration with the earthquake and vibration test motions recorded at the MRO. They are

tabulated in Table 3-4 and are discussed in the paragraphs that follow. The following paragraphs also discuss the identified values of the embankment spring stiffness k_{ye}, and how they compare with the value predicted using the simplified expression given in Equation 2-2 of Section 2.2.3.

(a) Transverse Abutment Stiffness k_y

Table 3-4 shows that the earthquake values of the transverse abutment stiffness k_y, which is the SSI parameter that was best constrained by the recorded earthquake motions are approximately ¼ of the vibration test values. This observation indicates that nonlinear response was significant during the earthquake and that the abutment response was an important contributor to this nonlinear behavior -- trends which are consistent with conclusions by Werner et. al. (1990) based on comparisons of normal mode parameters identified from the MRO's earthquake motions and vibration test motions. Table 3-4 also shows that the earthquake-induced values of k_y are in between the FHWA values for the "piles only" and "piles and footing" cases. This suggests that the stiffness contribution from the abutment footing (pile cap) was not as great as predicted from the engineering calculations, which treated the pile cap as a rigid footing embedded in an elastic half space characterized by a shear modulus that was 50 percent of the measured low-strain value. It is noted that this treatment of the pile cap could produce unrealistically large estimates of the abutment stiffness, especially for the MRO where the embankment side slopes are close to the pile cap. This interpretation is supported by Crouse (1992), who showed that the pile cap contribution to the low-strain stiffness calculation of k_y resulted in estimates of k_y that were greater than the values derived from the vibration test data. The occurrence of any settlement of the soils beneath the pile cap and separation of the soils away from the sides of the cap could also have contributed to this overestimation of the stiffness contribution of the pile cap by the engineering procedures.

(b) Abutment Rotational Stiffness $k_{x\theta}$

The abutment stiffness corresponding to rotations about the MRO's longitudinal (x-) axis, $k_{x\theta}$, was adequately constrained by the recorded earthquake motions. Table 3-4 shows that the earthquake values of this parameter are significantly smaller than the vibration-test values; these earthquake values are seen to range from about 0.1 to 0.75 of the vibration-test values and, for Case 5-1A (which is judged to be the most plausible set of model parameters estimated from the earthquake motions), the earthquake value of $k_{x\theta}$ is about ¼ of the vibration-test value. This is similar to the comparisons noted above for the transverse abutment stiffness k_y, and further supports the premise that the MRO experienced significant nonlinear response during the earthquake and that the abutments were an important contributor to this nonlinear behavior. Table 3-4 also shows that the earthquake values of $k_{x\theta}$ are in between the FHWA values for the "piles only" and "piles and footing" cases, indicating that the engineering procedures again have overestimated the contribution of the pile cap to the abutment stiffness.

(c) Rotational Stiffnesses $k_{x\theta}$' and $k_{z\theta}$

Because the identified values of the rotational stiffnesses $k_{x\theta}$' (at the base of the central pier) and $k_{z\theta}$ (at the abutment) are poorly constrained by the recorded earthquake motions, it is difficult to interpret the comparisons of these values with the values estimated using engineering procedures. For example, the $k_{x\theta}$' values shown for the Case 5-1A and 5-4A earthquake results are greater than the range of estimates from the vibration tests or from the FHWA and Novak methods. This is inconsistent with intuition and with the previous trends for k_y and $k_{x\theta}$, which were better constrained by the recorded earthquake motions.

(d) Embankment Stiffness k_{ye}

Table 3-4 does not contain results of engineering estimates of the embankment transverse stiffness k_{ye}, which is not usually included in bridge models for seismic analysis. It is noteworthy that, for the Case 5-1A model (in which the ATC-32 structural parameters are used together with the best estimate value of the embankment mass that is computed using Equation 2-1 of Section 2.2.3), Table 3-2 shows that the value of k_{ye} that was identified from the earthquake motions differed by only 18 percent from the initial estimate value computed from the Wilson and Tan (1990) approach (Equation 2-2 of Section 2.2.3). In addition, as discussed in Section 3.1.1, this identified value of k_{ye} was well constrained by the recorded earthquake motions. However, for the Case 5-4A model in which a larger embankment mass is used, the identified value of k_{ye} also increases substantially (as might be expected) and is not quite as well constrained by the recorded motions.

3.2 Structural Response

3.2.1 Bending Moments and Shear Forces in Structure

To assess the structural response of the MRO during the Imperial Valley Earthquake, we focused on the computed bending moments and shear forces at the following locations within the bridge: (a) the top and bottom of the pier; (b) in the deck adjacent to the abutment end wall; (c) at the midlength of one of the deck spans; and (d) within the flared segment of the deck alongside the solid segment. These results were compiled for a range of different sets of model parameter values that encompass various combinations of structural parameter, embankment mass, and soil spring stiffness values. The selection of each set of parameter values was guided not only by the optimum values obtained from our system identification, but also on the results of our previously described sensitivity studies. As a result, each assumed set of model parameter values led to fits between the recorded motions and the computed model motions that were comparable to those described in Section 3.1.2 and shown in Figures 3-1 and 3-2. In addition, we also included models where we assumed that the abutment's torsional spring stiffness, $k_{x\theta}$, was assumed to be fixed and then pinned, in order to assess how closely the stiffness value identified from the earthquake motions conformed to either of these idealizations.

The resulting matrix of parametric cases for which we computed the structural response is given in Table 3-5. Figures 3-4 to 3-6 provide example time histories of bending moment and shear forces at each of the above indicated locations (for Case 5-1A only), and Table 3-6 provides tabulations of peak values of the demand bending moments and shear forces at these locations and the corresponding demand-capacity ratios (for all of the parametric cases). These tabulations show that the earthquake demand bending moments and shear forces were all well within the MRO's first yield and ultimate capacity values. In this sense, the results are consistent with the excellent performance of the MRO during the Imperial Valley Earthquake. Other trends shown by these tabulations are as follows:

- The maximum demand shear forces and bending moments in the pier are not strongly affected by any of the parametric variations encompassed by Cases 5-1A through 5-1H. Also, the pier's maximum demand forces and moments for these cases are comparable to those obtained from the Case 5-2 model. The pier's shear forces and bending moments from Case 5-1I differ from the other results using the Case 5-1 models. However the Case 5-1I model corresponds to a pinned condition for $k_{x\theta}$, which is not considered to be a realistic value and was assumed only as an extreme lower bound for this particular spring stiffness.

- In the Case 5-1 parametric analyses, the assumed variations in the rotational spring stiffness at the base of the pier $k_{x\theta}$' that are encompassed by Cases 5-1A through 5-1C have a significant effect on the demand moments in the deck at the top of the pier, but not on the other demand moments and shear forces. The variations in the rotational spring stiffness at the abutment $k_{z\theta}$ that are encompassed by Cases 5-1A, 5-1D, and 5-1E have an important effect on the bending moments all along the deck. The principal effect of the variations in the torsional spring stiffness at the abutment $k_{x\theta}$ (Cases 5-1A, 5-1F, and 5-1G) is in the bending moment in the deck at the top of the central pier. The peak demand shear forces and bending moments computed assuming that $k_{x\theta}$ is fixed (Case 5-1H) are very similar to those obtained using the best estimate value of $k_{x\theta}$ (Case 5-1A).

- The use of gross section properties (Case 5-2) rather than the ATC-32 recommended properties (Case 5-1A) leads to substantial increases in the deck's demand moments along the midlength of its spans and above the central pier. The use of cracked section properties (Case 5-3) leads to a large increase in the demand bending moment and shear force at the end of the deck, and a sharp reduction in the deck's bending moment and shear force at the top of the pier.

- When the embankment mass is doubled, its effect can be seen by comparing the results from Cases 5-4A and 5-1A. These comparisons show that this doubling of the embankment mass reduces the bending moments at the top and bottom of the pier, substantially increases the bending moment at the end of the deck (due to the much larger value of $k_{z\theta}$ that was identified for the Case 5-4A model), and reduces the deck's bending moments at the midlength of each span and above the central pier.

- In the Case 5-4 parametric analyses, the variations in the values of the rotational spring at the base of the pier, $k_{x\theta}$', that are encompassed by Cases 5-4A through 5-4C have a particularly large effect when $k_{x\theta}$' is assumed to vanish (Case 5-4C). This assumption leads to a substantial increase (relative to Cases 5-4A and 5-4B) in the deck's demand bending moment and shear force at its end and at the midlength of its span, as well as an increase in the deck's bending moment at the top of the pier. This increased mass also causes a reduction in the shear forces along the pier and in the deck above the central pier. When the rotational spring at the abutment, $k_{z\theta}$, is reduced from a fixed to a pinned condition (Cases 5-4A, -D, and -E), the bending moments along the length of the deck are substantially increased and the bending moment at the end of the deck vanishes. The variations in the abutment's torsional spring stiffness, $k_{x\theta}$, that are encompassed by Cases 5-4A, -D, and -E affect the deck's demand bending moment and shear force above the central pier, and its shear force at the midlength of the span.

3.2.2 Abutment and Central Pier Foundation Spring Forces and Moments

An important element of our seismic analysis of the MRO is our assessment of the earthquake demands and capacities of the pile elements that support the abutments and the central pier. The input to our analysis procedure for the piles (see Sec. 2.5) consists of peak forces and/or moments in the various soil springs at the abutment and the base of the central pier, together with the maximum transverse shear force at the base of the pier (since our model does not include a transverse soil spring at that location). For this reason, we have tabulated these peak forces and moments from each of the parametric cases (Table 3-7), and have also provided representative time histories of these quantities from Case 5-1A only (Fig.3-7). Trends observed from our review of these tabulated results are as follows:

- The parametric variations encompassed by Cases 5-1A through 5-1G typically do not have significant effects on the maximum demand forces and moments in the soil springs. The only exception to this trend is the maximum moments in the rotational spring $k_{z\theta}$ at the abutment, which show large variations because of the large range in stiffnesses that was assumed for this spring. However, this large range of assumed stiffnesses for the $k_{z\theta}$ spring (which reflects the poor constraint of the stiffness value for this spring by the array of recorded earthquake motions at the MRO) do not lead to significant variations in any of the other spring forces and moments. In addition, the maximum spring forces and moments computed assuming that $k_{x\theta}$ is fixed (Case 5-1H) are very similar to those obtained using the best estimate value of $k_{x\theta}$ (Case 5-1A).

- The use of gross section properties for the structure (Case 5-2) rather than the ATC-32 properties results in maximum spring forces and moments that are typically comparable to those observed from Case 5-1A. The only exception to this trend are the maximum moments in the rotational spring $k_{x\theta}$' at the base of the central pier, which are about 20 percent lower for Case 5-2 than for Case 5-1A. This is due to the much lower value of the optimum value of the stiffness for this spring that was identified for Case 5-2 (see Table 3-2).

- The use of cracked section properties (Case 5-3) leads to a maximum demand force in the transverse abutment spring k_y that is somewhat larger than for Cases 5-1A through H and 5-2. In addition, because the system identification for Case 5-3 led to an optimum model in which $k_{z\theta}$ was fixed against rotations, the moment in the rotational abutment spring $k_{z\theta}$ is much larger for Case 5-3 than for Cases 5-D and 5-1E (for which finite nonzero values of $k_{z\theta}$ were used. The maximum force in the embankment spring k_{ye} is comparable for Cases 5-1A, 5-2, and Case 5-3, and the values of the moments in the torsional spring at the abutment ($k_{x\theta}$) and the rocking spring at the base of the pier ($k_{x\theta}$') are smaller for Case 5-3A.

- When the embankment mass is doubled (Case 5-4A), the largest overall effect (relative to Case 5-1A) is an increase in the maximum force in the embankment spring k_y by a factor that approaches 2.0. Among the parametric variations encompassed by Cases 5-4A through 5-4G, the variation that has the largest overall effect on the spring forces and moments is Case 5-4C in which the rotational spring $k_{x\theta}$' at the base of the pier is set to 0.0. This leads to: (a) a marked increase in the maximum force in the transverse abutment spring k_y and in the maximum moment in the abutment rotational spring $k_{z\theta}$; and (b) a substantial reduction in the maximum moment in the abutment rotational spring $k_{x\theta}$ and in the maximum shear force in the base of the central pier (relative to the corresponding demands for the other parametric cases under Case 5-4).

3.3 Pile Foundation Analysis

3.3.1 Input Foundation Loads

The foundation spring forces and moments discussed in Section 3.2.2 and the results from dynamic and static analysis for the MRO's vertical response that is presented below were used to select the input foundation loads for the pile foundation analysis.

(a) Dynamic Shear Forces, Overturning Moments, and Torsional Moments

Time histories of the transverse shear forces (F_y), overturning moments (M_x), and torsional moments (M_z) in the abutment, as well as the transverse shear force (F_y') and overturning moment (M_x') at the base of the central pier were computed from the dynamic analyses as summarized in Section 3.2.2. These time histories revealed that the maximum positive and maximum negative values of these quantities all occur at either 4.4 or 5.4 sec (Fig. 3-7). Representative values of these quantities were selected from Table 3-7 for the pile foundation analyses and are listed in Table 3-8. The values of F_y, F_y', M_x, and M_x' that are shown in Table 3-8 were obtained from the results for Case 5-1A, and the value shown for M_z was obtained from Case 5-D.

(b) Dynamic and Static Vertical Loads

Dynamic and static vertical loads at the abutment and pier foundations were also

computed for input into our pile foundation analyses. The dynamic vertical loads were calculated by analyzing a simplified model of the MRO using the SAP90 structural analysis program. For these calculations, the bridge deck was modeled using elastic beam elements with a bending rigidity (EI_{yy}) that was computed from the closed form solution for the natural frequency of the first symmetric mode of a two-span beam with fixed supports (Clough and Penzien, 1975). This natural frequency was specified to be 4.6 Hz, which is the frequency identified for the MRO's first symmetric vertical mode from application of MODE-ID to the recorded earthquake motions. The central pier was modeled using elastic beam elements whose axial rigidity (EA) was chosen to be the gross section value for the pier. Input motions at the ends of the deck and at the pinned central support were assumed to be the vertical motions recorded at the base of the pier during the earthquake. The damping ratio for all modes of the model was assumed to be 0.052, which is the damping value identified for the first vertical symmetric mode from this same application of MODE-ID.

Although this model is simplified, it is viewed as providing acceptable estimates of the dynamic loads at the MRO's foundations for purposes of estimating vertical loads for these pile foundation analyses. For example, we used fixed-support conditions at the abutments because this led to a reasonable estimate of the maximum vertical acceleration recorded at the midspan of the MRO during the earthquake, whereas the assumption of pinned support conditions (which was also considered as a possibility for this analysis) did not. Nevertheless, we found that analyses of the MRO's vertical response using both support conditions led to dynamic vertical loads at the abutment and central pier that were within about 20 percent; such differences are considered to be acceptable for purposes of this analysis. In addition, our use of the vertical motions recorded at the base of the central pier as input at the abutments as well as at the central support was based on our observation that these motions were not very different from the vertical motions recorded at the MRO's abutments (Werner et. al., 1987); therefore, the choice of whether to use the vertical motions recorded at the abutments or at the base of the central pier is not critical for this analysis. (It is noted that our use of a single input motion time history rather than multiple support motions was necessitated by the fact that the SAP90 structural analysis program cannot easily accommodate multiple support motions.)

Two sets of dynamic vertical loads, (denoted as F_z and F_z' for the abutments and central pier support respectively), that were obtained from our SAP90 analyses are shown in Table 3-8. One set corresponds to the loads that were computed at times of 4.4 and 5.4 sec., which are the times when the foundation shear forces, overturning moments, and torsional moments (F_y, M_x, M_z, F_y', and M_x') are largest. The second set contains the maximum positive and maximum negative values of F_z and F_z', and the times at which they occur. It is noted that the second set of force values are about 5-to-10 times larger than the first set.

(c) Static Vertical Loads

A static analysis of the MRO to compute dead loads at the base of each foundation support was carried out using SAP90. The model used for the static analysis differed from that used for the dynamic analysis in that vertical springs were included at the abutments and at the

base of the central pier. The values of these vertical spring stiffnesses (6.5×10^4 kip/ft at the abutments and 3.5×10^5 kip/ft at the base of the central pier) were estimated using the modified FHWA procedure that was recommended in D & M (1992). To be consistent with our assumed earthquake-induced (i.e., large-strain) values for the other foundation spring stiffnesses, we used soil shear moduli for these calculations that were 50 percent of the low-strain shear moduli obtained from our in situ soil tests. The results of limited parametric analyses indicated that the dead load distribution was not sensitive to reasonable variations in the foundation stiffness values.

3.3.2 Analysis Results

The loads listed in Table 3-8 were applied to nonlinear models of the abutment and central pier foundations. In these models, the loads were applied statically and were assumed to be resisted by (a) the piles and adjacent soil, (b) the soil supporting the pile caps, and (c) the soil against the sides of the caps. Usually, the latter two sources of load resistance are neglected. However, preliminary analysis revealed that the piles by themselves were not capable of resisting the full transverse demand load, F_y. Therefore, a decision was made to include the stiffness contribution provided by the soil around the pile cap. To be consistent with the approach used to estimate the abutment foundation stiffnesses, the contributions from the abutment walls (shearing resistance) and the wing walls were neglected. As noted in Section 2.5.2, the abutment wall shearing resistance is usually neglected, while the passive resistance of the soil against the wing walls is considered in Caltrans' current seismic evaluation procedures. Observations regarding the load distribution and capacities of the various elements comprising the MRO abutment foundation system are presented in Section 3.4.

A detailed description of the nonlinear model is presented in Appendix B and is summarized in this section. An approximate composite model was developed which considers the nonlinear load-deflection behavior of the piles, the pile cap acting as a footing, and the passive resistance of the soils against the side of the footing as separate and independent analyses (i.e., the complete static interaction of the various components that comprise the foundation system was neglected). The nonlinear force-deflection relationships for the piles were developed using the modified FHWA (1986) approach recommended by D & M (1992). Similar nonlinear relationships were developed for vertical and transverse loading of the footing (pile cap) by (a) computing the ultimate shearing and bearing capacities according to procedures in NAVFAC (1986); (b) computing an initial tangent stiffness from the embedded footing foundation stiffness values; and (c) selecting a hyperbolic curve with these initial tangent and ultimate capacity values. Because the footings are embedded, their ultimate shear resistance was approximated as the sum of the shear capacity of a surface footing and the ultimate passive resistance of the soil against the sides of the footing.

The solution procedure for the displacements of the nonlinear model due to the applied loads is described in Appendix B, and the results from the application of this procedure are presented in Table 3-9. This table shows that the transverse displacement computed for the abutment pile cap was 0.00069 ft., which was much smaller than the deflection of 0.033 ft. obtained by dividing the transverse load in Table 3-8 ($F_y = +2.4 \times 10^2$ kips) by the best estimate

of the abutment transverse stiffness (k_y = 7.3 x 10^3 kip/ft) that was identified from the MRO's recorded earthquake motions (Case 5-1A of Table 3-5). Because the displacements estimated with the model were too small, the above calculations were repeated for the pile group only. The resulting displacements (Table 3-9) were greater than 0.2 ft. because the pile-group capacity was exceeded. The above results suggest that (1) the piles were not the only elements carrying transverse load; and (2) the contribution of the pile cap is not as great as predicted by the nonlinear model.

The transverse displacements computed at the base of the central pier (Table 3-9) are qualitatively similar to the abutment displacements. The pier foundation displacements are small unless the contribution of the pile cap is ignored, which leads to large displacements in excess of 0.2 ft.

An indication of whether the transverse displacement computed by the nonlinear model is reasonable for the central pier was obtained by comparing this displacement (given as 0.0097 ft. in Table 3-9) with an estimate of the displacement that occurred during the earthquake. A lower bound estimate of this earthquake-induced displacement (0.0063 ft.) was computed by dividing the maximum shear force at the base of the central pier (F_y' = 3.8 x 10^2 kips in Table 3-8) by a representative stiffness computed from the forced vibration test data (k_y' = 6.0 x 10^4 kip/ft, from Crouse, 1992). The actual value of k_y' was presumably smaller during the earthquake, perhaps by as much as a factor of 2 less than the vibration-test value based on the estimated 50 percent reduction in soil shear modulus during the earthquake (Crouse and Hushmand, 1990). Thus, the agreement between the computed model displacement and the estimated earthquake-induced displacement at the central pier foundation is judged to be reasonable.

3.4 Assessment of Seismic Design Procedures

The results presented earlier in this chapter indicate that the earthquake demand bending moments and shear forces for the MRO's central pier and deck are well within the first yield and ultimate capacity values. These findings are consistent with the observed seismic performance of the MRO, which was undamaged from the Imperial Valley Earthquake motions despite the intense shaking recorded on the bridge (with peak accelerations in excess of 0.5 g).

3.4.1 Original Design

To use our dynamic analysis results to assess Caltrans' seismic design procedures for SBOs, we first compared the total lateral static seismic design force computed using Caltrans' procedures in effect when the MRO was designed vs. the time history of the total lateral force computed from our dynamic analysis for Case 5-1A. This total force from our dynamic analysis was computed as the time-dependent sum of the spring forces in the k_y spring at each abutment plus the shear force at the base of the central pier. We have not been able to obtain the actual design calculations for the MRO; however, the summary of Caltrans' past seismic design procedures given in the report by the Governor's Board of Inquiry following the 1989 Loma

Prieta Earthquake (Housner, 1990) indicated procedures dated 1965 that were in effect when the MRO was designed in 1968. These correspond to an equivalent static force method that was based in part on the lateral force requirements for buildings of the Structural Engineers Association of California.

When applied to the MRO, the above procedure leads to a maximum total earthquake force (to be applied horizontally at the center of gravity of the structure) that is 0.1 x the weight of the structure. Figure 3-8 shows that this seismic design force level is well below the total dynamic forces computed from our seismic analysis. Therefore, it is likely that the MRO's seismic resistance and capacity were probably controlled by the its design against dead loads and traffic loads, rather than against the low seismic design forces that were in effect when the MRO was designed. Based on these considerations, the excellent performance of the MRO during the Imperial Valley Earthquake was most likely due to its simple configuration (e.g., unskewed, monolithic abutments,etc.) and to its detailing. Regarding the detailing of the MRO's central pier, most bridge columns designed by Caltrans before the 1971 San Fernando Earthquake contained very little transverse shear reinforcement; this reinforcement typically consisted of #4 transverse peripheral hoops spaced at 12-inches to 18-inches on center, regardless of column size and area of longitudinal steel reinforcement (Roberts, 1991). However, the transverse steel reinforcement for the MRO's central pier was much more extensive, consisting of #5 spirals at a 5-inch pitch (see Appendix A). This undoubtedly was an important contributor to the MRO's excellent seismic performance during the Imperial Valley Earthquake. However, other elements of the MRO's detailing are substandard according to current design practice, such as: (a) insufficient development length of the #18 longitudinal steel from the central pier where it extends into the deck; (b) the lack of top steel in the central pier footing; and (c) the possible lack of a positive connection between the timber piles and the pile caps . Although these deficiencies did not affect the MRO's seismic performance during the Imperial Valley Earthquake, they could conceivably influence the potential for damage of the bridge under stronger and longer durations of shaking.

3.4.2 Current Seismic Design/Retrofit Procedures

(a) Overview

After the 1971 San Fernando Earthquake, Caltrans substantially extended their seismic design provisions to include ductile detailing requirements, and new seismic design criteria that incorporated: (a) the use of ARS spectra with a damping ratio of 0.05 for defining design spectra in terms of the maximum expected rock acceleration (A), the normalized rock response (R) and the soil amplification spectral ratio (S); and (b) the use of dynamic analysis together with period-dependent ductility and risk reduction factors (Z factors) to obtain corresponding seismic design forces. Over the years since 1971, new retrofit provisions were also developed and implemented that included the placement of cable restrainers to prevent separation at deck joints, and the strengthening of concrete columns and piers. Since the 1989 Loma Prieta Earthquake, Caltrans has been implementing a major seismic research program directed toward expansion and enhancement of their current procedures for the seismic design and retrofit of bridge structures,

abutments, and foundations. Revisions to Caltrans' current procedures based on current knowledge and on available results from their research program are being developed under the Caltrans-sponsored ATC-32 project (ATC, 1992). The evolution of Caltrans' seismic design and retrofit procedures since 1971 has been summarized by Roberts (1991).

Caltrans' current procedures for the seismic evaluation of short bridge overcrossing (SBO) structures are documented in their current seismic design standards (Caltrans, 1990), and in their recent Interim Memo to Designers 20-4 for seismic retrofit (Caltrans, 1992). This documentation indicates that the current procedure consists of the iterative approach shown in Figure 3-9 for assessing the SBO's seismic response to both longitudinal and transverse input motions represented by an appropriate ARS spectrum. To analyze the bridge's response to each direction of input motions, an elastic model of the bridge is developed which includes an initial estimate of the abutment's longitudinal or transverse stiffness (as discussed further in Section 3.4.2(b) below). Gross section values of the bending and torsional rigidities are used to model the bridge's structural elements, and are based on a preliminary design configuration (for a new bridge) or on the actual bridge configuration (for an existing bridge). The dynamic analysis of the SBO is then implemented, the bridge's responses to the longitudinal and transverse input motions are combined according to Caltrans procedures, and the computed abutment spring force is compared to a limiting value obtained as described below in Section 3.4.2(b). If this limiting value is exceeded, the abutment spring stiffness is reduced arbitrarily and the above process is repeated until the abutment force computed from the dynamic analysis is less than the limiting value. When this occurs, the structure's demand bending moments and shear forces are compared to capacity values, and design revision (for a new bridge) or retrofit (of an existing bridge) is required if the demand to capacity ratios exceed limits specified by Caltrans. Design revision or retrofit is also required if the computed abutment displacement exceeds 0.2 ft.

(b) Assessment of Caltrans Modeling Procedure for SBOs

Table 3-10 provides a comparison of MRO model parameters developed using Caltrans' current procedures vs. those identified from the Imperial Valley Earthquake motions for Case 5-1A. In this, two different estimates of the abutment translational spring stiffness have been computed under the Caltrans procedure, corresponding to two different approaches used by Caltrans to estimate the initial value of this stiffness parameter. Both approaches consider only (a) the passive resistance of the backfill soil against the wing wall; and (b) the piles supporting the abutment. The approaches differ only in the manner in which the passive resistance is considered. The first approach (termed Method A) is documented in Caltrans Bridge Design Aids 14-1 entitled "Dynamic Model Assumptions and Adjustments" (dated October 1989). It computes the passive resistance at the wing wall as the product of a unit stiffness of 200 kips/in per foot of length of the wall times the effective length of the wing wall (computed as 2/3 x the ratio of the area to the height of the wall). The second approach (Method B) has recently been developed to reduce the number of iterations in the seismic evaluation process. It computes the passive resistance as (7.7 ksf x effective wing wall area)/0.2 ft., where 7.7 ksf is an assumed limiting passive resistance of the soil, the effective wing wall area is taken to be 2/3 of the total area, and 0.2 ft. is the maximum allowable displacement assumed by Caltrans. In both methods,

both wing walls contribute to the total abutment stiffness, but not equally; i.e., the stiffness estimated for one wing wall is not reduced whereas the stiffness estimated for the other wing wall is multiplied by 1/3. For each method, the initial lateral stiffness contribution of each pile is assumed to be 40 kip/in., regardless of pile size and materials and the surrounding soil conditions. Finally, both methods are based on the same approach for computing the limiting value of the abutment spring force. This limiting force is computed as 7.7 ksf x [(2/3 of the area of the wing wall assumed to be fully effective) + (2/3 x 1/3 of the area of the wing wall that is assumed to be partially effective)].

Table 3-10 shows that the model parameters estimated using the Caltrans procedures differ from those of Case 5-1A in the following ways: (a) the Caltrans model of the structural elements is based on the use of gross section properties to compute the bending stiffnesses, whereas Case 5-1A incorporates the ATC-32 recommendations to reduce these stiffnesses to account for cracking of the concrete; (b) the Caltrans method neglects the mass of the abutment walls and pile cap as well as the rotational inertia of the structure, abutment, and central pier foundation, whereas the Case 5-1A model has included these inertial properties; (c) the Method A value of the abutment lateral stiffness (k_y) is much larger than that of Case 5-1A, while the Method B value of k_y is comparable to the Case 5-1A value; and (d) the Case 5-1A model includes the embankment's effective mass and transverse shear stiffness whereas the Caltrans model does not. It is noted that the values of the abutment rotational stiffnesses $k_{x\theta}$ and $k_{z\theta}$ that were identified from the MRO's earthquake motions for the Case 5-1A model compare closely to the fixed and pinned assumptions for these stiffnesses that are currently used by Caltrans. In addition, the identified value of the central pier's rotational stiffness $k_{x\theta}$' for the Case 5-1A model was found to be comparable to a fixed condition, which is also consistent with Caltrans' current modeling assumptions. However, as previously discussed, these identified values of $k_{z\theta}$ and $k_{x\theta}$' were not well constrained by the MRO's recorded earthquake motions.

To further compare the Caltrans and the Case 5-1A models, Table 3-11 shows the normal mode parameters for the MRO's first transverse mode that is computed using each model. This table shows that: (a) the natural frequency and mode shapes computed using the Caltrans Method A model do not compare well to those of Case 5-1A; (b) the natural frequency computed using the Caltrans Method B model is about 30 percent higher than that of Case 5-1A, whereas the mode shape computed using the Method B model is nearly identical to that of Case 5-1A; and (c) the damping ratio of 0.05 that is used for the Caltrans models is much lower than the damping ratio of 0.26 identified from the MRO's earthquake motions for the Case 5-1A model.

As a final comparison, we subjected the Caltrans models to the MRO's recorded earthquake motions at the base of the central pier (which are the same input motions used to compute the MRO's seismic response using the Case 5-1A model), and then compared the resulting seismic response results to those obtained using the Case 5-1A model. These comparisons for the same set of input motions are intended to show how differences between the Case 5-1A model and the Caltrans modeling procedures affect the MRO's computed seismic response. The results of the comparisons (Table 3-12) show that Caltrans' Method A model leads to peak seismic responses that are substantially different (and typically lower) than those

obtained using the Case 5-1A model. The Method B model leads to maximum responses that are generally comparable to those from the Case 5-1A model (except for the abutment transverse spring force, transverse displacement, and overturning moment which are 25 to 42 percent higher for Case 5-1A). It is noted that the maximum transverse spring forces shown in Table 3-12 for both Caltrans models are below the limiting force capacity (computed to be 1209 kips); therefore, no iteration to reduce the abutment forces was required for either model. Also, to explain why the maximum seismic responses computed from the two Caltrans models are typically lower than or comparable to those from the Case 5-1A model despite the much lower damping ratio used in the Caltrans models, we plotted the 5-percent damped and 26-percent damped response spectra for the transverse input motions to the seismic analyses (i.e., the MRO's transverse earthquake motions recorded at the base of its central pier). This plot (Fig. 3-10) shows that the higher natural frequencies of the two Caltrans models (4.1 and 3.1 Hz) vs. that of the Case 5-1A model (2.6 Hz) will tend to reduce the computed seismic response and to thereby offset the effect of the smaller damping ratio that is used in the Caltrans models.

(c) Abutment Modeling Considerations

Although Caltrans' seismic evaluation procedure for abutments appears reasonable based on the MRO case history, there is some question as to whether their methods to compute foundation stiffnesses and capacities are oversimplified and whether the deflection limit of 0.2 ft is too large. For example, the assumption of a lateral pile capacity of 40 kips regardless of the soil and pile properties is obviously inappropriate for detailed analysis of a pile foundation system. Such detailed analysis were conducted for the MRO abutment piles based on in situ soil properties and timber pile properties extracted from the technical literature. The lateral capacity of each pile was estimated using the BMCOL 76 program and found to be approximately 15-20 kips per pile. Assuming the smaller value of 15 kips, the total capacity of the pile group (7 piles) was on the order of 100 kips. According to Caltrans' evaluation procedure, the wing wall is the only other abutment element that is assumed to resist transverse loads. However, approximate hand calculations show that MRO's wing walls probably could not have absorbed the 150 kips (= 250 kips total abutment load - 100 kips total pile load) that they would have needed to carry if they were the only other lateral load carrying element of the abutment system. Based on (a) the assumption that one wing wall resists the lateral load, (b) the structural drawings of the MRO wing wall that are shown in Appendix A, (c) a concrete strength of $f'_c = 5166$ psi at the time of the earthquake (Table 2-1), and (d) an assumed yield stress of $f_y = 45$ ksi for the reinforcing steel, we estimated that the moment capacity of the wing wall was roughly 1/2 of the maximum demand moment developed during the earthquake. Because the wing walls did not suffer any apparent damage, the applied load was probably much less than 150 kips. This conclusion is not as obvious (and possibly cannot be drawn) if the load was distributed between the two wing walls as suggested by the Caltrans procedure (2/3 and 1/3 distribution), and/or if each pile carried 20 kips of lateral load instead of 15 kips. Despite this uncertainty, the dimensions and materials properties of the MRO's wing wall clearly demonstrate that this element behaves as a flexible plate rather than a rigid retaining wall. This wing wall will certainly fail at loads much smaller than those required to mobilize the full passive resistance of the soil between the wing walls. According to Caltrans' seismic evaluation procedure, this

passive load is approximately 700 kips for one MRO wing wall.

The MRO's wing walls, which have limited capacity based on our analysis, are probably not the primary load-carrying element of the abutment system. Reasonable analytical predictions of the transverse deflection of the MRO abutment during the earthquake were obtained using the model described in Appendix B by allowing the pile-cap/soil system (rather than the wing walls) to carry load in addition to that absorbed by the piles. For friction piles in cohesive soil similar to the backfill of the MRO embankments, it is reasonable to assume that a significant portion of the load is transferred directly from the buried pile cap to the adjacent soil though (a) shearing of the soil in contact with the bottom of the pile cap, and to some extent (b) the passive resistance of the soil against the side of the cap. Also, some fraction of the load is certainly carried by the shearing resistance of the soil against the end wall.

TABLE 3-1
MATRIX OF CASES FOR MODEL PARAMETER IDENTIFICATION

CASE NO.	STRUCTURAL PARAMETERS	EMBANKMENT MASS
5-1	ATC-32 Recommendations: Pier: $EI_{xx} = 0.5\ (EI_{xx})_g$ Deck: $EI_{zz} = 0.75\ (EI_{zz})_g$ $GJ = GJ_g$	Best estimate value computed as described in Section 2.2.3 (Eq 2-1). $m_e = 1.01 \times 10^2$ kip-sec^2/ft
5-2	Gross Section Properties for Pier and Deck.	Same as Case 5-1.
5-3	Cracked Section Properties for Pier and Deck.	Same as Case 5-1.
5-4	Same as Case 5-1.	Twice the embankment mass from Case 5-1: $m_e = 2.02 \times 10^2$ kip-sec^2/ft

Note: Subscript "g" denotes gross section properties. Refer to Table 2-2 for values of bending and torsional rigidities for each segment of deck.

TABLE 3-2
SYSTEM IDENTIFICATION RESULTS

CASE		OPTIMUM VALUES OF $\theta_i^{(K)}$					Measure-of-Fit Parameter $J(\underline{\theta})$
No.	Description	$\theta(k_y)$	$\theta(k_{x\Theta})$	$\theta(k_{z\Theta})$	$\theta(k_{x\Theta}')$	$\theta(k_{ye})$	
5-1A	ATC-32 Structural Parameters. Best Estimate Value of M_e (Eq. 2-1 of Section 2.2.3).	0.73 (0.64 - 0.85)	0.77 (0.39 - 1.41)	0.0 (0.0 - 5.15)	9.14 (1.22 - Fixed)	1.18 (0.99 - 1.38)	0.4166 (0.418)
5-2	Gross Section Properties. Best Estimate Value of M_e.	0.78	0.63	0.0	0.44	1.32	0.4145
5-3	Cracked Section Properties. Best Estimate Value of M_e.	1.07	Fixed	Fixed	0.27	Fixed	0.4260
5-4A	ATC-32 Structural Parameters. Twice the Best Estimate Value of M_e.	0.65 (0.60 - 0.70)	0.36 (0.28 - 0.49)	Fixed (0.05 - Fixed)	Fixed (1.34 - Fixed)	4.09 (2.99 - 6.70)	0.4169 (0.418)

Note: (1) For the i^{th} identified model parameter, $\theta_i^{(K)}$ is defined as:

$$\theta_i^{(K)} = \frac{k_i}{\overline{k_i}}$$

where k_i is the identified value of the parameter and $\overline{k}_i$ is the initial estimate value. The initial estimate values used for the five spring stiffnesses identified for the MRO model are as follows:

$\overline{k}_y = 1.0 \times 10^4$ kip/ft $\quad \overline{k}_{z\theta} = 7.2 \times 10^6$ kip-ft/rad $\quad \overline{k}_{ye} = 7.6 \times 10^4$ kip/ft

$\overline{k}_{x\theta} = 6.2 \times 10^6$ kip-ft/rad $\quad \overline{k}_{x\theta}' = 5.0 \times 10^6$ kip-ft/rad

(2) Ranges of soil spring stiffness values shown in parentheses for Cases 5-1 and 5-4 correspond to results from sensitivity studies described in Section 2.3.2.

TABLE 3-3
PARAMETERS FOR FIRST TRANSVERSE MODE
COMPUTED FROM FINITE ELEMENT MODEL OF MRO

Case		Natural Frequency (hz)	Damping Ratio	Mode Shape Amplitudes at Instrument Locations					
				Transverse Translation				Rotation About X-Axis	
No.	Description			ϕ_{ye}	ϕ_{ya}	$\phi_{y\text{-}ms}$	$\phi_{y\text{-}cp}$	$\phi_{\theta\text{-}ms}$	$\phi_{\theta\text{-}cp}$
5-1A	ATC-32 Structural Properties. Best Estimate Value of M_e (Eq 2-1 of Section 2.2.3).	2.63	0.26	0.074	0.699	0.937	1.000	-0.027	-0.039
5-2	Gross Section Properties. Best Estimate Value of M_e.	2.62	0.25	0.069	0.707	0.932	1.000	-0.028	-0.039
5-3	Cracked Section Properties. Best Estimate Value of M_e.	2.53	0.19	0.001	0.511	0.814	1.000	-0.037	-0.054
5-4A	ATC-32 Structural Properties. Twice the Best Estimate Value of M_e.	2.61	0.24	0.022	0.904	0.975	1.000	-0.038	-0.048

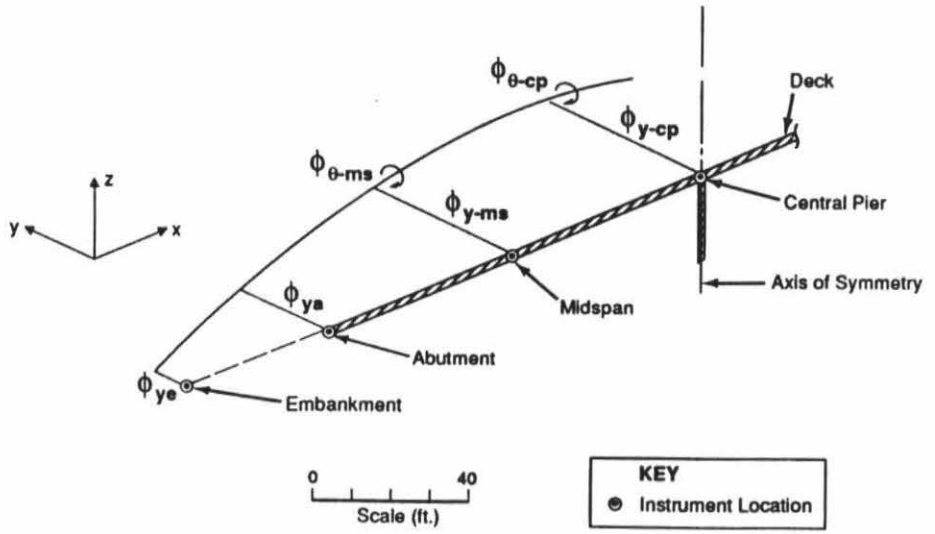

TABLE 3-4
COMPARISON OF SOIL SPRING STIFFNESSES ESTIMATED FROM ENGINEERING PROCEDURES, RECORDED EARTHQUAKE MOTIONS, AND FORCED VIBRATION TEST DATA

Element		Engineering Procedures					System Identification Results from Recorded Earthquake Motions						Forced Vibration Tests
		Piles Only		Piles and Footing		Piles & Footing Side	Case 5-1A		Case 5-4A		Case 5-2	Case 5-3	Range of Estimates from Table 1 of Crouse (1992)
		FHWA (1986)	Novak et. al (1991)	FHWA (1986)	Novak et. al (1991)	Novak et. al (1991)	Best Estimate	Range from Sensitivity Evaluation	Best Estimate	Range from Sensitivity Evaluation	Best Estimate	Best Estimate	
Pier	$k_{x\theta}'$ (kip-ft) rad	$1.6\times10_{6}$	5.1×10^{6}	$4.6\times10_{6}$	8.1×10^{6}	6.6×10^{6}	4.6×10^{7}	6.1×10^{6} to Fixed	Fixed	6.7×10^{6} to Fixed	2.2×10^{6}	1.4×10^{6}	$(2.9 \text{ to } 9.0)\times10^{6}$
Abutment	k_{y} (kip/ft)	$1.3\times10_{3}$	2.0×10^{4}	$3.6\times10_{4}$	4.6×10^{4}	2.7×10^{4}	7.3×10^{3}	$(6.4 - 8.5)\times10^{3}$	6.5×10^{3}	$(6.0 - 7.0)\times10^{3}$	7.8×10^{3}	10.7×10^{3}	$(2.5 \text{ to } 3.8)\times10^{4}$
	$k_{z\theta}$ (kip-ft) rad	$1.5\times10_{5}$	2.3×10^{6}	$5.7\times10_{6}$	7.4×10^{6}	4.5×10^{6}	0.0	$(0.0 - 3.7)\times10^{6}$	Fixed	3.6×10^{5} to Fixed	0.0	Fixed	$(8.0 \text{ to } 36.0)\times10^{6}$
	$k_{x\theta}$ (kip-ft) rad (top of pile cap)	$1.0\times10_{6}$	$1.5\times10a^{7}$	$5.7\times10_{6}$	1.8×10^{7}	1.5×10^{7}	5.3×10^{6}	$(2.9 - 9.4)\times10^{6}$	2.7×10^{6}	$(2.2 - 3.6)\times10^{6}$	4.5×10^{6}	Fixed	$(1.4 \text{ to } 2.6)\times10^{7}$
	$k_{x\theta}$ (kip-ft) rad (mid-depth of deck)	$9.0\times10_{5}$	1.4×10^{7}	$5.4\times10_{6}$	1.5×10^{7}	1.3×10^{7}	4.7×10^{6}	$(2.4 - 8.7)\times10^{6}$	2.2×10^{6}	$(1.7 - 3.0)\times10^{6}$	3.9×10^{6}	Fixed	---

Note: (1) $k'_{x\theta}$ for central pier computed at top of pile cap.

(2) Values of $k_{x\theta}$ for abutments that are computed at top of pile cap and at mid-depth of deck are related through rigid body transformation.

TABLE 3-5
CASES TO INVESTIGATE EFFECTS OF MODEL PARAMETER SENSITIVITY ON COMPUTED FORCES AND MOMENTS

Case		Values of $\theta_i^{(K)}$				
No.	Description	$\theta(k_y)$	$\theta(k_{x\theta})$	$\theta(k_{z\theta})$	$\theta(k_{x\theta}')$	$\theta(k_{ye})$
5-1	ATC-32 Structural Parameters. Best Estimate Value of M_e (Eq 2-1).					
	5-1A: Optimum $\theta_i^{(K)}$	0.73	0.77	0.0	9.14	1.18
	5-1B: Original Estimate of $k_{x\theta}'$	0.73	0.77	0.0	1.00	1.18
	5-1C: Fixed Value of $k_{x\theta}'$	0.73	0.77	0.0	Fixed	1.18
	5-1D: Original Estimate of $k_{z\theta}$	0.73	0.77	1.0	9.14	1.18
	5-1E: Increased Value of $k_{z\theta}$	0.73	0.77	5.2	9.14	1.18
	5-1F: Reduced Value of $k_{x\theta}$	0.73	0.39	0.0	9.14	1.18
	5-1G: Increased Value of $k_{x\theta}$	0.73	1.41	0.0	9.14	1.18
	5-1H: Fixed Value of $k_{x\theta}$	0.73	Fixed	0.0	9.14	1.18
	5-1I: Pinned value of $k_{x\theta}$	0.73	0.0	0.0	9.14	1.18
5-2	Gross Section Properties. Best Estimate Value of M_e.					
	Optimum $\theta_i^{(K)}$	0.78	0.63	0.0	0.44	1.32
5-3	Cracked Section Properties. Best Estimate Value of M_e.					
	Optimum $\theta_i^{(K)}$	1.07	Fixed	Fixed	0.27	Fixed
5-4	ATC-32 Structural Parameters. 2 × Best Estimate Value of M_e.					
	5-4A: Optimum $\theta_i^{(k)}$	0.65	0.36	Fixed	Fixed	4.10
	5-4B: Original Estimate of $k_{x\theta}'$	0.65	0.36	Fixed	1.00	4.10
	5-4C: Pinned Value of $k_{x\theta}'$	0.65	0.36	Fixed	0.0	4.10
	5-4D: Original Estimate of $k_{z\theta}$	0.65	0.36	1.00	Fixed	4.10
	5-4E: Pinned Value of $k_{z\theta}$	0.65	0.36	0.0	Fixed	4.10
	5-4F: Reduced Value of $k_{x\theta}$	0.65	0.28	Fixed	Fixed	4.10
	5-4G: Increased Value of $k_{x\theta}$	0.65	0.49	Fixed	Fixed	4.10

Note: As noted in Table 3-2, $\theta_i^{(K)}$ for the i^{th} identified model parameter is defined as:

$$\theta_i^{(K)} = \frac{k_i}{\overline{k_i}}$$

where k_i is the identified value of the parameter and $\overline{k}_i$ is the initial estimate value. (See Table 3-2 for the $\overline{k}_i$ values used for each parameter.)

TABLE 3-6
MAXIMUM MOMENT AND SHEAR IN DECK AND CENTRAL PIER

CASE	Central Pier				Deck (end)		Deck (mid-span)		Deck (top of pier)	
	Mtop (k-ft)	Mbot (k-ft)	Vtop (kips)	Vbot (kips)	Mrz (k-ft)	Vy (kips)	Mrz (k-ft)	Vy (kips)	Mrz (k-ft)	Vy (kips)
5-1A	3040.00	4775.00	377.40	385.30	18.14	164.60	5249.00	20.45	1860.00	139.30
D/Y	0.52	0.82	---	---	0.00	---	0.11	---	0.03	---
D/C	0.39	0.61	0.41	0.42	0.00	0.09	0.07	0.01	0.02	0.08
5-1B	3136.00	4216.00	354.40	363.10	19.96	182.40	6135.00	19.14	3473.00	126.60
D/Y	0.54	0.72	---	---	0.00	---	0.13	---	0.05	---
D/C	0.40	0.53	0.38	0.39	0.00	0.10	0.08	0.01	0.03	0.07
5-1C	3031.00	4842.00	380.10	387.80	17.90	162.20	5131.00	21.02	1654.00	141.10
D/Y	0.52	0.83	---	---	0.00	---	0.11	---	0.02	---
D/C	0.38	0.61	0.41	0.42	0.00	0.09	0.07	0.01	0.02	0.08
5-1D	2975.00	4657.00	368.30	376.20	1068.00	168.50	4348.00	19.09	1418.00	135.40
D/Y	0.51	0.80	---	---	0.04	---	0.09	---	0.02	---
D/C	0.38	0.59	0.40	0.41	0.03	0.09	0.06	0.01	0.01	0.07
5-1E	2872.00	4494.00	355.40	363.40	2766.00	174.00	2918.00	17.33	1189.00	129.10
D/Y	0.49	0.77	---	---	0.09	---	0.06	---	0.02	---
D/C	0.36	0.57	0.38	0.39	0.07	0.10	0.04	0.01	0.01	0.07
5-1F	2669.00	4717.00	356.50	364.20	19.21	173.10	5706.00	19.83	2843.00	129.40
D/Y	0.46	0.81	---	---	0.00	---	0.12	---	0.04	---
D/C	0.34	0.60	0.39	0.39	0.00	0.09	0.08	0.01	0.03	0.07
5-1G	3220.00	4783.00	386.70	394.40	17.29	158.90	4944.00	18.58	1295.00	144.70
D/Y	0.55	0.82	---	---	0.00	---	0.11	---	0.02	---
D/C	0.41	0.61	0.42	0.43	0.00	0.09	0.07	0.01	0.01	0.08
5-1H	3453.00	4818.00	399.60	407.60	16.37	152.60	4607.00	22.30	1286.00	150.80
D/Y	0.59	0.83	---	---	0.00	---	0.10	---	0.02	---
D/C	0.44	0.61	0.43	0.44	0.00	0.08	0.06	0.01	0.01	0.08
5-1I	2525.00	3663.00	242.90	248.50	17.39	231.60	9554.00	112.30	12730.00	98.88
D/Y	0.43	0.63	---	---	0.00	---	0.20	---	0.18	---
D/C	0.32	0.46	0.26	0.27	0.00	0.13	0.13	0.06	0.12	0.05
5-2	3085.00	3783.00	330.20	339.30	16.96	191.80	6625.00	21.13	4454.00	115.40
D/Y	0.53	0.65	---	---	0.00	---	0.14	---	0.06	---
D/C	0.39	0.48	0.36	0.37	0.00	0.11	0.09	0.01	0.04	0.06
5-3	2314.00	1999.00	204.70	215.50	7784.00	243.20	1708.00	86.77	2845.00	48.64
D/Y	0.40	0.34	---	---	0.26	---	0.04	---	0.04	---
D/C	0.29	0.25	0.22	0.23	0.18	0.13	0.02	0.05	0.03	0.03
5-4A	2200.00	4054.00	300.80	308.20	4837.00	187.40	1646.00	23.77	961.20	104.10
D/Y	0.38	0.70	---	---	0.16	---	0.04	---	0.01	---
D/C	0.28	0.51	0.33	0.33	0.11	0.10	0.02	0.01	0.01	0.06
5-4B	2230.00	3458.00	273.30	281.20	5713.00	207.00	1737.00	40.74	852.60	89.06
D/Y	0.38	0.59	---	---	0.19	---	0.04	---	0.01	---
D/C	0.28	0.44	0.30	0.30	0.14	0.11	0.02	0.02	0.01	0.05
5-4C	2317.00	96.52	102.90	113.20	10300.00	304.40	2146.00	134.40	5560.00	10.73
D/Y	0.40	0.02	---	---	0.34	---	0.05	---	0.08	---
D/C	0.29	0.01	0.11	0.12	0.24	0.17	0.03	0.07	0.05	0.01
5-4D	2400.00	4437.00	329.90	337.20	1200.00	174.90	4668.00	18.15	2233.00	117.60
D/Y	0.41	0.76	---	---	0.04	---	0.10	---	0.03	---
D/C	0.30	0.56	0.36	0.36	0.03	0.10	0.06	0.01	0.02	0.06
5-4E	2471.00	4558.00	339.30	346.60	17.23	170.20	5665.00	19.23	3044.00	122.20
D/Y	0.42	0.78	---	---	0.00	---	0.12	---	0.04	---
D/C	0.31	0.58	0.37	0.37	0.00	0.09	0.08	0.01	0.03	0.07
5-4F	2043.00	4114.00	276.90	303.00	5298.00	199.60	1718.00	31.03	693.60	100.30
D/Y	0.35	0.71	---	---	0.18	---	0.04	---	0.01	---
D/C	0.26	0.52	0.30	0.33	0.13	0.11	0.02	0.02	0.01	0.06
5-4G	2428.00	4215.00	320.70	327.60	4632.00	186.90	1666.00	16.84	941.50	113.20
D/Y	0.42	0.72	---	---	0.15	---	0.04	---	0.01	---
D/C	0.31	0.53	0.35	0.35	0.11	0.10	0.02	0.01	0.01	0.06
Maximum	3453.00	4842.00	399.60	407.60	10300.00	304.40	9554.00	134.40	12730.00	150.80
Minimum	2043.00	96.52	102.90	113.20	16.96	158.90	1646.00	16.84	693.60	10.73
Max. D/Y	0.55	0.83	0.00	0.00	0.34	0.00	0.14	0.00	0.08	0.00
Min. D/Y	0.35	0.02	0.00	0.00	0.00	0.00	0.04	0.00	0.01	0.00
Max. D/C	0.41	0.61	0.42	0.43	0.24	0.17	0.09	0.07	0.05	0.08
Min. D/C	0.26	0.01	0.11	0.12	0.00	0.09	0.02	0.01	0.01	0.01

Note :
D = Demand
C = Capacity in bending or shear (Table 2-3)
Y = Moment at first yield (Table 2-3)

TABLE 3–7
MAXIMUM FORCES AND MOMENTS IN SOIL SPRINGS

CASE	ABUTMENT SPRINGS			BASE OF PIER		EMBANKMENT SPRING
	Fy (kips)	Mx (k–ft)	Mz (k–ft)	Fy' (kips)	Mx' (k–ft)	Fye (kips)
5–1A	−2.11E+02	−2.06E+03	0.00E+00	−3.85E+02	−4.33E+03	−1.21E+03
	2.42E+02	2.46E+03	0.00E+00	3.52E+02	4.78E+03	1.24E+03
5–1B	−2.25E+02	−2.04E+03	0.00E+00	−3.63E+02	−3.79E+03	−1.22E+03
	2.61E+02	2.45E+03	0.00E+00	3.27E+02	4.25E+03	1.26E+03
5–1C	−2.09E+02	−2.06E+03	0.00E+00	−3.88E+02	−4.40E+03	−1.21E+03
	2.40E+02	2.45E+03	0.00E+00	3.56E+02	4.84E+03	1.24E+03
5–1D	−2.15E+02	−2.02E+03	−1.08E+03	−3.76E+02	−4.25E+03	−1.22E+03
	2.47E+02	2.40E+03	8.67E+02	3.46E+02	4.66E+03	1.25E+03
5–1E	−2.22E+02	−1.97E+03	−2.77E+03	−3.63E+02	−4.12E+03	−1.23E+03
	2.55E+02	2.31E+03	2.26E+03	3.36E+02	4.50E+03	1.26E+03
5–1F	−2.16E+02	−1.96E+03	0.00E+00	−3.64E+02	−4.26E+03	−1.21E+03
	2.50E+02	2.39E+03	0.00E+00	3.34E+02	4.72E+03	1.25E+03
5–1G	−2.08E+02	−2.09E+03	0.00E+00	−3.94E+02	−4.35E+03	−1.21E+03
	2.37E+02	2.45E+03	0.00E+00	3.61E+02	4.79E+03	1.24E+03
5–1H	−2.04E+02	−2.18E+03	0.00E+00	−4.08E+02	−4.39E+03	−1.20E+03
	2.31E+02	2.50E+03	0.00E+00	3.72E+02	4.82E+03	1.24E+03
5–1I	−2.95E+02	0.00E+00	0.00E+00	−2.49E+02	−3.67E+03	−1.12E+03
	2.36E+02	0.00E+00	0.00E+00	1.90E+02	3.12E+03	1.30E+03
5–2	−2.33E+02	−2.06E+03	0.00E+00	−3.39E+02	−3.45E+03	−1.23E+03
	2.70E+02	2.47E+03	0.00E+00	3.10E+02	3.85E+03	1.26E+03
5–3	−2.93E+02	−1.43E+03	−7.78E+03	−2.16E+02	−1.78E+03	−1.20E+03
	3.23E+02	1.64E+03	6.86E+03	1.96E+02	1.99E+03	1.30E+03
5–4A	−2.34E+02	−1.69E+03	−4.84E+03	−3.08E+02	−3.76E+03	−2.20E+03
	2.66E+02	2.04E+03	4.04E+03	2.91E+02	4.05E+03	2.37E+03
5–4B	−2.51E+02	−1.64E+03	−5.71E+03	−2.82E+02	−3.19E+03	−2.22E+03
	2.87E+02	1.99E+03	4.79E+03	2.62E+02	3.49E+03	2.38E+03
5–4C	−3.27E+02	−1.34E+03	−1.03E+04	−1.13E+02	0.00E+00	−2.27E+03
	3.86E+02	1.68E+03	8.57E+03	1.04E+02	0.00E+00	2.45E+03
5–4D	−2.21E+02	−1.81E+03	−1.21E+03	−3.37E+02	−4.05E+03	−2.18E+03
	2.51E+02	2.20E+03	9.93E+02	3.13E+02	4.44E+03	2.35E+03
5–4E	−2.16E+02	−1.85E+03	0.00E+00	−3.47E+02	−4.14E+03	−2.17E+03
	2.45E+02	2.25E+03	0.00E+00	3.21E+02	4.56E+03	2.34E+03
5–4F	−2.41E+02	−1.66E+03	−5.30E+03	−3.03E+02	−3.75E+03	−2.21E+03
	2.81E+02	2.06E+03	4.30E+03	2.84E+02	4.11E+03	2.37E+03
5–4G	−2.36E+02	−1.75E+03	−4.63E+03	−3.28E+02	−3.83E+03	−2.21E+03
	2.70E+02	2.11E+03	3.84E+03	3.02E+02	4.22E+03	2.36E+03
Max. Positive	3.86E+02	2.50E+03	8.57E+03	3.72E+02	4.84E+03	2.45E+03
Max. Negative	−3.27E+02	−2.18E+03	−1.03E+04	−4.08E+02	−4.40E+03	−2.27E+03

Note: See following page for spring force and moment notation.

TABLE 3-7 (continued)

Spring Force and Moment Notation is as follows:

Abutment:

F_y = maximum force in transverse spring with stiffness k_y
M_x = maximum moment in rotational spring with stiffness $k_{x\theta}$
M_z = maximum moment in rotational spring with stiffness $k_{z\theta}$

Central Pier Foundation

$F_{y'}$ = maximum shear force at base of pier
M_x' = maximum moment in rotational spring with stiffness $k_{x\theta}'$

Embankment

F_{ye} = maximum force in transverse spring with stiffness k_{ye}

TABLE 3-8
INPUT LOADS FROM DYNAMIC ANALYSIS RESULTS FOR USE IN NONLINEAR FOUNDATION ANALYSES

ELEMENT	LOAD COMPONENT [1]	MAXIMUM VALUE
Abutment	F_y (kips) x 10^2	+2.4 @ 4.4 sec -2.1 @ 5.4 sec
	M_x (kip-ft) x 10^3	+2.5 @ 4.4 sec -2.1 @ 5.4 sec
	M_z (kip-ft) x 10^3	+1.0 @ 5.4 sec -1.0 @ 4.4 sec
	F_z (kip) x 10 (dynamic vertical force @ 4.4 sec and 5.4 sec)	+2.6 @ 4.4 sec +2.6 @ 5.4 sec
	F_z (kip) x 10 (maximum dynamic vertical force)	+15.0 @ 2.64 sec -12.0 @ 3.20 sec
	F_z (kip) x 10^2 (static dead load)	5.8
Central Pier Foundation	F_y' (kip) x 10^2	+3.5 @ 5.4 sec -3.8 @ 4.4 sec
	M_x' (kip-ft) x 10^3	+4.8 @ 4.4 sec -4.3 @ 5.4 sec
	F_z' (kip) x 10 (dynamic vertical force @ 4.4 sec and 5.4 sec)	+3.5 @ 4.4 sec +3.5 @ 5.4 sec
	F_z' (kip x 10) (maximum dynamic vertical force)	28.0 @ 2.64 sec -23.0 @ 3.20 sec
	F_z' (kip) x 10^2 (static dead load)	9.1

Note: (1) F_y, M_x, M_z, F_y', and M_x' notation defined in Table 3-7.

TABLE 3-9
EARTHQUAKE-INDUCED TRANSVERSE DISPLACEMENT OF PILE CAP ESTIMATED FROM NONLINEAR ANALYSIS

FOUNDATION	CONTRIBUTING FOUNDATION ELEMENTS	TRANSVERSE DISPLACEMENT OF PILE CAP (ft)
Abutment	Piles and Pile Cap	6.9×10^{-4}
	Piles Only	>0.2
Central Pier	Piles and Pile Cap	9.7×10^{-3}
	Piles Only	>0.2

TABLE 3-10
COMPARISON OF MRO MODEL PARAMETERS FROM CALTRANS PROCEDURES AND FROM EARTHQUAKE MOTIONS (CASE 5-1A)

Parameter	Caltrans	Case 5-1A
Structural Stiffnesses[1]:		
Deck	EI_g, GJ_g	0.75 EI_g, GJ_g
Central Pier	EI_g	0.5 EI_g
Mass (Translational):		
Structure	Included	Included
Abutments	Neglected	Included
Rotational Moment of Inertia:		
Structure	Neglected	Included
Abutments	Neglected	Included
Abutment Stiffnesses:		
k_y (kip/ft)	29243 (Method A) 8000 (Method B)	7300
$k_{x\theta}$ (kip-ft/rad)	Fixed	≈ Fixed
$k_{z\theta}$ (kip-ft/rad)	Pinned	≈ Pinned
Stiffness at Base of Pier:		
$k_{x\theta}'$ (kip-ft/rad)	Fixed	≈ Fixed
Embankment:		
Mass (kip-sec^2/ft)	Not Included	1.0×10^2
k_{ye} (kip/ft)	Not Included	9.0×10^4
Damping Ratio for First Transverse Mode:	0.05	0.26

[1]Quantities EI_g and GJ_g denote gross section bending and torsional rigidities respectively.

TABLE 3-11
COMPARISONS OF NORMAL MODE PARAMETERS FROM CALTRANS MODELS AND FROM EARTHQUAKE MOTIONS (CASE 5-1A)

Parameter	Caltrans		Case 5-1A
	Method A	Method B	
Natural Frequency (Hz)	4.1	3.4	2.6
Damping Ratio	0.05	0.05	0.26
Mode Shape:			
Abutment	0.28	0.69	0.70
Midlength of Span	0.81	0.93	0.94
Above Central Pier	1.00	1.00	1.00

TABLE 3-12
COMPARISONS OF PEAK SEISMIC RESPONSES FROM CALTRANS MODELS AND FROM EARTHQUAKE MOTIONS (CASE 5-1A)

Response	Caltrans		Case 5-1A
	Method A	Method B	
Bending Moment at Base of Pier (kip-ft)	3735 (D/Y = 0.64)	5358 (D/Y = 0.92)	4775 (D/Y = 0.82)
Shear Force at Base of Pier (kip)	287 (D/C = 0.31)	411 (D/C = 0.44)	385 (D/C = 0.42)
Bending Moment at Mid-Span of Deck (kip-ft)	7759 (D/C = 0.11)	5809 (D/C = 0.08)	5249 (D/C = 0.07)
Abutment: Transverse Spring Force (kip) Transverse Displacement (ft) Overturning Moment (kip-ft)	 217 0.007 1392	 194 0.024 2000	 242 0.033 2460

Note:
D = Demand
C = Capacity in bending or shear (Table 2-3)
Y = Moment at first yield (Table 2-3

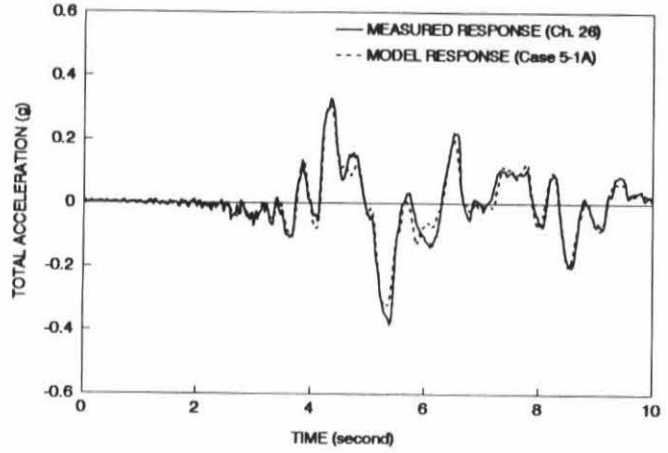

a) North Embankment

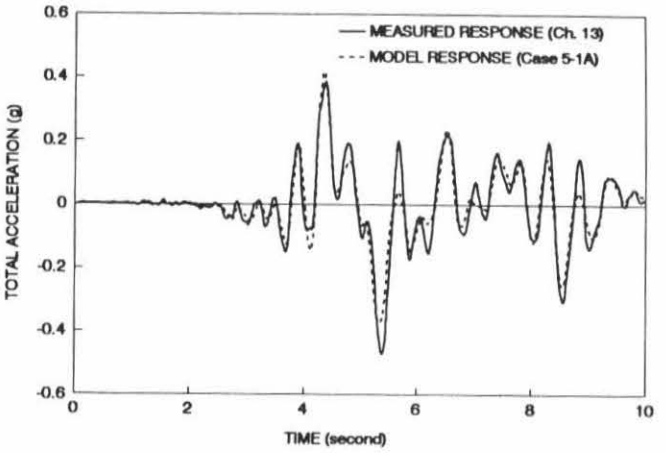

b) North Abutment

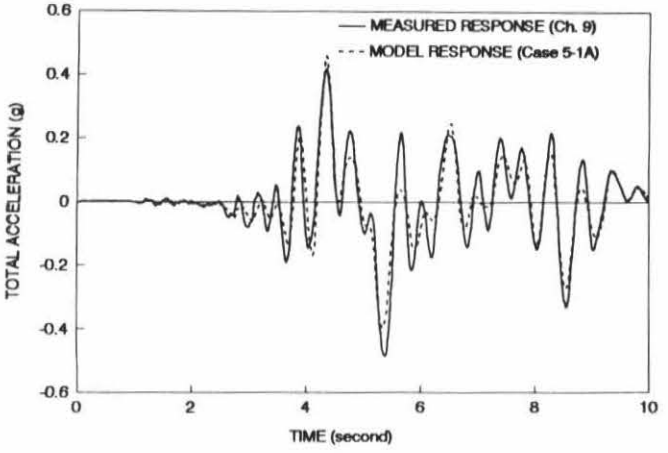

c) Midlength of North Span

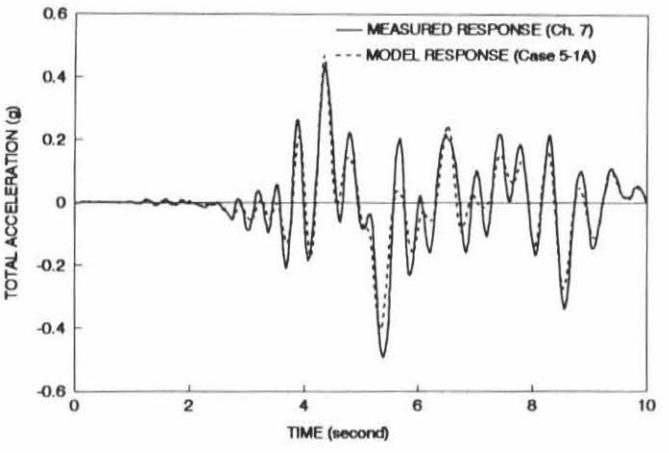

d) Top of Central Pier

FIGURE 3-1

COMPARISONS BETWEEN MEASURED AND MODEL RESPONSE: TRANSVERSE HORIZONTAL ACCELERATIONS

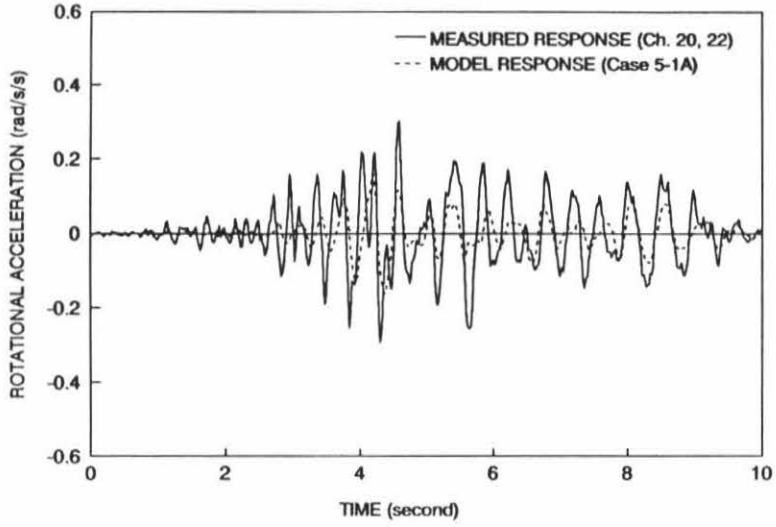

a) Rotation at Midlength of North Span

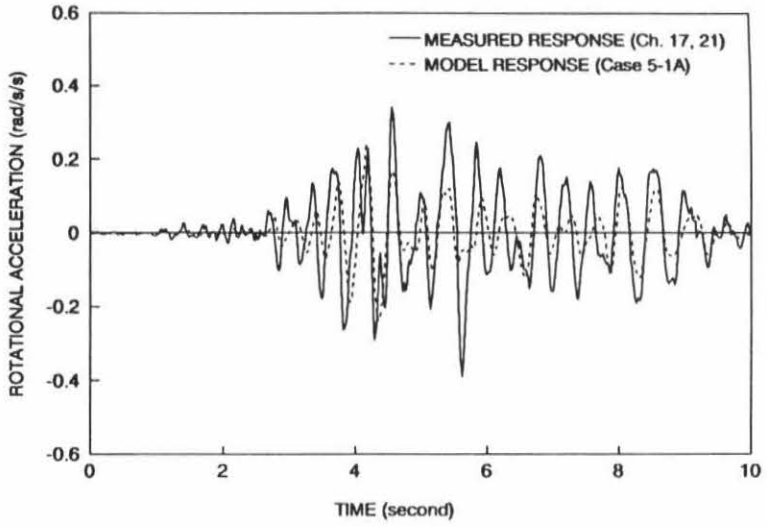

b) Rotation at Top of Central Pier

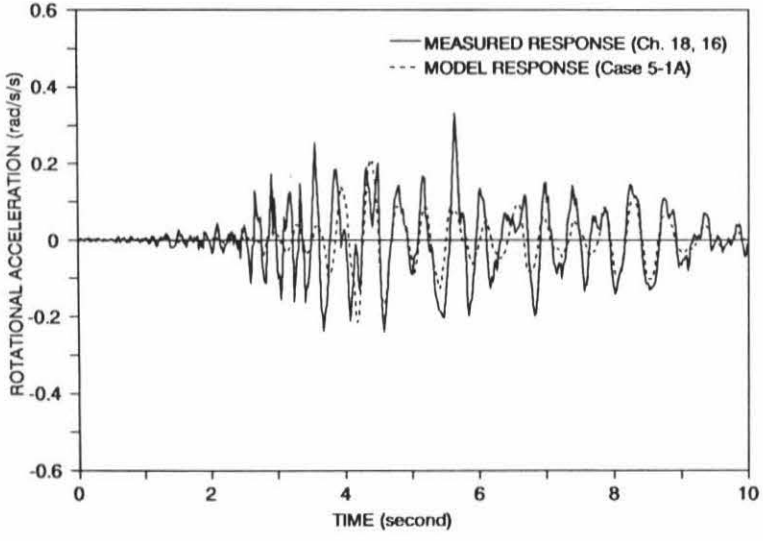

c) Rotation at Midlength of South Span

FIGURE 3-2

COMPARISONS BETWEEN MEASURED AND MODEL RESPONSE: ROTATIONAL ACCELERATIONS (ABOUT X-AXIS)

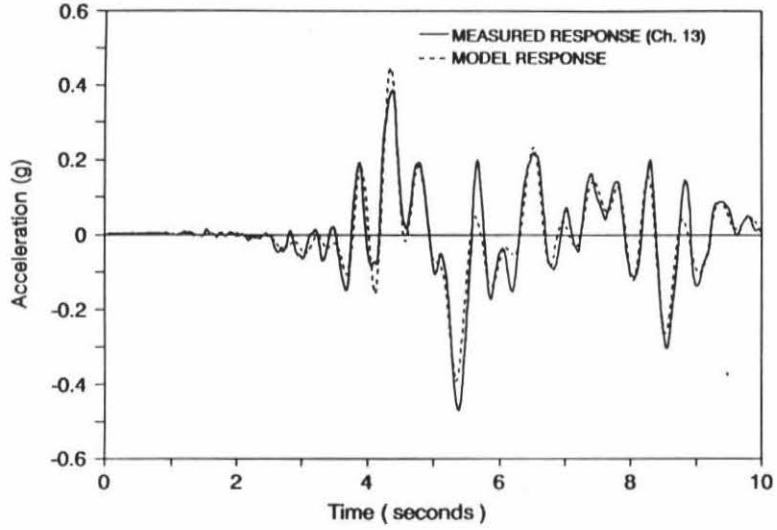

a) Translation at North Abutment

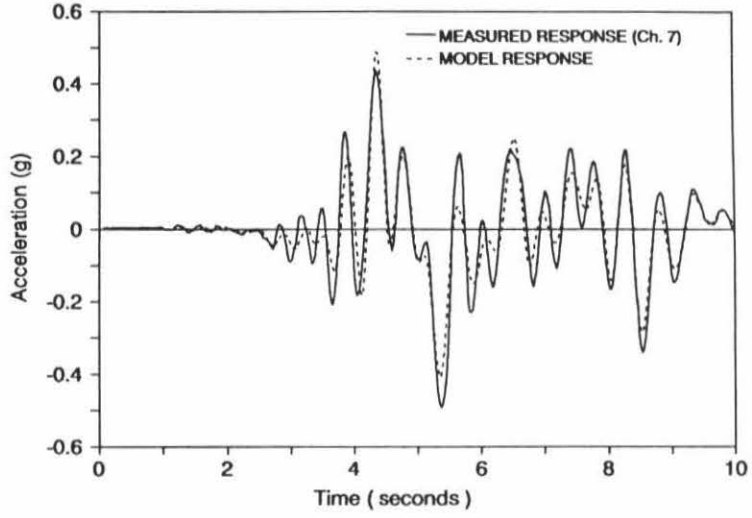

b) Translation at Top of Central Pier

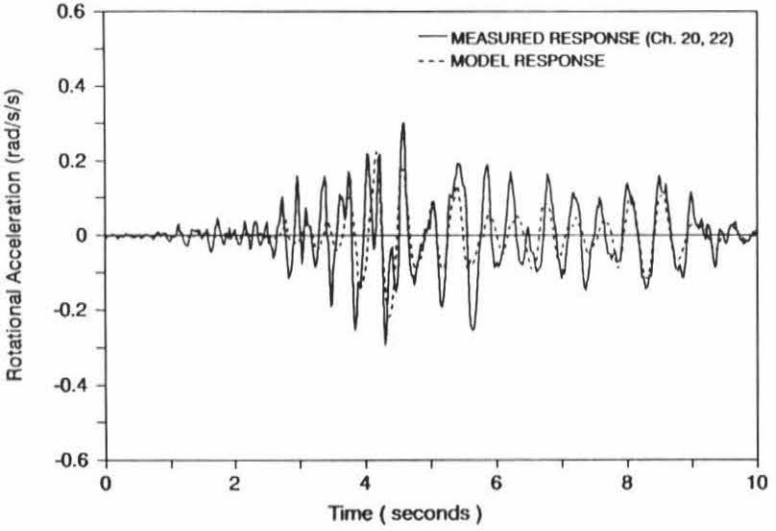

c) Rotation at Midlength of North Span

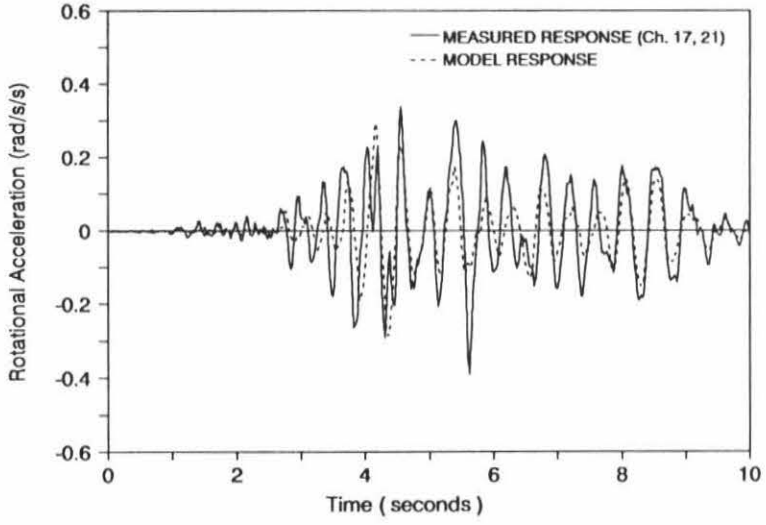

d) Rotation at Top of Central Pier

FIGURE 3-3
COMPARISONS BETWEEN MEASURED AND MODEL RESPONSE USING MODE-ID

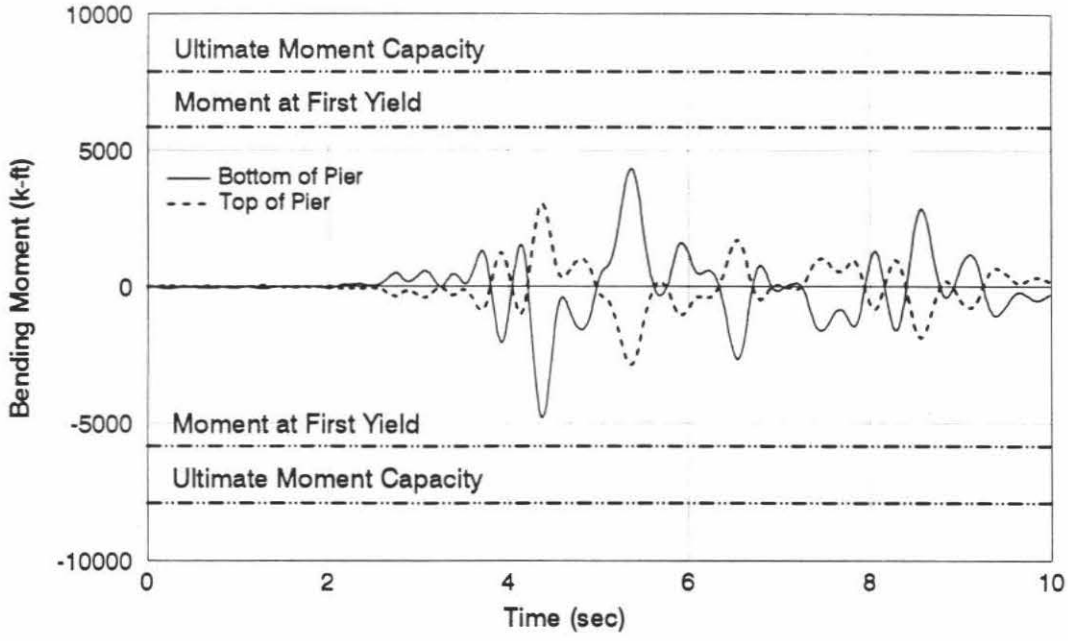

a) Bending Moment

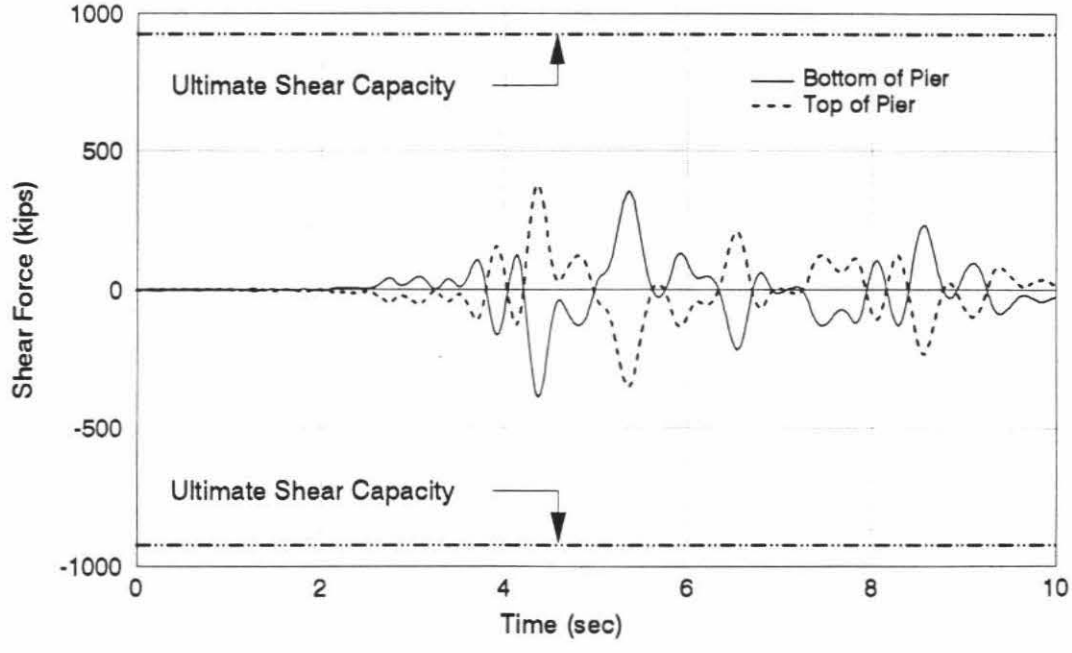

b) Shear Force

FIGURE 3-4

BENDING MOMENTS AND SHEAR FORCES CENTRAL PIER (CASE 5-1A)

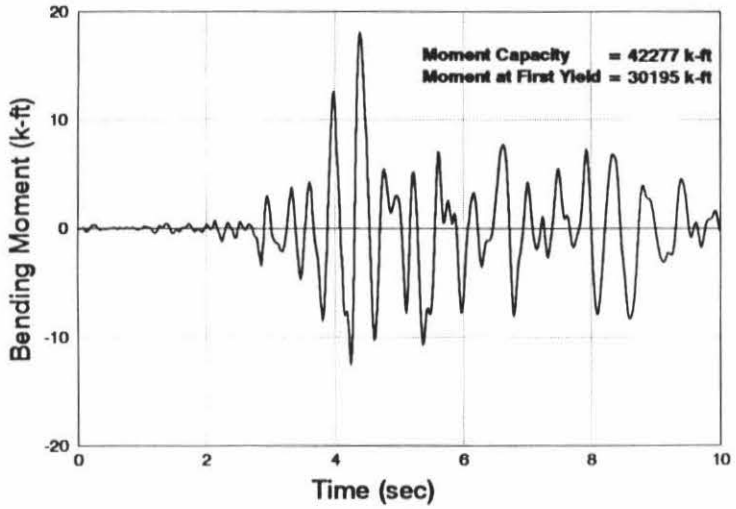

a) Adjacent to Abutment

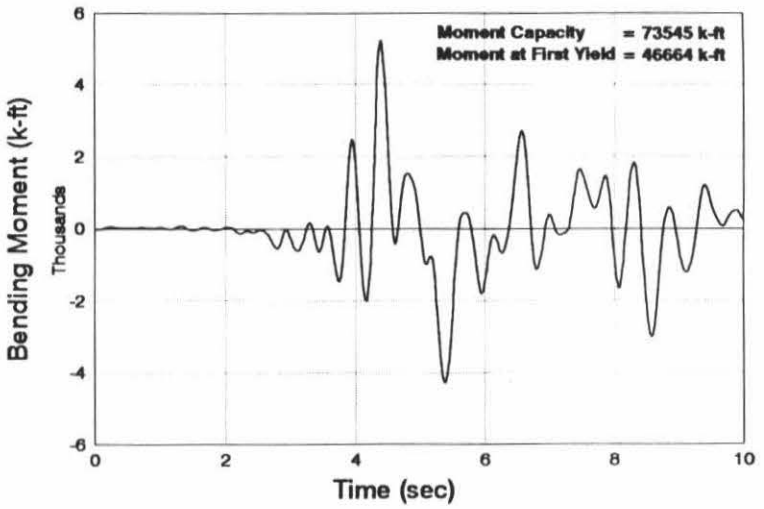

b) Midlength of Span

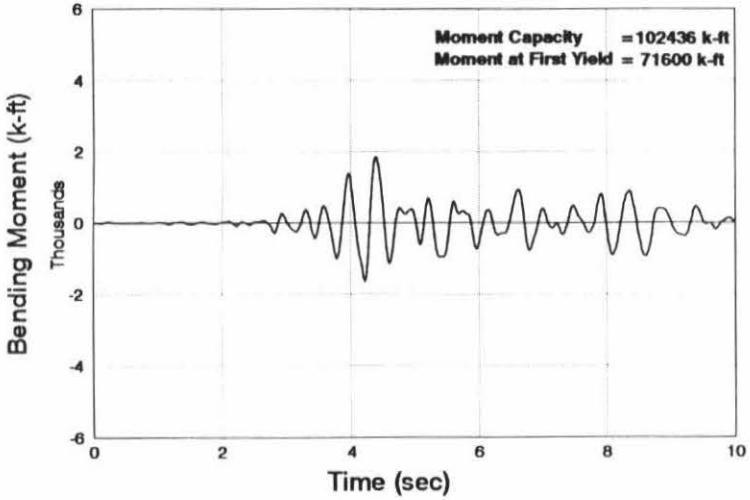

c) Above Central Pier

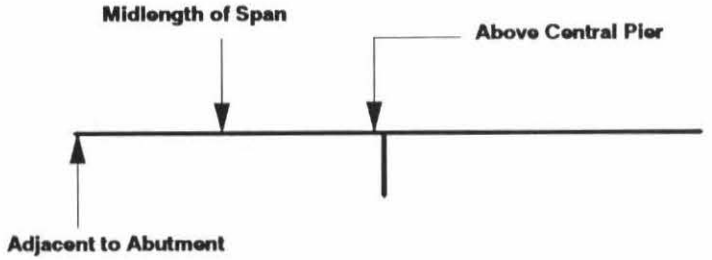

Note : Scale for vertical axis different for a vs. b and c

FIGURE 3-5

BENDING MOMENTS ALONG DECK (CASE 5-1A)

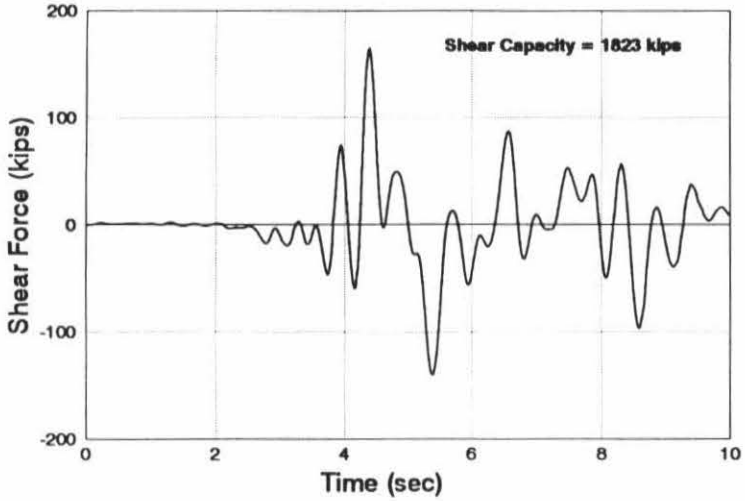

a) Adjacent to Abutment

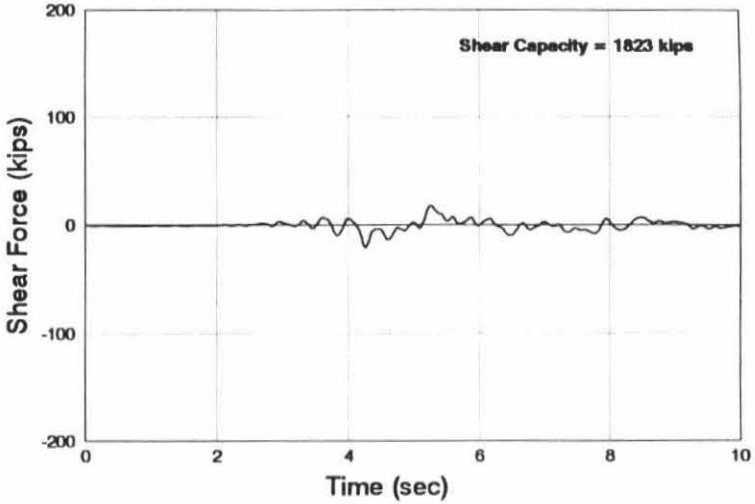

b) Midlength of Span

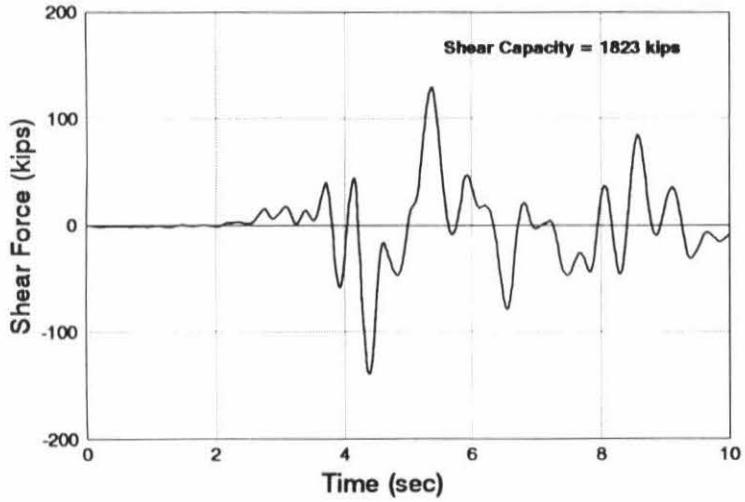

c) Above Central Pier

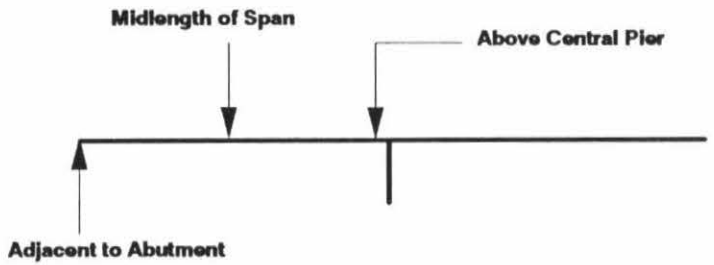

FIGURE 3-6

SHEAR FORCES ALONG DECK (CASE 5-1A)

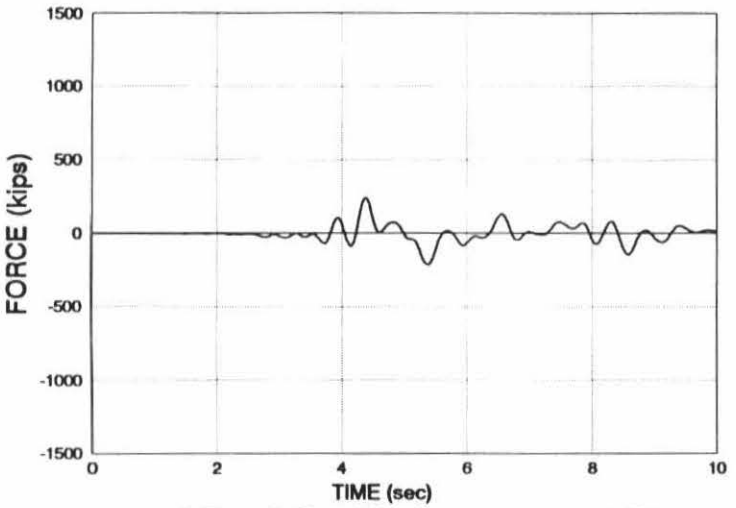

a) Translational Spring at Abutment, Ky

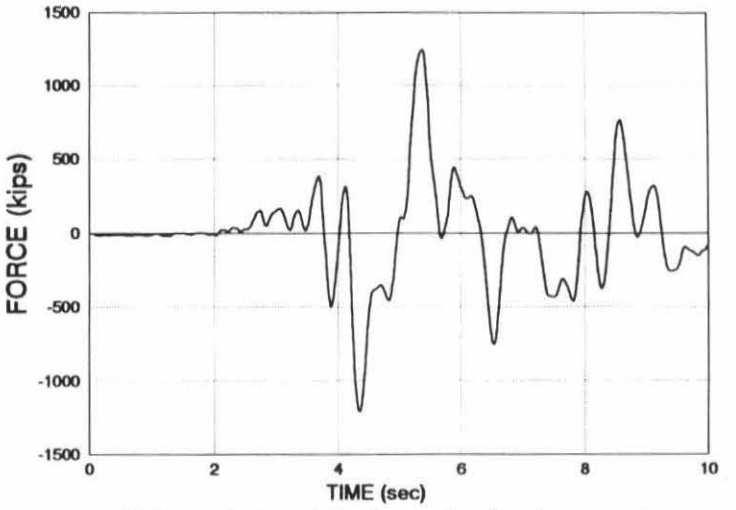

b) Translational Spring at Embankment, Kye

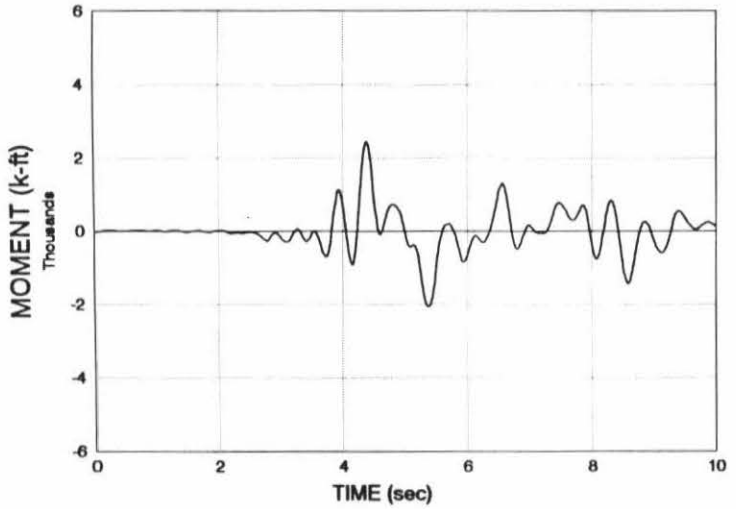

c) Rotational Spring at Abutment, Kxr

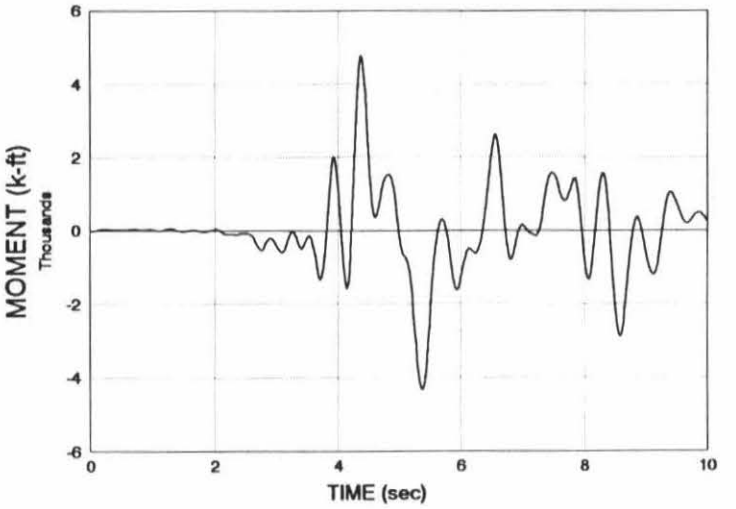

d) Rotational Spring at Base of Pier, K'xr

FIGURE 3-7

FORCES AND MOMENTS IN SOIL SPRINGS (CASE 5-1A)

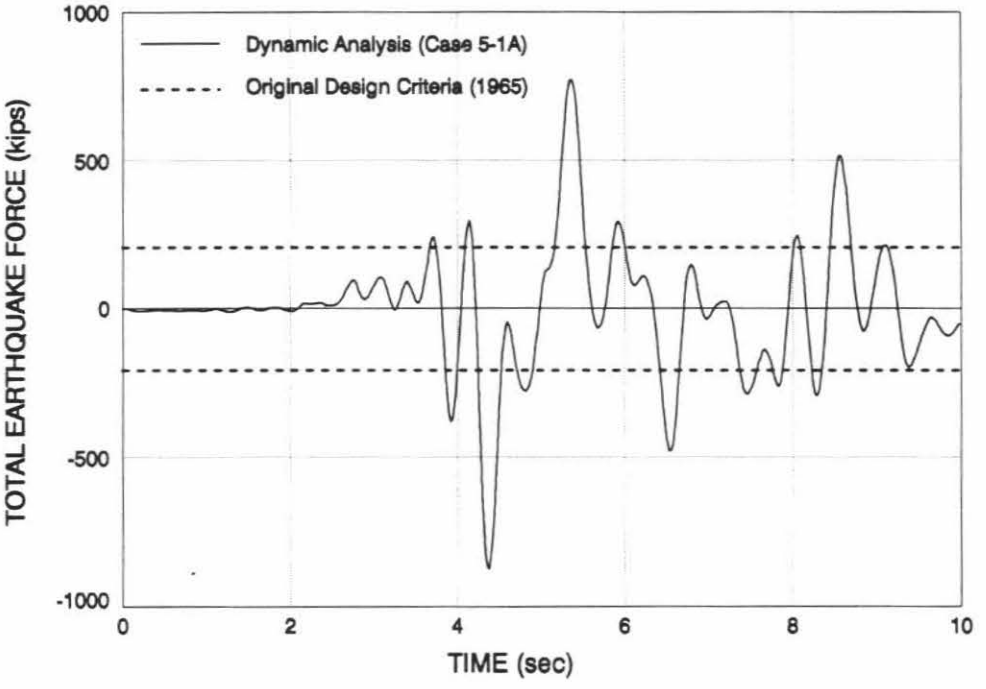

FIGURE 3-8

COMPARISON OF TOTAL EARTHQUAKE FORCE FROM DYNAMIC ANALYSIS AND FROM ORIGINAL (1965) DESIGN CRITERIA FOR MRO

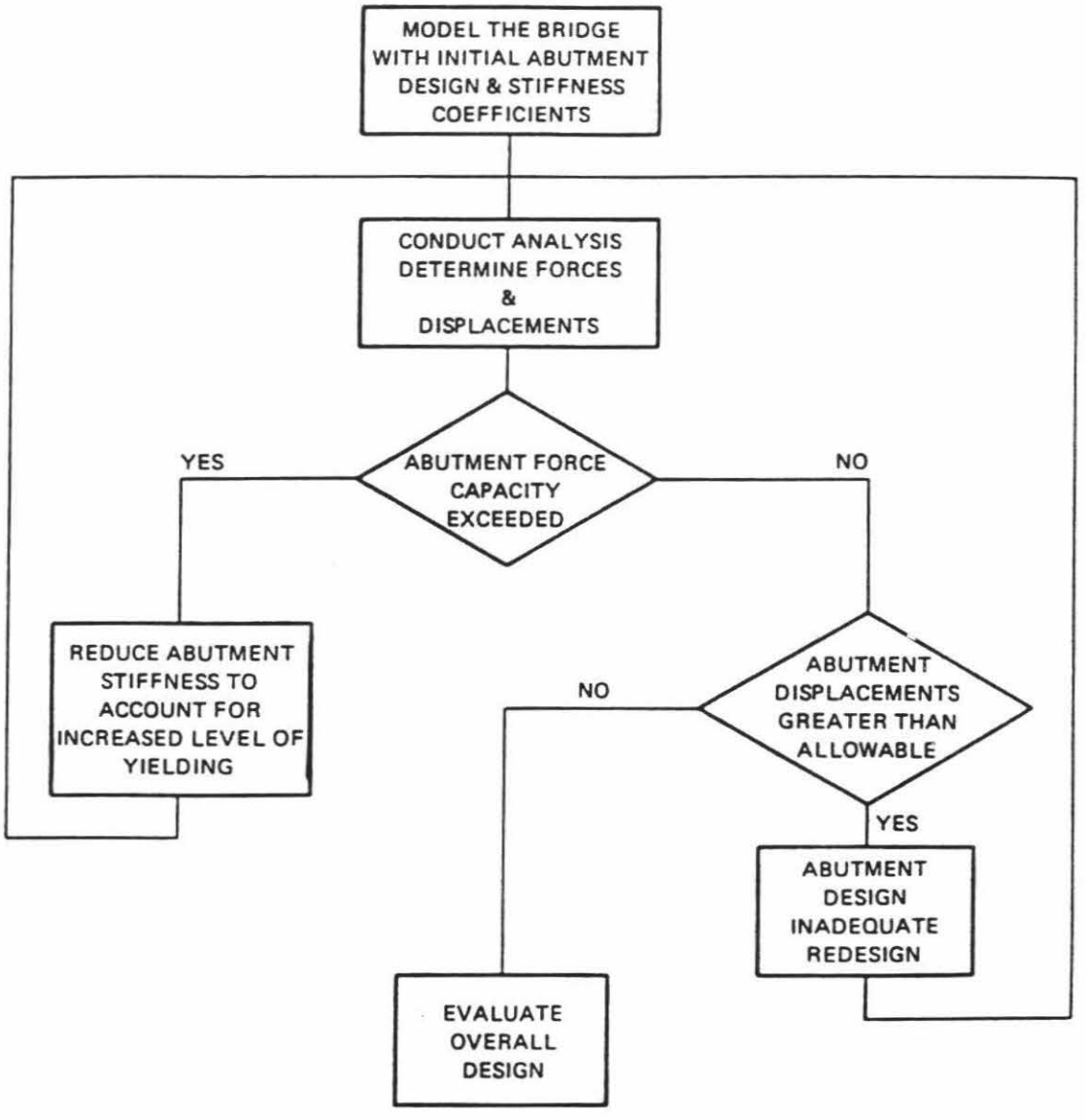

FIGURE 3-9

CALTRANS ITERATIVE SEISMIC EVALUATION PROCEDURE

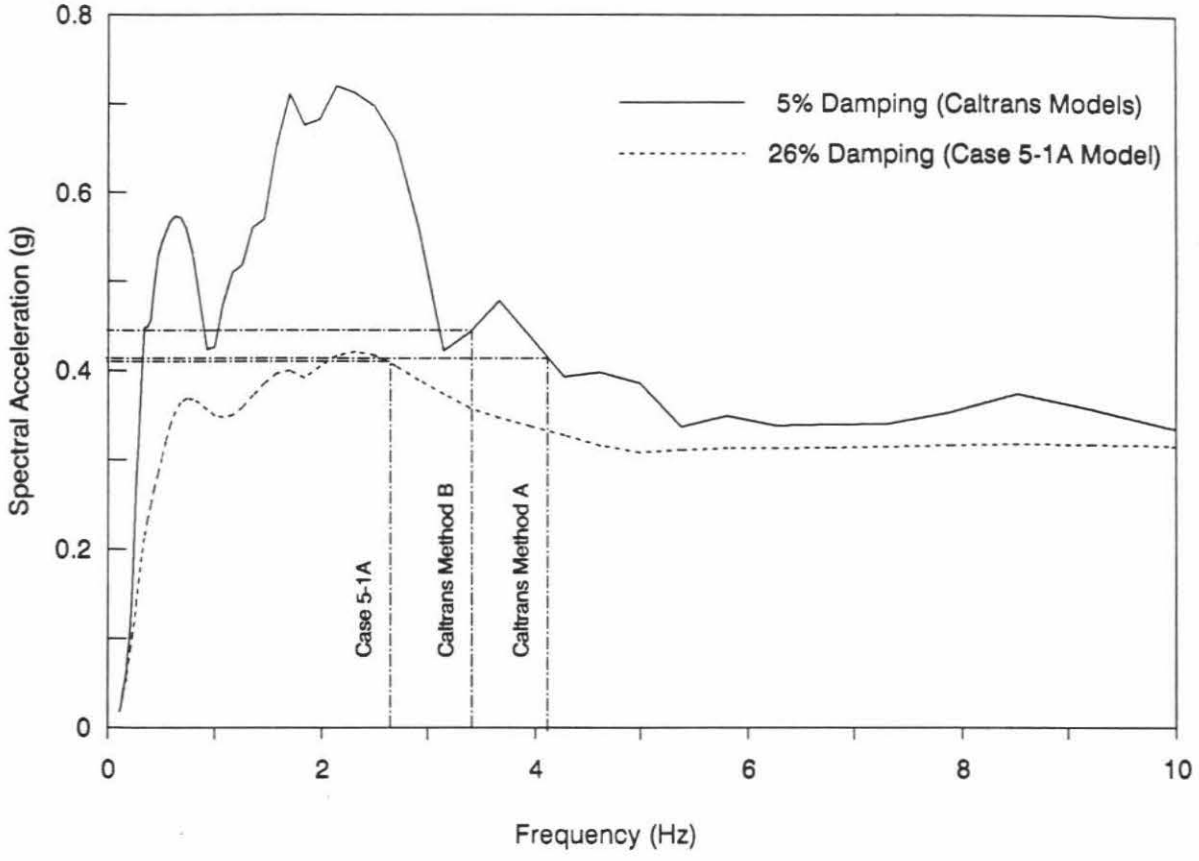

FIGURE 3-10

RESPONSE SPECTRA OF INPUT MOTION FOR SEISMIC ANALYSES OF MRO (CHANNEL 2 OF RECORDED EARTHQUAKE MOTIONS)

CHAPTER 4
CONCLUDING COMMENTS

4.1 Evaluation and Applicability of Procedures and Results

The results presented in this report are the culmination of extensive evaluations of the seismic and dynamic response characteristics of the bridge-soil system at the MRO. These evaluations have been based on system identification of the MRO's recorded motions from the 1979 Imperial Valley Earthquake, full scale dynamic testing of the MRO, in situ testing of the site soil materials, and testing of concrete cores extracted from the MRO's central pier. The resulting bridge model parameters obtained from these procedures led to plausible comparisons with values of the parameters that were estimated from our prior dynamic tests of the MRO and from engineering analyses. In addition, our seismic analyses of the MRO using these parameters led to earthquake demand values of the bending moments and shear forces along the deck and central pier foundation that were well within first yield and ultimate capacity values of these quantities. These demand vs. capacity comparisons are consistent with the observed seismic performance of the MRO, which was undamaged despite the strong levels of shaking experienced by the bridge during the Imperial Valley Earthquake. Therefore, it is our view that the model parameters developed for the MRO from this project can serve as an excellent basis for calibrating improved modeling and seismic evaluation procedures in the future. In addition, the system identification procedures used to estimate these parameters can also be applied to future earthquake motion arrays at bridges in order to further calibrate, assess, and improve bridge modeling and seismic evaluation procedures.

A principal objective of these seismic analyses has been to assess Caltrans' original seismic design that was in effect during the original design of the MRO, and also to assess Caltrans' current seismic evaluation procedures for short bridge overcrossing structures. Our conclusions from these assessments (which are discussed in detail in Section 3.4) are summarized in the remainder of this chapter.

4.2 Assessment of Original Design

Caltrans' seismic design criteria that was in effect at the time of the design of the MRO in 1968 was based on an equivalent static lateral force that was found to be well below the dynamic values of the total lateral force computed from our seismic analysis. This comparison, when considered together with the MRO's excellent seismic performance during the Imperial Valley Earthquake, indicates that the MRO's inherent seismic resistance and capacity was probably controlled by its design against dead loads and traffic loads rather than the low seismic design forces that were considered at that time. In view of this, the MRO's excellent seismic performance was most likely due to such factors as: (a) the simple configuration of the MRO (e.g., unskewed, monolithic abutments, etc.), which is a type of configuration that has exhibited favorable performance during past earthquakes; and (b) the use of relatively tightly-pitched spiral steel as the transverse reinforcement for the MRO's central pier, which was well beyond Caltrans' more typical practice at the time for the transverse reinforcement of bridge columns.

However, other elements of the MRO's original design and detailing are substandard according to Caltrans' current design practice, but did not affect the seismic response during these particular earthquake motions; these include the insufficient development length of the central pier's longitudinal steel where it extends into the deck, the lack of top steel in the central pier's footing, and the possible lack of a positive connection between the timber piles and the pile cap.

4.3 Assessment of Current Seismic Evaluation Procedures

Caltrans' current evaluation procedures for the seismic design of new bridges and the retrofit of existing bridges are summarized in Section 3.4.2. Our conclusions from our use of the MRO's recorded motions and seismic analyses to assess these procedures are summarized in the following paragraphs.

4.3.1 Abutment Evaluation Procedures

The results from these seismic analyses have clearly demonstrated that SSI at the abutments is a particularly important element of the seismic response of short bridge overcrossing structures subjected to transverse input motions. Therefore, current Caltrans procedures for the seismic evaluation of abutments should be upgraded to incorporate consideration of the actual configuration and properties of the wing walls, pile cap, and piles as well as the properties of the adjacent and underlying soil materials. Our analysis of the MRO's abutments shows that the relative contributions of these various elements to the overall stiffness and capacity of the abutments is complex and not readily estimated using current engineering procedures. Furthermore, there is currently a lack of experimental data from abutment test programs that could provide insights for improving the state-of-practice for evaluating abutment seismic response characteristics. However, such data are anticipated in the near future upon completion of the detailed abutment test program that is now being carried out at the University of California at Davis under Caltrans sponsorship. Furthermore, the abutment model parameters and seismic response characteristics established from our detailed analysis of the MRO's strong motion records and also from our full-scale dynamic tests of the MRO can, together with appropriate engineering analysis procedures, provide a valuable additional basis for improving current abutment seismic evaluation procedures.

4.3.2 Modal Damping Ratios

The results of this evaluation of the MRO's strong motion records have led to bridge models with modal damping ratios for the bridge's first transverse mode of vibration that range from 0.19 to 0.26; similar results were also obtained from parallel studies of these records (Vrontinos, et. al., 1993). These results suggest that the modal damping ratio of 0.05 that is used in Caltrans' current seismic evaluation procedures may be unduly conservative for modes with significant SSI and that, for such modes, larger values are more appropriate. However, detailed evaluation of the MRO's modal damping ratio has shown that, of all the modal parameters, the damping ratio is particularly sensitive to differences in model characteristics, the segment of the recorded motions used to identify the bridge's modal parameters, and the uncertainties associated

with using a linear classical mode model to represent the seismic response characteristics of a highly nonlinear bridge-soil system (Tsai, Werner, and Mahin, 1993). Furthermore, as described in that report, the current experimental bridge damping data base is nearly entirely comprised of damping ratios that were estimated from very small dynamic excitations, and are therefore too low to be representative of earthquake-induced damping levels. In addition, the only reliable earthquake-induced bridge damping data have been developed from the MRO's strong motion records from the Imperial Valley Earthquake. Therefore, although the use of a modal damping ratio larger than 0.05 is indicated, particularly for bridges with significant SSI, we suggest that caution be exercised in using overly large damping values for the seismic evaluation of bridges until more damping estimates from recorded earthquake motions at additional bridges are obtained.

4.3.3 Structural Parameters

The equivalent elastic parameters used to model the bridge structure should consider the effects of potential degree of cracking of the concrete anticipated for the deck and central pier elements. It is our view that the parameters recommended under the ATC-32 project are appropriate for this purpose. The results of this study show that the use of these structural parameters together with plausible values of embankment mass and soil spring stiffness lead to computed seismic responses of the MRO that compare closely with the recorded earthquake motions and are also consistent with the bridge's observed seismic performance. In addition, we recommend that the capacity of the central pier be evaluated on the basis of relative displacement and shear capacities as described by Moehle and Aschheim (1993) and summarized in Section 2.6.2.

4.3.4 Embankment Modeling

The effects of the elevated embankment in amplifying the input motions into the abutments represents an important element of the seismic response of short bridge overcrossing structures to transverse input motions. Therefore, these effects should be incorporated into bridge modeling procedures for seismic analysis of these response characteristics, through the use of an effective embankment mass and transverse shear stiffness. Simple procedures for estimating this mass and stiffness have been developed and used in our seismic analyses of the MRO. In this, it is noteworthy that, for a model that incorporated the ATC-32 structural parameters and a best estimate value of the embankment mass that was computed using Equation 2-1 of Section 2.2.3, our system identification of the earthquake motions led to a value of the embankment stiffness that compared closely to the stiffness value estimated using the Wilson-Tan (1990) procedure (see Eq. 2-2).

4.4 Strong Motion Instrumentation of Bridges

One of the end products of the investigation of the MRO that was conducted by the University of Nevada at Reno and Dames & Moore has been the recommendation of improved

strong motion instrumentation of the bridge (Crouse, Werner, Douglas, and Beck, 1991). This improved instrumentation will lead to strong motion record arrays during future earthquakes that will provide more complete data for evaluating the MRO's seismic response characteristics (and particularly SSI effects) than were obtained from the bridge motions recorded during the Imperial Valley Earthquake. The recommended instrumentation has since been deployed by the California Division of Mines & Geology (CDMG).

We strongly suggest that the basic principles upon which these recommendations were based should be followed when planning future arrays of strong motion instruments at bridges in California and when expanding existing arrays. In addition, the results of our evaluation of the MRO's strong motion records from the Imperial Valley Earthquake that are described in this report demonstrate the invaluable information for evaluating bridge modeling procedures, seismic response characteristics, and seismic design procedures that can be obtained from extensive arrays of strong motion records. Accordingly, our recommendations along these lines are as follows:

- Our use of the MRO's recorded earthquake motions as a basis for modeling and interpreting its seismic response characteristics was hampered by insufficient instrumentation at the bridge's abutments and central pier footing, and also by possible incoherence of the recorded free field motions over the distance between the free field instrument and the bridge. Therefore, care should be taken when planning arrays of strong motion instruments at key bridge structures to be sure that: (a) the translational and rotational motions at the supports of the bridge are recorded, in order to adequately represent the key "input motions" that will affect the bridge's seismic response; and (b) free field instruments should be placed as close as possible to the bridge (with due regard to possible contamination by SSI) to minimize problems with possible incoherence. In addition, the instrumentation along the bridge itself should be placed at ample locations to capture its key translational and rotational response characteristics. Such planning will greatly enhance the value of future arrays of strong motion records as a tool for assessing bridge response characteristics, design procedures, and modeling requirements.

- Caltrans should initiate detailed studies of the numerous arrays of recorded earthquake motions that have been obtained at the Painter Street Overcrossing in Northern California, to gain insight into its seismic response characteristics and to further evaluate seismic design procedures for bridges. Although the instrumentation of this bridge has certain limitations (i.e., the placement of instrumentation on one side only of this skewed bridge and the extended distance between the free field instrument and the bridge), a wealth of strong motion records has been obtained at the bridge during several past earthquakes. These records should be analyzed using established system identification and engineering procedures. The results of these analyses should serve to supplement the initial study of the records from the 1992 Petrolia Earthquake that is now being supported by CDMG.

- Caltrans should work with CDMG to enhance the strong motion instrumentation of bridges throughout the state. This should include the deployment of additional instruments at existing bridges that are now currently instrumented, where necessary to

better represent their seismic response characteristics. In addition, the number of bridges that are instrumented should be increased. The planning of this instrumentation program should incorporate careful evaluation of potential seismic response characteristics of candidate bridges (including effects of SSI and possible free field incoherence) so that a sufficient number and locations of free field and bridge instruments are deployed to: (a) adequately represent the response characteristics of the bridges during future earthquakes; and (b) facilitate the implementation of studies of the type described in this report that could provide insight into seismic design, evaluation, and modeling requirements for bridges.

REFERENCES

Applied Technology Council (ATC) (1992). ATC-32 -- Review and Revision of Caltrans Seismic Design Procedures for Bridges. Redwood City CA, Draft Interim Report to California Department of Transportation, Sacramento CA, December.

Beck, J. L. (1978). Determining Models of Structures from Earthquake Records. Report No. EERL 78-01, Earthquake Engineering Research Laboratory, California Institute of Technology, Pasadena CA, June.

Beck, J. L. (1989). "Statistical System Identification of Structures", Proceedings of Fifth International Conference on Structural Safety and Reliability, San Francisco CA, August.

California Department of Transportation (Caltrans) (1990). Structures Seismic Design References, Division of Structures, Sacramento CA, June.

California Department of Transportation (Caltrans) (1992). Interim Memo to Designers 20-4, Division of Structures, Sacramento CA, April.

Clough, R. W. and Penzien, J. (1975). Dynamics of Structures, McGraw-Hill, Inc., 633 pp.

Crouse, C. B. (1992). Estimation of Foundation Stiffnesses of Meloland Road Overcrossing Bridge from Forced Vibration Data. Dames & Moore, Seattle WA, Report to California Department of Transportation, Sacramento CA, August.

Crouse, C. B. and Hushmand, B. (1990). "Soil-Structure Interaction and Nonlinear Site Response at the Differential Array Accelerograph Station", Proceedings of 4th U. S. National Conference on Earthquake Engineering, Volume 3, Palm Springs CA, May, pp 815-823.

Crouse, C. B., Price, T., and Mitchell, R. (1992). "Evaluation of Methods to Estimate Pile Foundation Stiffnesses for Bridges", Proceedings of 8th U.S.-Japan Bridge engineering Workshop, Chicago IL, May.

Crouse, C. B., Werner, S. D., Douglas, B. M., and Beck, J. L. (1991). Strong Motion Instrumentation Plan for the Meloland Road Overcrossing, Report prepared for California Department of Transportation, Sacramento CA, Dames & Moore, Seattle WA, March.

Dames & Moore (D & M) (1992). Task 1 Report -- Evaluation of Methods to Estimate Stiffness and Damping of Bridge Foundations. Report to Washington Department of Transportation, Olympia WA, Dames & Moore, Seattle WA, April.

Douglas, B. M., Norris, G., Dodd, L., and Richardson, J. (1984). "Behavior of the Meloland Road Overcrossing during the 1979 Imperial Valley Earthquake", Seismic Research for Highway Bridges (U.S.-Japan Program), Department of Civil Engineering, University of Pittsburgh, Pittsburgh PA, June, pp 339-366.

Douglas, B. M., Maragakis, E. A., Vrontinos, S., and Douglas, B. J. (1990). "Analytical Studies of the Static and Dynamic response of the Meloland Road Overcrossing", Proceedings of the 4th U. S. National Conference on Earthquake Engineering, Vol. 1, Palm Springs CA, May, pp 987-992.

Douglas, B. M., Maragakis, E. A., and Vrontinos, S., (1991). "Parameter Identification Studies of the Meloland Road Overcrossing", Proceedings of Pacific Conference on Earthquake Engineering, Vol. 1, University of Aukland, Aukland, New Zealand, November 20-23, pp 105-116.

Douglas, B. M., Crouse, C. B., Werner, S. D., and Maragakis, E. A. (1993). Quick Release Dynamic Tests of the Meloland Road Overcrossing. Report prepared for California Department of Transportation, Sacramento CA, Center for Civil Engineering Research, University of Nevada, Reno NV, In press.

Federal Highway Administration (FHWA) (1986). "Seismic Design of Highway Bridge Foundations," FHWA Report Nos. FHWA/RD-861, FHWA/RD-86/102, and RHWA/RD-86/103. Turner-Fairbanks Highway Research Center, McLean VA, June.

Housner, G. W. (ch.) (1990). Competing Against Time. Report to Governor George Deukmejian from the Governor's Board of Inquiry of the 1989 Loma Prieta Earthquake, May.

Katafygiotis, L. S. (1991). Treatment of Model Uncertainties in Structural Dynamics. Report No. EERL 91-01, Earthquake Engineering Research Laboratory, California Institute of Technology, Pasadena CA, May.

Klein, G. (1992). Compressive Strength Tests of Concrete Cores from Meloland Road Overcrossing (Bridge No. 58-215), California Department of Transportation, Sacramento CA, Communication to S. D. Werner of Dames & Moore, October.

Mason, A. B., Beck, J. L., Chen, J., and Ullmann, R. R. (1989). "Modal Parameter Identification of an Offshore Platform from Earthquake Response Records", Seismic Engineering: Research and Practice, American Society of Civil Engineers, New York NY, May 1-5, pp 217-226.

Moehle, J. (1993). Personal Communication to S. D. Werner of Dames & Moore, January.

Moehle, J. and Aschheim, M. (1993). Evaluation of Column Deformation Capacity, Report to Dames & Moore prepared under Caltrans Contract No. 59Q122, University of California, Berkeley CA, April.

Naval Facilities Engineering Command (NAVFAC) (1986). Foundations and Earth Structures, DM-7.02, Department of the Navy, Washington D.C., September.

Novak, M., Sheta, M., El-Hifnawy, L., El-Marsafawi, H., and Ramadan, O. (1991). DYNA 3, A Computer Program for Calculation of Foundation Response to Dynamic Loads, User Manual, University of Western Ontario Geotechnical Research Centre, Report No. GEOP 90-02, Vol 1, Rev. 2.

Roberts, J. E. (1991). "Recent Advances in Seismic Design and Retrofit of California Bridges". Proceedings of the 3rd U. S. Conference on Lifeline Earthquake Engineering, ASCE Technical Council on Lifeline Earthquake Engineering, Monograph No. 4, August 22-23, pp 52-64.

Scott, B. D., Park, R., and Priestley, M. J. N. (1982). "Stress-Strain Behavior of Concrete Confined by Overlapping Hoops at Low and High Strain Rates", Journal of the American Concrete Institute, Vol. 79, No. 1, January-February, pp 13-27.

Tsai, N. C., Werner, S. D., and Mahin, S. A. (1993). Compilation and Evaluation of Current Bridge Damping Data Base. Report to California Department of Transportation under Contract No. 59Q122, Dames & Moore, Oakland CA, February.

Vrontinos, S., Douglas, B. M., and Maragakas, E. A. (1993). "System Identification of the Meloland Road Overcrossing using Static and Dynamic Field Test Data". Structural Engineering in Natural Hazards Mitigation, Vol. 1, Proceedings of Papers presented at ASCE Structures Congress, Irvine CA, April,

Wallace, J. W. and Moehle, J. (1989). BIAX: A Computer Program for the Analysis of Reinforced Concrete Sections. Report No. UCB/SEMM-89/12, Dept. of Civil Engineering, University of California, Berkeley CA, July.

Werner, S. D., Beck, J. L., and Levine, M. (1987). "Seismic Response Evaluation of Meloland Road Overpass using 1979 Imperial Valley Earthquake Records". Journal of Earthquake Engineering and Structural Dynamics, Vol. 15, No. 2, February, pp 249-274.

Werner, S. D., Beck, J. L., and Nisar, A. (1990). "Full-Scale Dynamic Tests and Seismic Excitation of a Bridge Structure". Proceedings of the 4th U. S. National Conference on Earthquake Engineering, Vol. 1, Palm Springs CA, May, pp 1037-1046.

Werner, S. D., Nisar, A., and Beck, J. L. (1992). Assessment of UBC Seismic Design Provisions using System Identification of Recorded Earthquake Motions. Report to National Science Foundation, Washington D. C. under Grant No. BCS-9011136, Dames & Moore, Oakland CA, January.

Wilson, E. L. and Habibullah, A. (1989). SAP90, A Series of Computer Programs for the Static and Dynamic Finite Element Analysis of Structures, Users Manual, Computers & Structures Inc., Berkeley CA, July.

Wilson, J. and Tan, B. S. (1990). "Bridge Abutments: Formulation of Simple Model for Earthquake Response Analysis". Journal of Engineering Mechanics, American Society of Civil Engineers, Vol. 116, No. 8, August, pp 1828-1856.

Wood, S. L. (1991). "Evaluation of Long Term Properties of Concrete", ACI Materials Journal, Vol. 88, No. 6, November - December, pp 630-643.

APPENDIX A

SELECTED STRUCTURAL DRAWINGS FOR MELOLAND ROAD OVERCROSSING

I-008-2(23)117

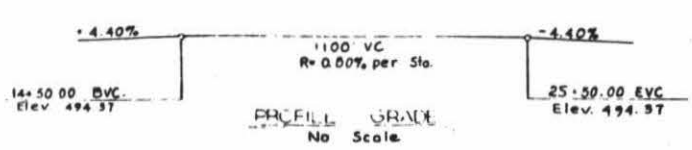

PROFILE GRADE
No Scale.

APPROXIMATE QUANTITIES

FURNISH CONCRETE PILING (CLASS II)	990	LF
FURNISH CONCRETE PILING (CLASS III)	1,175	LF
DRIVE CONCRETE PILES	39	EA
BRIDGE APPROACH GUARD RAILING (TYPE 8)	238	LF
METAL RAILING (TYPE 11)	498	LF

FINAL QUANTITIES

STRUCTURE EXCAVATION (BRIDGE)	180	CY
STRUCTURE BACKFILL (BRIDGE)	130	CY
STRUCTURE CONCRETE (BRIDGE)	555	CY
BAR REINFORCING STEEL (BRIDGE)	160,000	LB

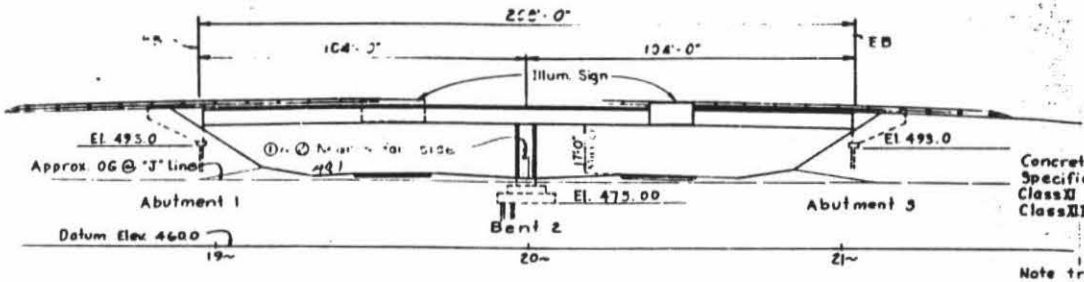

ELEVATION
Scale 1"=20'

Concrete piles (45 ton bearing)
Specified tip elev. 455.0 Estimated tip Elev. 450.0
Class XI @ Abutments
Class XII @ Bents

Note treated timber piles may be used at contractor's option. The engineers estimated is based on the conc. pile.

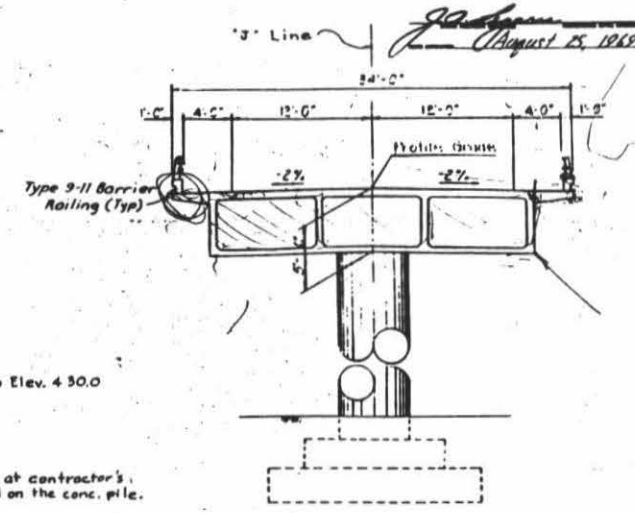

TYPICAL SECTION
Scale 3/16"=1'-0"

AS BUILT PLANS
Contract No. 11-029824
Date Completed 7-1-71
Document No. A0000858

INDEX TO PLANS

SHEET NO	TITLE
1	General Plan
2	Grid Grades
3	Foundation Plan
4	Abutment Details
5	Bent Details
6	Typical Section & Girder Layout
7	Girder Reinforcement
8	Corrosion Resistant Concrete Pile Details 45 Ton
9	Log of Test Borings
	Std. Plans Dated July 1969
A62-B1	Exc. & Backfill Br. & Walls-Limits of Payment
B0-1	Bridge Details
B0-5	" "
B7-1	Box Grd. Details
B11-36	B.A.G.R. Type 8 (Layout)
B11-37	" " " (Details)
B11-43	Metal Railing Det - Types 9 10 & 11
B11-45	Barrier Railing Type 9-11

NO AS BUILT
CORRECTIONS BY R J Dryden
CONTRACT NO. 029823

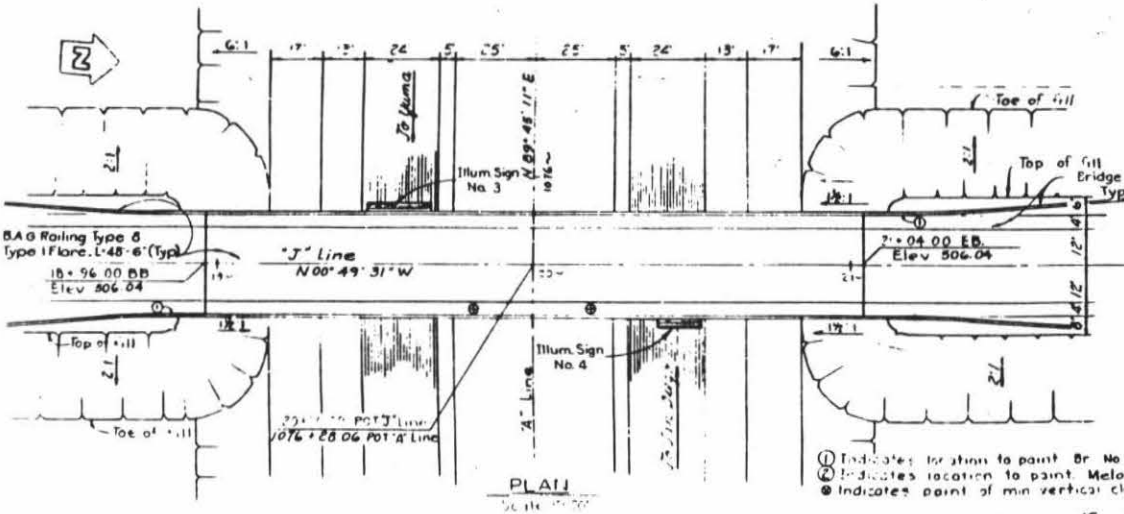

PLAN
Scale 1"=50'

① Indicates location to paint Br. No. 58-215 and year.
② Indicates location to paint Meloland Rd. O.C.
@ Indicates point of min. vertical clearance.

For General Notes see "Foundation Plan" sheet

For Loading Notes and Alternative

DESIGN SECTION ... 14

DESIGN	M. Ansley	CHECK	A.E. Spence
DETAILS	J.H.B.	CHECK	A.E. Spence
LAYOUT	T.H.	CHECK	A.E. Spence
QUANTITIES		CHECK	
SPECIFICATIONS		CHECK	

Supervising Engineer: A.P. Orozco
Project Engineer: O. Bendeff

STATE OF CALIFORNIA
DEPARTMENT OF PUBLIC WORKS
DIVISION OF HIGHWAYS

MELOLAND ROAD OVERCROSSING

LOCATED APPROX. 3.4 MILES E. OF EXISTING STATE ROUTE 111 AND APPROX. 2.1 MILES S. OF EXISTING U.S. 8 (80) ROUTE 80
IN IMPERIAL COUNTY

GENERAL PLAN

BRIDGE NO.	58-215	POST MILE	43.6	DRAWING NO.	58215-1	SHEET NO.	1

Designed plans bearing earlier revision dates ——

WO 029821
CU 11205

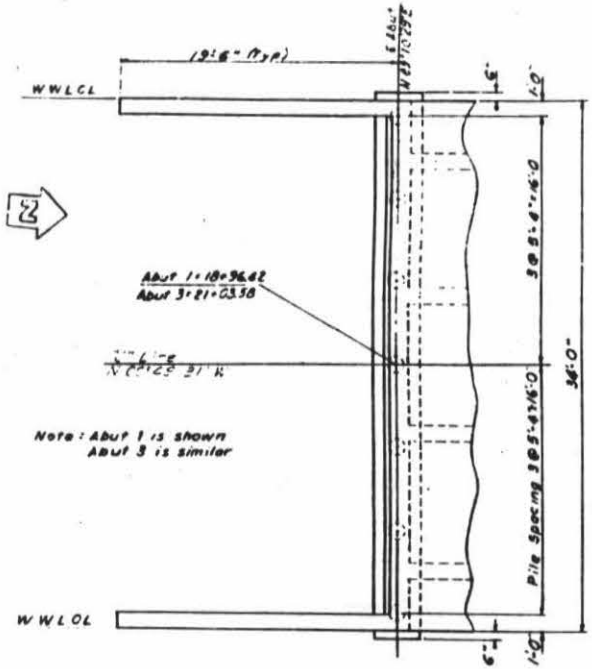

PLAN
Scale 1/8" = 1'-0"

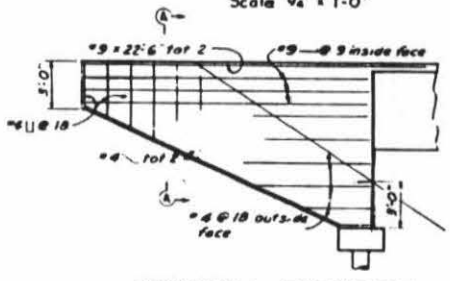

WINGWALL ELEVATION
Scale 1/4" = 1'-0"

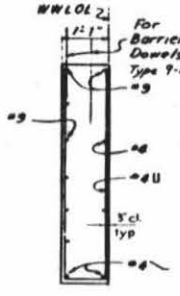

SECTION A-A
Scale 1/4" = 1'-0"

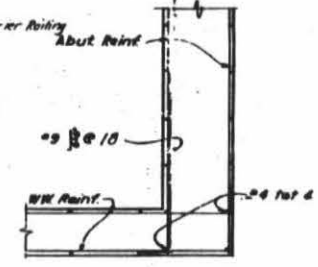

CORNER DETAIL
Scale 1/4" = 1'-0"

OPTION	"A"	"B"	"C"
Concrete Pile	1'-6"	6"	3"
Timber Pile	1'-9"	9"	6"

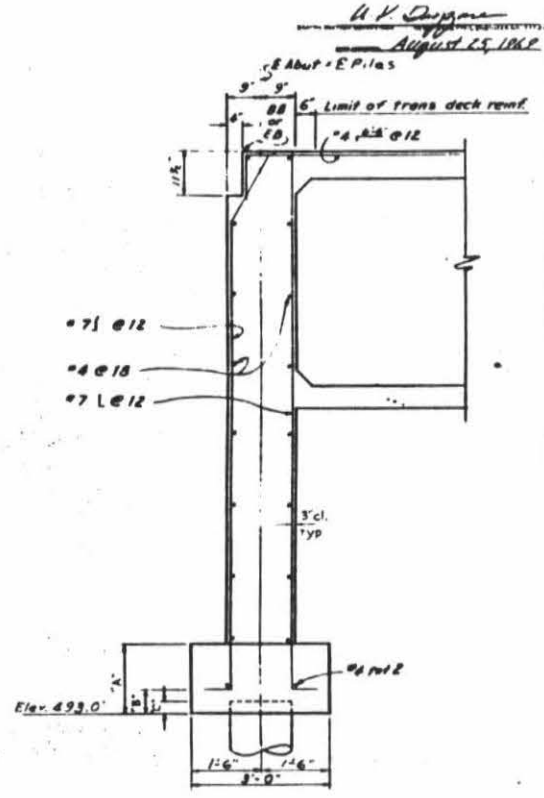

ABUTMENT SECTION
Scale 1/4" = 1'-0"

AS BUILT PLANS
Contract No. 11-029824
Date Completed 7-1-71
Document No. A0009853

NO AS BUILT
CORRECTIONS BY
CONTRACT NO.

DESIGN SECTION 14
Project Engineer O. Bruide.

STATE OF CALIFORNIA
TRANSPORTATION AGENCY
DEPARTMENT OF PUBLIC WORKS
DIVISION OF HIGHWAYS

MELOLAND ROAD OVERCROSSING

ABUTMENT DETAILS

58-215 | 43.6 | 582/5-4 | 4

WO
CU

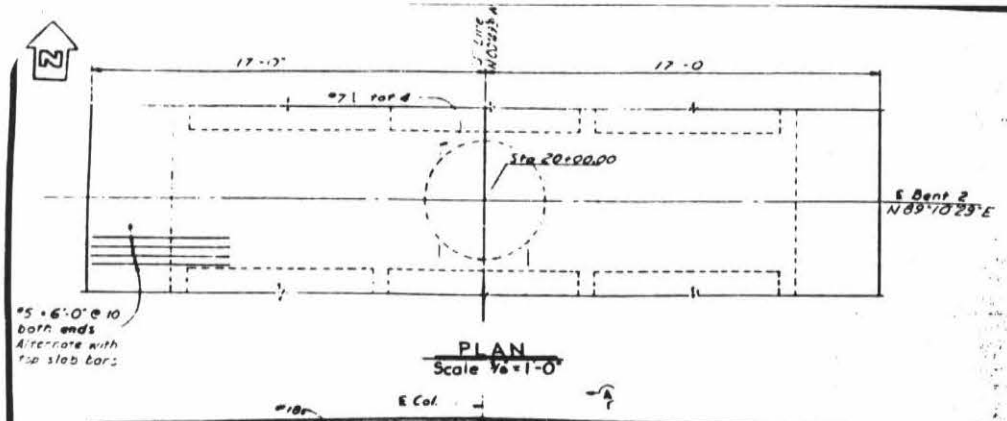

PLAN
Scale 1/8" = 1'-0"

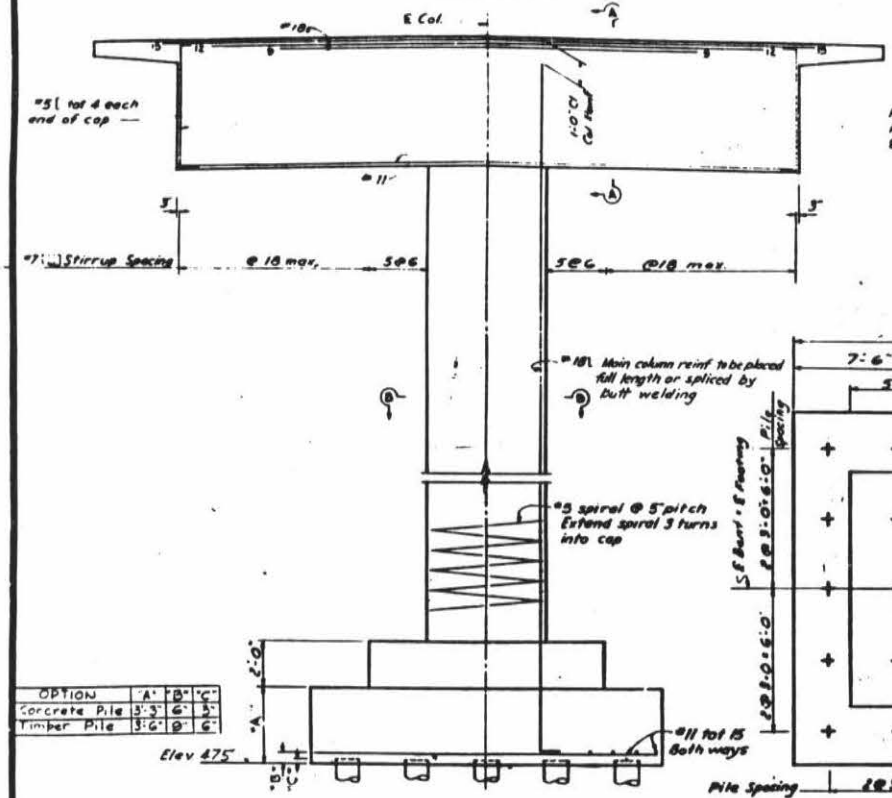

ELEVATION
Scale 1/8" = 1'-0"

Numbers at ends of bars indicate length in feet from E Col.

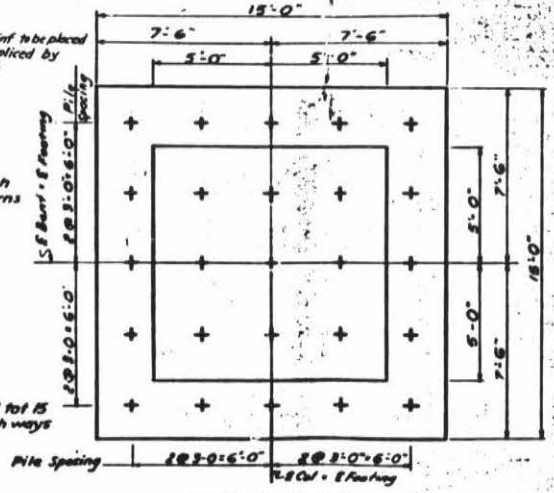

FOOTING PLAN
Scale 1/8" = 1'-0"

Indicates length of #19s

E Bent 2

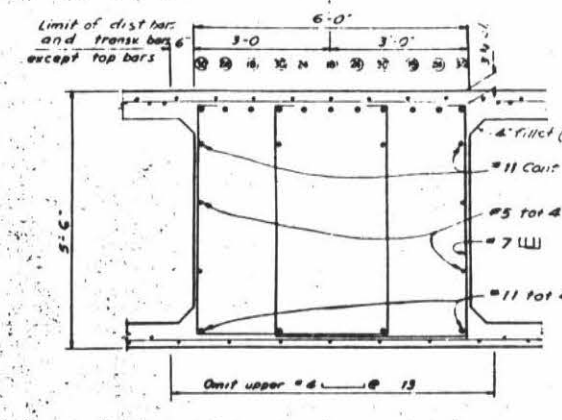

SECTION A-A
Scale 1/8" = 1'-0"

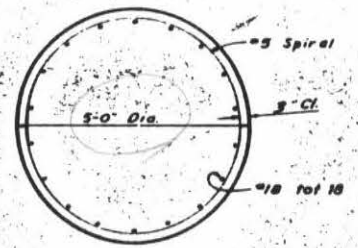

SECTION B-B
Scale 3/4" = 1'-0"

AS BUILT PLANS
Contract No. 11-029824
Date Completed 7-1-71
Document No. A0000858

NO AS BUILT
CORRECTIONS BY
CONTRACT NO.

11	Imv	0	Rec'd PSR 3 8/11

August 25, 1

DESIGN SECTION 14

O. Bender

M.F. Crowley
H.E. Shuck
8-3-60
H.E. Shuck
Ken Johnson

MELOLAND ROAD OVERCROSSING

BENT DETAILS

58-215 | 43.6 | 57215 5 | 5

APPENDIX B

PROCEDURE FOR NONLINEAR STATIC ANALYSIS OF PILE-FOUNDATION SYSTEMS

TABLE OF CONTENTS

Section — Page

1.0 INTRODUCTION 1

2.0 PILE FOUNDATION ELEMENT LOAD-DEFLECTION RELATIONSHIPS 2
- 2.1 PILE HEAD LOAD-DEFLECTION RELATIONSHIPS 2
  - 2.1.1 Estimation of Pile Parameters 2
  - 2.1.2 Computation of t-z Curves 3
  - 2.1.3 Computation of q-z Curve 5
  - 2.1.4 Computation of p-y Curves 6
  - 2.1.5 BMCOL-76 Analysis 8
- 2.2 PILE CAP STIFFNESSES AND CAPACITIES 9
  - 2.2.1 Calculation of Footing Stiffnesses 9
  - 2.2.2 Calculation of Footing Capacities 11

3.0 PILE CAP RESTORING FORCE COMPUTATION 14
- 3.1 INDUCED PILE HEAD DEFLECTIONS 14
- 3.2 PILE HEAD DEFLECTIONS IN LOCAL (BATTERED) COORDINATES 15
- 3.3 PILE HEAD REACTION FORCES 16
- 3.4 BATTER PILE REACTION FORCES 16
- 3.5 FLEXIBILITY OF PILE-CAP TO PILE-HEAD CONNECTION 16
- 3.6 PILE HEAD/PILE CAP CONNECTION CAPACITIES 19
- 3.7 INDUCED PILE CAP REACTION FORCES 19

4.0 MULTI-VARIABLE NEWTON-RAPHSON ROOT FINDING METHOD 20
- 4.1 MATHEMATICAL THEORY 21
- 4.2 APPLICATION TO PILEGRP 21

5.0 REFERENCES 23

Notation 24

STATIC ANALYSIS OF NON-LINEAR PILE FOUNDATION SYSTEMS

1.0 INTRODUCTION

Dames and Moore has developed the computer program PILEGRP to model the behavior of non-linear pile foundation systems at or near maximum load capacity. PILEGRP calculates pile cap deflections and pile head deflections and reaction forces for a given input pile cap loading, configuration, and pile properties. Figure 1.1 shows the sign convention for the PILEGRP model. The origin for the coordinate system is located at the geometric center of the pile cap-pile group system. All pile heads are assumed to lie in the horizontal (x-y) plane. The location of the applied loading and calculated deflections is Point O, at the top of the pile cap, a specified thickness t above the origin on the z-axis.

The pile cap is assumed to be rigid and massless. Each pile is assumed to behave as a linear elastic beam-column supported by a non-linear medium . For purposes of modelling, the resistance of the pile cap is represented by a set on non-linear reaction springs located at Point O. Each pile is modelled by a set of non-linear reaction springs at the location of the pile head.

Evaluation of structural systems with material non-linearity is complicated since it is often difficult to determine the manner in which different structural elements interact with one another. For the analysis herein, a method analogous to linear finite element structural analysis is adopted. The linear method is comprised of three steps, each of which has a non-linear counterpart. First, an element stiffness matrix must be developed for each member in the structural system. In the non-linear system, each component of the stiffness matrix is represented by a non-linear load-deflection relationship, computed as described in Section 2.0. The next step of the linear method is to compute a global stiffness matrix comprised of the stiffness contributions of the structural elements, relating structural deflections to applied forces. In PILEGRP, the structural forces are computed for a given deflection by evaluating the effects of pile batter, pile head/pile cap connection capacity and stiffness, and the geometry of the PILEGRP system (Section 3.0). Finally, the response of a linear system is computed by straightforward inversion of the linear structural stiffness matrix. Structural response of a non-linear system generally cannot be calculated directly, and can only be computed by an iterative method. In PILEGRP, a multi-variate form of the Newton-Raphson method is used to evaluate global structural response (Section 4.0). A flowchart of the PILEGRP program structure is shown in Figure 1.2.

2.0 PILE FOUNDATION ELEMENT LOAD-DEFLECTION RELATIONSHIPS

PILEGRP models the pile cap system as a rigid, massless pile cap supported by non-linear reaction springs representing the piles and the effect of the soil surrounding the pile cap. Reaction springs for the pile heads are evaluated by considering the stiffness properties of the linear elastic pile and the load-deflection properties of the supporting soil mass (Section 2.1). Reaction springs for pile cap proper are modelled by analogy with an equivalent rectangular footing (Section 2.2).

2.1 PILE HEAD LOAD-DEFLECTION RELATIONSHIPS

Individual pile head reaction spring load-deflection relationships are computed at the point where the piles enter the abutment footing. Several steps are involved in this calculation. First, the appropriate parameters of the piles are estimated (Section 2.1.1) and used in the calculation of the so-called t-z (vertical load - vertical deflection), Q-z (tip load - tip deflection), and p-y (lateral load - lateral deflection) curves. Load-deflection relationships are evaluated for the low-strain case by using low-strain soil properties; if high strain relationships are desired, the t-z and p-y curves should be reduced by 50% prior to input to BMCOL-76 (Lam, 1989). Although it is theoretically possible to reduce the pile head load-deflection curves because of pile-soil-pile interaction, this is not done herein because of the difficulty of accurately quantifying these group effects.

The t-z and p-y curves specify the resistances provided by the soil bearing against the pile subjected to vertical and axial loads, and can be visualized as the force-deformation relationships of springs attached to small incremental pile segments comprising the pile. The Q-z curve is simply the force-deflection relationship of the pile tip and end-bearing soils. The calculation of the t-z and Q-z curves is illustrated in Sections 2.1.2 and 2.1.3, respectively; the p-y curve calculation is illustrated in Section 2.1.4. These curves, as well as the stiffness properties of the pile, are input to the computer program BMCOL-76 (Matlock et al, 1981) , which computes the load-deflection curves of the pile head under either the pinned-head or fixed-head condition for pile-head fixity. Similar results are obtained if another commercially avaiable beam-column program, such as COM624, is used.

2.1.1 Estimation of Pile Parameters

The required pile parameters can be calculated or approximated from the known dimensions of the pile. In the calculation of t-z and Q-z curves, the relevant parameters are the pile perimeter, s, and gross cross-sectional area of the pile, A. For the p-y curves, the required parameter is the width of the pile normal to the applied lateral load, D. Also, the BMCOL-76 program requires the stiffness properties, EA and EI, and the length of the pile.

The definitions of these quantities vary slightly for different types of piles, as described below.

If solid circular or rectangular piles are used, the pile parameters are readily defined from the pile geometry. The definitions of s, A, and D may be directly applied to the pile section. In the calculation of the stiffness properties of the pile, the products EA and EI are calculated based on the gross properties of the pile section. Note that for a rectangular section, there may be different values of D and EI for each direction of applied lateral load.

For pipe or H-piles, the definitions of the pile parameters vary. The parameters relating to the calculation of t-z, Q-z, and p-y curves, s, A, and D, are based on gross pile properties. For a pipe pile, these values are calculated for a section equivalent to the outside diameter of the pile. For an H-pile, it is assumed that the soil trapped between the flanges will successfully mobilize the supporting soil mass, so the parameters s, A, and D are calculated based on the properties of a rectangle circumscribing the pile section. The stiffness properties for both pipe and H-piles are calculated based on the area of the pile material, and not the gross section properties.

For composite piles, the parameters s, A, and D are once again based on gross section properties. The stiffness properties EA and EI for the pile can be computed by calculating values of EA and EI for each pile component and summing the contributions. For example, for a pipe pile backfilled with concrete, EA for the pile is computed by calculating EA for the pipe pile section, based on the area of steel in the pile cross-section, then calculating EA for the enclosed circular section of concrete, and finally by adding the results.

Several examples of the appropriate values for s, A, D, and EA are shown in Figure 2.1

2.1.2 Computation of t-z Curves

The procedure for computing the t-z curve was adapted from information in Vijayvergiya (1977), Scott (1981), API-RP2A (1991), and NAVFAC (1986). The general formula relating the axial resistance (force) provided by the soil per unit pile length, t, and vertical pile deflection, z, is (Vijayvergiya, 1977).

$$t = t_{max} \tanh(z / z_{ref}) \qquad (2.1)$$

where t_{max} is the maximum resistance and z_{ref} is a reference deflection. The form of this hyperbolic t-z curve is plotted in Figure 2.2. The parameters, t_{max} and z_{ref}, are computed from the following formulas:

$$t_{max} = f \cdot s \tag{2.2}$$

$$z_{ref} = f / \bar{k} \tag{2.3}$$

where f is the pile-shaft friction in units of stress, s is the equivalent pile perimeter (see Section 2.1), and $\bar{k}$ is a stiffness parameter given by (Scott, 1981),

$$\bar{k} = G\pi / 2s \tag{2.4}$$

In Equation (2.4), G is the low-strain soil shear modulus. As shown in Figure 2.2, the initial slope of the t-z curve is $\bar{k} \cdot s$.

The pile-shaft friction is computed from the following formula in API RP2A (1991):

$$f = \begin{cases} c & (\textit{cohesive soils}) \\ Kp_o \tan\delta & (\textit{cohesionless soils}) \end{cases} \tag{2.5}$$

where

	c	=	undrained shear strength or cohesion of soil,
	K	=	coefficient of lateral earth pressure (ratio of horizontal to vertical normal effective stress),
	p_o	=	effective overburden pressure at point in question, and
	δ	=	friction angle between soil and pile wall.

According to API RP2A (1991),

$$K = \begin{cases} 0.8 & (\textit{open-ended piles}) \\ 1.0 & (\textit{closed-ended or plugged piles}) \end{cases} \tag{2.6}$$

Although values of δ are suggested in API RP2A, the following values are preferred (NAVFAC, 1986)

$$\delta = \begin{cases} 20^\circ \text{ (steel piles)} \\ 0.75\phi \text{ (concrete and timber piles)} \end{cases} \quad (2.7)$$

where ϕ is the friction angle (in degrees) of the cohesionless soil.

2.1.3 Computation of q-z Curve

The procedure for computing the Q-z curve for each pile tip was adapted from information in Vijayvergiya (1977), Scott (1981), API-RP2A (1991), and NAVFAC (1986). This formulation is similar to that for the t-z curves. The general formula relating the resistance (vertical force) provided by soil bearing against the pile tip, Q, and the vertical tip deflection, z, is (Vijayvergiya, 1977)

$$Q = Q_{max} \tanh(z / z_{ref}) \quad (2.8)$$

where Q_{max} is the maximum resistance and z_{ref} is a reference deflection. These parameters are computed from the following formulas:

$$Q_{max} = Aq \quad (2.9)$$

$$z_{ref} = q / \bar{k}_t \quad (2.10)$$

where A is the cross-sectional area of the pile, q is the unit end bearing in units of stress, and $\bar{k}_t$ is a stiffness parameter given by Scott (1981),

$$\bar{k}_t = G\pi / 4s \quad (2.11)$$

The initial slope of the Q-z curve is $\bar{k}_t \cdot A$, as shown in Figure 2.3.

The unit end bearing, q, is given by (API RP2A, 1991),

$$q = \begin{cases} 9c & (cohesive\ soils) \\ p_o N_q & (cohesionless\ soils) \end{cases} \tag{2.12}$$

where c = undrained shear strength,

p_o = effective overburden pressure at the pile tip, and

N_q = dimensionless bearing capacity factor.

Values of N_q as a function of friction angle, ϕ, are provided in Table 2.1, taken from NAVFAC (1986).

For situations where the piles bear on bedrock, the development of Q-z curves is not recommended. In this case, the axial displacement of the pile tip is set equal to zero.

2.1.4 Computation of p-y Curves

The procedure for computing the p-y curves was taken from API RP2A (1991). In this reference, formulas are provided that relate the lateral resistance (load) provided by the soil per unit length of pile, p, and the lateral pile deflection, y. The same functional form used for the t-z and Q-z curves (i.e. Eqns. 2.1 and 2.8), is also used for the p-y curves for sands. A different functional form is used for clays.

p-y Curves for Sands. The general formula for the p-y curve is

$$p = \overline{A} p_u \tanh(y / y_c) \tag{2.13}$$

where: $\overline{A}$ is a factor to account for cyclic or static loading conditions; p_u is the ultimate bearing capacity at depth H and is in units of force/length; and, y_c is a reference length. The parameters $\overline{A}$, p_u, and y_c are computed from the following formulas:

$$\bar{A} = 0.9 \text{ (cyclic or earthquake loads)} \tag{2.14}$$

$$p_u = \min \begin{Bmatrix} (C_1 H + C_2 D) p_o \\ C_3 D p_o \end{Bmatrix} \tag{2.15}$$

$$y_c = \frac{\bar{A} p_u}{kH} \tag{2.16}$$

where: C_1, C_2, and C_3 are functions of friction angle, ϕ, and are plotted in Figure 2.4; D is the average (or equivalent) pile diameter; p_o is the effective overburden pressure at depth H; and, k is the modulus of subgrade reaction in units of force/length^3 and is given in Figure 2.5 as a function of ϕ. For cylindrical piles of constant cross section, D is the outside pile diameter; for tapered cylindrical piles that are fully embedded in the soil, D is the average pile diameter from the pile top to depth, H. For floating tapered piles, D is the average pile diameter from the ground surface to depth, H.

The notation, min { }, in Equation (2.15) for p_u means that the value of p_u to be used is the smaller of the two values obtained from the top and bottom expressions with the { }.

p-y Curves for Clay. The general formula for the p-y curve is

$$p = \begin{cases} 1/2 p_u' (y/y_c)^{1/3}, & y \le 8y_c \\ p_u', & y > 8y_c \end{cases} \tag{2.17}$$

where p_u' is the ultimate resistance in units of force/length of pile, and y_c is a reference length.

The parameters p_u' and y_c are computed from the following formulas:

$$p_u' = \min \begin{Bmatrix} 3cD + p_o D + JcH \\ 9cD \end{Bmatrix} \tag{2.18}$$

$$y_c = 2.5\epsilon_c D \qquad (2.19)$$

where, as before: c is the undrained shear strength; p_o is the effective overburden pressure, H is the depth, and D is the average or equivalent pile diameter. The parameter, J, is a dimensionless empirical constant ranging from 0.25 (soft clays) to 0.5 (medium and stiff clays), and the parameter, ϵ_c is the strain which occurs at one-half the maximum undrained compressive strength. The parameter, ϵ_c , usually ranges between 0.005 and 0.020. In the absence of field or laboratory test data, the values recommended for J and ϵ_c are summarized in Table 2.2.

TABLE 2.2
RECOMMENDED VALUES OF J AND ϵ_c FOR CLAY

CLAY CONSISTENCY	J	ϵ_c
Soft	0.25	0.020
Medium	0.50	0.010
Stiff	0.50	0.005

2.1.5 BMCOL-76 Analysis

In general, it is necessary to develop a relationship between each of the six force quantities and all six of the deflection quantities, 36 relationships in all. Some of these relationships, fortunately, can be eliminated from consideration immediately. For example, resistance of the pile to rotation about its vertical axis (torsion) is considered negligible. Also, there is no interaction among the pile translational force components, e.g. the x- and y-direction force components. Thus, for a generic pile, there are nine load-deflection relationships of interest, given by $F_{x,x}^{F}$, $F_{y,y}^{F}$, $F_{z,z}$, $F_{\theta x,\theta x}$, $F_{\theta y,\theta y}$, $F_{\theta x,y}$, $F_{\theta y,x}$, $F_{x,\theta y}$, and $F_{y,\theta x}$, where the notation $F_{i,j}$ indicates the force component associated with the i degree of freedom when the pile is subjected to deflection associated with the j degree of freedom, and all other degrees of freedom are set to zero, and the superscript F indicates a fixed head (zero rotation) condition. Since PILEGRP considers the case of a flexible connection between the pile cap and pile head, as described in Section 3.5, it is also necessary to develop additional relationships for $F_{x,x}^{P}$ and $F_{y,y}^{P}$, where the superscript P indicates a pinned head condition. If the pile is symmetric, e.g. cylindrical or square, the quantities for the x and y direction are interchangeable, and $F_{y,y}^{F}$, $F_{y,y}^{P}$, $F_{\theta x,\theta x}$, $F_{\theta x,y}$, and $F_{y,\theta x}$ become redundant.

Input for the BMCOL-76 program consists of the pile parameters discussed in Section 2.1.1 and the non-linear soil response springs, i.e. t-z, Q-z, and p-y curves, discussed in Sections 2.1.2, 2.1.3, and 2.1.4, respectively. Input files are prepared for the axial load case, the lateral load case with pinned pile head condition,

the lateral load case with fixed pile head condition, and the lateral moment (swaying) case with lateral deflection set to zero. If the pile is not symmetric about its vertical axis, one set of lateral load input files is required for each direction. Load-deflection curves for response of the pile head are developed by instructing the BMCOL-76 program to evaluate pile response to a sequence of load conditions. A deflection is computed for each applied load, yielding one point on the load-deflection curve. Examples of such load-deflection curves are shown in Figures 2.6-2.10.

2.2 PILE CAP STIFFNESSES AND CAPACITIES

PILEGRP models the pile cap as a footing fully embedded in the surrounding soil. It should be noted that modelling the pile cap as an embedded footing implicitly neglects the presence of the piles. Therefore, it may be appropriate to reduce the stiffness and capacity quantities discussed in this section to account for such effects as settlement of the soil mass away from the base of the pile cap. It is believed that the resistance of the pile cap is adequately modelled by considering only contributions from the pile cap and neglecting other elements such as end- and wingwalls. However, the procedure in Section 3.0 is not limited by this exclusion; reactions due to any additional contributing elements can be considered by including additional reaction springs placed at Point O.

The resistance of the pile cap is modelled by one non-linear reaction spring for each of the six components of deflection. The initial tangent stiffness of each spring is calculated according to the methodology presented in the FHWA report "Seismic Design of Highway Bridge Foundations" (Section 2.2.1). The ultimate capacity of the footing (cap) is computed for each deflection component using the ultimate soil stresses defined in NAVFAC (1986) (Section 2.2.2). Interpolation between the initial and ultimate conditions is performed via a hyperbolic tangent curve that has an initial slope equal to the static stiffness and that approaches the footing capacity for large deflections.

2.2.1 Calculation of Footing Stiffnesses

The theoretical model for estimating the stiffnesses of an embedded footing is taken from pages 40-51 of Volume II of the FHWA (1986) report. The model consists of a rigid massless footing in a linear elastic half space. The elastic properties characterizing the half space are Poisson's Ratio, ν, and shear modulus, G.

The origin of the global coordinate system for the footing is located on the top face of the footing at its geometric center, as for PILEGRP, but the orientation is different from the orientation of the global coordinate system used by PILEGRP for the pile-group stiffness calculations. However, this change in orientation only causes

a change in the stiffness values which represent interaction between the different components of deflection, e.g. horizontal deflection and horizontal moment. These interaction terms are considered negligible for footings supporting abutments and intermediate pier foundations.

The stiffnesses values for an embedded rectangular footing are approximated by (FHWA, 1986)

$$K_i = \alpha_i \cdot \beta_i \cdot K_i^o \tag{2.20}$$

where: K_i^o is the stiffness value of an equivalent circular surface footing, α is a scalar factor that accounts for the shape of the footing, β is a scalar factor that accounts for the embedment of the footing, and the subscript i indicates the ith component of footing deflection.

The values of K_i^o are calculated using the following formulas:

$$\textit{Vertical translation}: \quad K_z^o = \frac{4GR}{1 - \nu} \tag{2.23}$$

$$\textit{Horizontal translation}: \quad K_x^o = K_y^o = \frac{8GR}{2 - \nu} \tag{2.24}$$

$$\textit{Rotation about vertical axis}: \quad K_{\theta z}^o = \frac{16GR_z^3}{3} \tag{2.25}$$

$$\textit{Rotation about x horizontal axis}: \quad K_{\theta x}^o = \frac{8GR_x^3}{3(1 - \nu)} \tag{2.26}$$

$$\textit{Rotation about y horizontal axis: } K^{o}_{\theta y} = \frac{8GR_y^3}{3(1 - \nu)} \qquad (2.27)$$

where R, R_x, R_y, and R_z are the equivalent radii for translation and rotation. The formulas for R are given in Figure 2.11, taken from the aforementioned FHWA (1986) report.

The shape factors, α_i, for the various stiffnesses are plotted as a function of the footing length to width ratio, L/B, in Figure 2.12 (FHWA, 1986). The embedment factors, β_i, are plotted in Figure 2.13 as a function of the footing thickness to equivalent radius ratio (FHWA, 1986). for translational stiffnesses, R is used to compute this ratio; for rotational stiffnesses, $K_{\theta x}$, $K_{\theta y}$, and $K_{\theta z}$, the appropriate values of equivalent radius are R_x, R_y and R_z, respectively (Figure 2.11).

In order to compute the footing stiffness values, values of G and ν for an equivalent half space must be estimated from a soil profile that usually consists of more than one soil layer, each one having different elastic properties. Gazetas (1983) recommends that the values of G and ν at a depth h beneath the bottom of the footing be used for all components of footing deflection, where h is equal to the equivalent radius for translation, i.e.

$$h = R = \left(\frac{4BL}{\pi}\right)^{1/2} \qquad (2.26)$$

where 4BL is the area of the rectangular footing of width 2B and length 2L (see Figure 2.11).

2.2.2 Calculation of Footing Capacities

Footing capacity is computed considering three principal modes of resistance of the supporting soil mass, vertical bearing capacity, passive pressure against the side of the footing, and sliding of the bottom of the footing over the soil mass.

The vertical bearing capacity is given by the following equation from NAVFAC (1986),

$$q_{ult} = cN_c(1 + 0.3\frac{B}{L}) + \gamma tN_q + 0.8\gamma BN_\gamma \quad (2.27)$$

where c is the cohesion of the soil, L and B are the footing half-length and half-width, respectively, t is the depth of embedment or the footing thickness, whichever is less, γ is the unit weight of the soil, and N_c, N_q, and N_γ are dimensionless bearing capacity factors. Values of N_c, N_q, and N_γ as a function of soil friction angle, ϕ, are given in Figure 2.14.

The passive pressure bearing against the side of the footing is given by

$$\sigma_p = \gamma z\tan^2(45 + \frac{\Phi}{2}) + 2c\tan(45 + \frac{\Phi}{2}) \quad (2.28)$$

where z is the depth below the soil surface, or the top of the footing, whichever is less. The force resultant of passive pressure, integrated over the thickness of the footing, is given by

$$P_p = \frac{1}{2}\gamma t^2\tan^2(45 + \frac{\Phi}{2}) + 2ct\tan(45 + \frac{\Phi}{2}) \quad (2.29)$$

where P_p is the passive force per unit length along the footing.

The resistance of the soil mass to sliding of the footing is given by

$$f_{ult} = C + \sigma_z\tan\delta \quad (2.30)$$

where C is the cohesion of the supporting soil, δ is the angle of friction between the footing and the supporting soil mass, and σ_z is the applied vertical stress. σ_z is typically caused by a vertical load applied to the entire cap. Substituting the magnitude of the applied vertical load divided by the area of the footing for σ_z in Equation 2.30,

$$f_{ult} = C + \frac{F_z}{4BL}\tan\delta \quad (2.31)$$

Since it is inconvenient to have the lateral capacity of the footing depend on the value of the axial load

being applied, it is recommended to set F_z equal to that portion of the axial component of load caused by the static (dead) load and carried by the pile cap for use in Equation 2.31. F_z is affected by the presence of the piles and possible gapping between the soil and the base of the pile cap. Typically, F_z is somewhat less than the total vertical load applied to the pilecap/abutement system.

In computing footing capacities from the above ultimate stresses, it is assumed that there is a straight-line distribution of stresses at the interface between the soil and the footing. Capacity is defined as the load at which the soil supporting the footing undergoes incipient failure.

The axial and rocking capacities of the footing can be calculated directly from the footing dimensions and the ultimate bearing capacity, q_{ult}, for the soil. The axial footing capacity is simply the maximum bearing pressure times the area of the footing

$$(F_z)_{max} = 4BLq_{ult} \tag{2.32}$$

Assuming a linear stress distribution in the soil, the moments about the x- and y-axes at incipient bearing failure of the soil are given by

$$(M_x)_{max} = \frac{4}{3}BL^2q_{ult} \tag{2.33}$$

$$(M_y)_{max} = \frac{4}{3}LB^2q_{ult} \tag{2.34}$$

The lateral and torsional capacities of the footing are computed from the footing dimensions and the calculated values of P_p and f_{ult}. The lateral force capacity of the footing consists of a passive pressure component, equal to the magnitude of the passive pressure diagram resultant, P_p, times the width of the footing perpendicular to the load, and a sliding component, equal to the ultimate shear stress at the base of the footing times the area of the footing. Mathematically, the two lateral force capacities are expressed as

$$(F_x)_{max} = 2LP_p + 4BLC + F_z\tan\delta \tag{2.35}$$

$$(F_y)_{max} = 2BP_p + 4BLC + F_z\tan\delta \qquad (2,36)$$

where F_z is numerically equal to the static dead load, as mentioned above.

Similarly, the torsional moment capacity of the footing consists of a component due to passive pressure and a component due to sliding. The torsional moment at incipient soil failure is given by

$$(M_z)_{max} = \frac{4}{3}P_p(B^2 + L^2) + \frac{1}{3}\sqrt{B^2 + L^2}[4BLC + F_z\tan\delta] \qquad (2.37)$$

It should be noted that there is interaction between the axial and rocking capacities and between the lateral and torsional capacities. For example, the maximum moment which the footing can support is reduced in the presence of axial load. This effect is not considered herein, although defining capacity using an incipient failure criterion will compensate for this omission by slightly underpredicting the rocking and torsional capacities of the footing.

3.0 PILE CAP RESTORING FORCE COMPUTATION

The computation of pile cap reaction forces arising from a given pile cap deflection is completed by executing the following procedure for each pile in the pile group. First, the 6-components of pile head deflection are calculated from the pile cap deflection vector and the location of the pile with respect to the Point O (Section 3.1). If the pile is battered, the pile head deflection vector in global coordinates is transformed into local coordinates for the equivalent vertical pile (Section 3.2). The pile-head restoring force vector is then computed from the non-linear load-deflection curves estimated for the pile head as specified in Section 2.1. The pile-head force vector in local pile coordinates is then transformed back into global coordinates, if necessary (Section 3.4). Adjustments are made for the flexibility (Section 3.5) and capacity (Section 3.6) of the pile head/pile cap connection. Finally, pile group forces are calculated by summing the force and moment contributions of the individual piles and of the pile cap (Section 3.7).

3.1 INDUCED PILE HEAD DEFLECTIONS

Since the pile cap is considered rigid, it is possible to compute the deflections of a pile head, given the 6-

component deflection vector for the pile cap and the location of the pile head with respect to Point O. Translational and rotational deflections of the pile cap may be transferred directly to the pile heads. Unless the pile head is located at Point O, rotations of the pile cap induce an additional component of translation at the pile head equal in magnitude to the cap rotation times the moment arm. The relationships can be expressed in the following form

$$\underline{X}_{CAP} = \begin{bmatrix} U \\ V \\ W \\ \Theta_x \\ \Theta_y \\ \Theta_z \end{bmatrix} \text{----------} > \underline{X}_{PILE} = \begin{bmatrix} U - t\Theta_y - y_P\Theta_z \\ V + t\Theta_x + x_p\Theta_z \\ W + y_p\Theta_x - x_p\Theta_y \\ \Theta_x \\ \Theta_y \\ \Theta_z \end{bmatrix} \quad (3.1)$$

where $\underline{X}_{CAP}$ and $\underline{X}_{PILE}$ indicate deflections of the pile cap and pile head, respectively, x_p and y_p represent the location of the pile head with respect to Point O, t is the height above the origin of Point O, and the arrow indicates induced deflections.

3.2 PILE HEAD DEFLECTIONS IN LOCAL (BATTERED) COORDINATES

Pile head load-deflection characteristics may be readily calculated for a vertical pile, as described in Section 2.1. For battered piles, the load deflection relations are evaluated by subjecting the computed vertical relationships to a coordinate transformation. In PILEGRP, a local coordinate system for the vertical pile is defined as follows; the local x-axis corresponds to one direction in the horizontal plane (longitudinal), the local y-axis is perpendicular to the x-axis in the horizontal plane (transverse), and the local z-axis is parallel to the vertical axis of the pile.

The transformation between this local coordinate system and the global pile cap system is fully defined by the following two parameters:

α = the angle in the horizontal plane between the global x-axis of the pile cap and the plane of batter of the pile (x-z plane in the local coordinate system)

ϕ = the angle between the global z-axis of the pile cap and the local z-axis of the battered pile

This relationship is shown graphically in Figure 3.1, where the angles α and ϕ are positive as shown.

Deflections at the pile head in global pile cap coordinates, represented by $\underline{X}_{PILE}$, can be transformed into

local pile coordinates via the following transformation.

$$\begin{bmatrix} u \\ v \\ w \\ \theta_x \\ \theta_y \\ \theta_z \end{bmatrix} = \begin{bmatrix} \cos\phi\cos\alpha & \cos\phi\sin\alpha & -\sin\phi & 0 & 0 & 0 \\ -\sin\alpha & \cos\alpha & 0 & 0 & 0 & 0 \\ \sin\phi\cos\alpha & \sin\phi\sin\alpha & \cos\phi & 0 & 0 & 0 \\ 0 & 0 & 0 & \cos\phi\cos\alpha & \cos\phi\sin\alpha & -\sin\phi \\ 0 & 0 & 0 & -\sin\alpha & \cos\alpha & 0 \\ 0 & 0 & 0 & \sin\phi\cos\alpha & \sin\phi\sin\alpha & \cos\phi \end{bmatrix} \begin{bmatrix} U \\ V \\ W \\ \Theta_x \\ \Theta_y \\ \Theta_z \end{bmatrix} \quad (3.2)$$

Equation 3.2 can alternatively be written as $\underline{x}_{PILE} = \Lambda * \underline{X}_{PILE}$.

3.3 PILE HEAD REACTION FORCES

Reaction forces at the head of each pile, or equivalent vertical pile, for battered piles, in local vertical pile coordinates are computed by linearly interpolating the discrete load-deflection curves developed in Section 2.1. This process results in one complete 6-component force vector at the head of each pile for both pinned and fixed conditions.

3.4 BATTER PILE REACTION FORCES

If a pile is battered, it is necessary to transform the pile head forces (moments) for a vertical pile from the local (vertical) coordinate system to the global pile cap coordinate system. This is achieved by inverting Equation 3.2.

It is important to note that Equation 3.2 applies to forces as well as displacements and that Λ, being a coordinate rotation matrix, is orthogonal. This implies that the inverse of Λ is its transpose, i.e. $\Lambda^{-1} = \Lambda^{T}$. Therefore, we have the relationship between pile head forces in the local coordinate system $\underline{f}_{PILE}$ and pile head forces in the global coordinate system $\underline{F}_{PILE}$ given by

$$f_{PILE} = \Lambda F_{PILE} \quad (3.3)$$

and the inverse of this relationship given by

$$E = \Lambda^T f_{PILE} \tag{3.4}$$

Equation 3.4 is directly applied to the pile head forces in order to effect the required transformation.

3.5 FLEXIBILITY OF PILE-CAP TO PILE-HEAD CONNECTION

Equations governing the force transfer from a pile head to a pile cap via a flexible moment connection are derived through analogy with a similar linear elastic system. In the analogous system, the pile is replaced with a prismatic cantilever of stiffness EI and length L. The connection between the pile head and pile cap is modelled as a linear elastic rotational spring of stiffness K_o placed between the location of moment application (pile cap) and the end of the cantilever (pile head). A graphical representation of the model is shown in Figure 3.2. The three degrees of freedom indicated in Figure 3.2 are the lateral deflection (shear) of the cantilever, rotation of the end of the cantilever, and rotation of the free end of the rotational spring. From finite element theory, the stiffness matrix for this system is given by,

$$\begin{bmatrix} P \\ M_1 \\ M \end{bmatrix} = \begin{bmatrix} 12EI/L^3 & -6EI/L^2 & 0 \\ -6EI/L^2 & 4EI/L + K_o & -K_o \\ 0 & -K_o & K_o \end{bmatrix} \begin{bmatrix} u \\ \theta_1 \\ \theta \end{bmatrix} \tag{3.5}$$

Since in the pile cap model the applied moment is located at the pile head/pile cap connection, rather than at the pile head, we wish to eliminate the degree of freedom associated with the pile head (end of cantilever) moment. Application of static condensation (Holzer, 1985) yields the following reduced stiffness matrix

$$\begin{bmatrix} P \\ M \end{bmatrix} = \begin{bmatrix} 12EI/L^3 & \dfrac{1 + K_oL/EI}{4 + K_oL/EI} & -6EI/L^2 & \dfrac{K_oL/EI}{4 + K_oL/EI} \\ -6EI/L^2 & \dfrac{K_oL/EI}{4 + K_oL/EI} & 4EI/L & \dfrac{K_oL/EI}{4 + K_oL/EI} \end{bmatrix} \begin{bmatrix} u \\ \theta \end{bmatrix} \tag{3.6}$$

It is noted that each of the terms in the new stiffness matrix is defined in terms of the elements of the simple cantilever stiffness matrix and the ratio K_oL/EI. It is further noted that the term EI/L is the rotational stiffness of a cantilever which is allowed to deflect freely. Therefore, the quantity K_oL/EI can be interpreted as the

ratio of the stiffness of the connection spring to the stiffness of the cantilever. Since the numerical value of the connection spring stiffness K_o often cannot be calculated directly, and must be set to infinity for the fixed condition, it is convenient to define the quantity

$$R = \frac{\frac{K_o L}{EI}}{4 + \frac{K_o L}{EI}} \tag{3.7}$$

where R is the ratio of the moment at the connection for a fixed condition to the moment at the connection for a flexible condition. This "fixity ratio" varies from R=0 (pinned condition) to R=1 (fixed condition). The reduced stiffness matrix is now given by,

$$\begin{bmatrix} P \\ M \end{bmatrix} = \begin{bmatrix} \frac{3EI}{L^3}(1-R) + \frac{12EI}{L^3}R & \frac{-6EI}{L^2}R \\ \frac{-6EI}{L^2}R & \frac{4EI}{L}R \end{bmatrix} \begin{bmatrix} u \\ \theta \end{bmatrix} \tag{3.8}$$

Thus, it is possible to represent the stiffness properties of the spring-cantilever system rather simply in terms of the properties of the simple cantilever, which are known, and the fixity ratio R which can easily be calculated or estimated. The above analysis applies to any system in which the load-deflection relationships are linear elastic and contains no simplifying assumptions regarding the model shown in Figure 3.2; the solution is exact.

In order to apply Equation 3.8 to a system in which the load-deflection relationships are non-linear, we first carry out the implied matrix multiplication and collect terms,

$$\begin{aligned} P &= \left[\frac{3EI}{L^3}u\right](1-R) + \left[\frac{12EI}{L^3}u - \frac{6EI}{L^2}\theta\right]R \\ M &= \left[\frac{-6EI}{L^2}u + \frac{4EI}{L}\theta\right]R \end{aligned} \tag{3.9}$$

The bracketed quantities in Equation 3.9 may be interpreted as force quantities calculated for the limiting fixed and pinned head conditions. To cast Equation 3.9 in a form which can be applied to non-linear analysis, we rewrite these force terms as

$$\begin{aligned} P &= P^P(u)\,(1-R) + P^F(u,\theta)\,R \\ M &= M^F(u,\theta)\,R \end{aligned} \qquad (3.10)$$

where $P^P(u)$ represents the pinned-head pile force corresponding to the deflection u and $P^F(u,\theta)$ and $M^F(u,\theta)$ represent the fixed-head pile force and moment, respectively, which are induced by the deflection u and rotation θ. Note that, since the fixed-head force and moment quantities are functions of u and θ, it is possible to include interaction effects between force and rotation, or moment and deflection, at this time.

If the construction of the pile head/pile cap connection is well understood, the fixity ratio can be calculated by substituting values of K_o, which is computed from the properties of the connection, and EI/L, which is approximated by the initial slope of the moment-rotation curve for the unrestrained pile head, into Equation 3.7. If a value of K_o cannot be calculated directly, the value of the fixity ratio may subjectively estimated to lie in the range R=0 (pinned) to R=1 (fixed). The resulting fixity ratio applies only to moment fixity in the horizontal plane of the global coordinate system. Equation 3.10 should be used only after the modifications dealing with batter effects have been applied to the load-deflection curves from Section 2.1.

3.6 PILE HEAD/PILE CAP CONNECTION CAPACITIES

After all adjustments have been made to account for batter and connection flexibility effects, a check is made of pile connection capacity. Capacities for four different failure modes are evaluated, punching failure of the pile cap, pull-out of the pile head from the pile cap, and moment failure at the pile head/pile cap connection about both horizontal axes.

If punching failure occurs, it is assumed that the pile cap has suffered a severe loss of structural integrity, and is no longer able to transfer moment about either of the horizontal axes to the pile head. Likewise, pull-out failure is assumed to indicate a loss of moment capacity in both horizontal directions. Moment failure is interpreted as an indication that the tensile capacity of the pile head/pile cap connection has been exceeded, implying that no tensile forces can be transferred to the pile head. Compressive forces, however, are unaffected.

Failure conditions are evaluated by checking that each component of the force vector lies within an acceptable range. Due to modelling difficulties, force interaction between load conditions is neglected, i.e. coupling between axial load and bending moment. Failure modes are assumed to be brittle; there is no residual strength in the connection components which have failed.

3.7 INDUCED PILE CAP REACTION FORCES

Performing a procedure similar to that described in Section 3.1, the reaction forces and moments induced at Point O by the reaction forces applied at the pile head can be evaluated. The forces and moments may be translated directly from the pile head to Point O, while an additional moment is generated by the pile head forces, equal in magnitude to the reaction force times the moment arm. This relationship is given by

$$\underline{F}_{PILE} = \begin{bmatrix} F_X \\ F_y \\ F_z \\ M_x \\ M_y \\ M_z \end{bmatrix} \text{----------} > \underline{F}^{O}_{PILE} = \begin{bmatrix} F_x \\ F_y \\ F_z \\ M_x + y_p F_x + tF_y \\ M_y - x_p F_x - tF_x \\ M_z + x_p F_y - y_p F_x \end{bmatrix} \quad (3.11)$$

where $\underline{F}_{PILE}$ and $\underline{F}^{O}_{PILE}$ indicate force vectors at the pile head and Point O, respectively. The force vector induced at Point O by the entire pile group is simply the summation of the $\underline{F}^{O}_{PILE}$ terms for each pile.

The reaction force vector for the entire pile cap system is the sum of the contributions of the pile group and the pile cap itself. The pile cap is modelled as an equivalent rectangular footing as discussed in Section 2.2. Since the origin of the equivalent footing is defined at the same point as the pile cap deflections, Point O, computation of the six- component reaction force vector for the pile cap involves only evaluating the load-deflection curves developed in Section 2.2 at the deflection components of $\underline{X}_{CAP}$.

4.0 MULTI-VARIABLE NEWTON-RAPHSON ROOT FINDING METHOD

Pile foundation displacement under applied loading is evaluated by numerically inverting the method described in Section 3.0; this step in the analysis is analogous to inverting the stiffness matrix of a linear structural system. The

procedure in Section 3.0 can be expressed as the computation of induced foundations loads, $\underline{F}_{CAP}$, as a function of pile cap displacement, $\underline{X}_{CAP}$. It is possible to find the displacement $\underline{X}_{CAP}$ corresponding to the foundation loading $\underline{F}^*$ by iteratively solving for the root of $\underline{F}_{CAP}(\underline{X}_{CAP}) - \underline{F}^* = 0$. In the PILEGRP program, foundation response is evaluated using the multi-variate Newton-Raphson method. The theory of this method is an extension of the well-known single-variable Newton's method (Section 4.1). The particulars of the application to PILEGRP are described in Section 4.2.In the PILEGRP program, foundation response is evaluated using the multi-variate Newton-Raphson method. The theory of this method is an extension of the well-known single-variable Newton's method (Section 4.1). The particulars of the application to PILEGRP are described in Section 4.2

4.1 MATHEMATICAL THEORY

In the single variable case, the Newton-Raphson method can be used to find a solution to the equation g(x) = 0 as follows; (1) an initial estimate of x is made (x^0), (2) the function g(x) and its derivative g'(x) are evaluated for $x = x^0$, (3) by assuming that the shape of the function g(x) at $x=x^0$ is similar to the tangent line, a second approximation of the root (x^1) is computed at the root of the tangent line, and (4) using x^1 in place of x^0, return to step (2), iterating until the desired tolerance is reached. Figure 4.1 shows a graphical representation of this procedure. Mathematically, the Newton-Raphson method can be written as

$$x^{i+1} = x^i - \frac{g(x^i)}{g'(x^i)}$$
$$g'(x^i)\,(x^{i+1}-x^i) = -g(x^i) \qquad (4.1)$$

where the superscripts i and i+1 indicate that values are appropriate at the i^{th} and $(i+1)^{th}$ iteration, respectively.

In the multi-variable case, x and f are replaced by the vectors $\underline{X}$ and $\underline{G}$, respectively, where the components X_j of $\underline{X}$ are scalar constants and the components G_j of $\underline{G}$ are scalar functions of one or more components of $\underline{X}$. The derivative of the scalar function g(x), given by g'(x), is replaced by the Jacobian matrix J, where the components J_{ij} of J are given by

$$J_{ij} = \frac{\partial G_i}{\partial X_j} \qquad (4.2)$$

The multi-variable analogy to Equation 4.1 is given by

$$J(X^{i+1})\ (X^{i+1} - X^i) = - G(X^i) \tag{4.3}$$

4.2 APPLICATION TO PILEGRP

The PILEGRP program applies Equation 4.3 directly to invert the solution presented in Section 3.0. For the pile cap model used thus far, the function $\underline{F}_{CAP} - \underline{F}^*$, where $\underline{F}_{CAP}$ is the cap reaction force corresponding to the deflection $\underline{X}$ and $\underline{F}^*$ is the applied load vector, is the dependent variable $\underline{G}$ in Equation 4.3 and the displacement vector for the pile cap is the independent variable $\underline{X}$. The equation which must, therefore, be solved at each iteration step is

$$J\ (X^i)\ (X^{i+1} - X^i) = - (F_{CAP}(X_i) - F^*) \tag{4.4}$$

Note that the term $(\underline{X}^{i+1} - \underline{X}^i)$ can be interpreted as the incremental deflection vector, the right-hand side term $(\underline{F}_{CAP}(\underline{X}^i) - \underline{F}^*)$ can be interpreted as an incremental load vector, and the Jacobian of the function $\underline{G}(\underline{X})$ can be interpreted as a stiffness of the pile cap at the deflection $\underline{X}$. Thus, the non-linear pile cap deflection problem can be reduced to a series of linear problems.

Since expressions for the components of $\underline{F}_{CAP}(\underline{X}^i)$ do not exist in closed form, the partial derivatives which make up the Jacobian must be estimated by numerical methods. The components J_{ij} of J are approximated by the finite difference approximation

$$J_{ij} = \frac{\left[(F_{CAP})_i\ (X^i + \Delta_j\ \underline{e}_j) - (F_{CAP})_i\ (X^i - \Delta_j\ \underline{e}_j)\right]}{2\Delta_j} \tag{4.5}$$

where $\underline{e}_j$ represents a vector with all zeroes, except for a 1 in the j^{th} position, e.g.
$\underline{e}_2 = (0, 1, 0, 0, 0, 0)^T$, and Δ_j is a small scalar quantity used to perturb the solution $\underline{F}_{CAP}(\underline{X}^i)$. It is necessary to define distinct Δ_j for different components of deflection of the pile cap due to the large disparity in the magnitudes of translations and rotations. The values of Δ_j have been arbitrarily chosen to be approximately two orders of

magnitude smaller than the values of corresponding displacements which can be reasonably expected.

Iteration is said to have converged when the quantity $|\underline{X}^{i+1} - \underline{X}^{i}|/|\underline{X}^{i}| < \epsilon$ or $|\underline{F}_{CAP}(\underline{X}^{i})-\underline{F}^{*}|/|\underline{F}^{*}| < \epsilon$, where the notation $|\underline{x}|$ indicates the magnitude of the vector $\underline{x}$ and ϵ is a specified tolerance.

5.0 REFERENCES

API RP 2A, 1991, "API Recommended Practice for Planning, Designing and Constructing Fixed Offshore Platforms," 19th edition, American Petroleum Institute, Washington, D.C.

Gazetas, G., 1991, "Foundation Vibrations," Foundation Engineering Handbook, 2nd Edition, H.Y.Fang, ed, Van Nostrand Reinhold, pp. 553-593.

Holzer, S.M., 1985, Computer Analysis of Structures: Matrix Structural Analysis Structured Programming, Elsevier Science Publishing Co., Inc., pp. 196-214.

Lam, I.P., 1989, Personal Communication.

Lam, I.P., and G.R. Martin, 1986, "Seismic Design of Highway Bridge Foundations," FHWA Report Nos. FHWA/RD-861, FHWA/RD-86/102, FHWA/RD-86/103.

Matlock, H., Bogard, D., and Lam, I.P., 1981, "BMCOL 76: A Compute Program for the Analysis of Beam Columns Under Static Axial and Lateral Loading," In-House Documentation Report, Ertec, Inc., June.

NAVFAC, 1986, "Foundations and Earth Structures," NAVFAC DM 7.02, Dept. of Navy.

Wang, S., and Reese, L., "Analysis of Piles Under Lateral Load - Computer Program COM624P for the Microcomputer," FHWA Report No. FHWA-SA-91-002.

Scott, R.F., 1981, Foundation Analysis, Prentice-Hall.

Vijayvergiya, V.N., "Load-Movement Characteristics of Piles," Paper presented in the Port 77 Conference, Long Beach, CA, March 1977.

Notation

α, ϕ	pile batter parameters
α_i	footing stiffness shape factor
β_i	footing stiffness embedment factor
γ	unit weight of soil
δ	soil-foundation element friction angle
Δ_j	finite difference quantity used to estimate derivatives of pile cap force component j
ϵ	convergence criteria for root-solving routine
ϵ_c	clay parameter equal to the strain at one-half the maximum deviator stress in the undrained triaxial test
θ_x, θ_y, θ_z	local coordinate system components of pile head rotation in x-, y-, and z-directions, respectively
Θ_x, Θ_y, Θ_z	global coordinate system components of pile head rotation in x-, y-, and z-directions, respectively
Λ	transformation matrix from global to local (battered) pile coordinates
ν	Poisson's ratio of soil
σ_z	passive pressure of soil mass
ϕ	soil friction angle
A	cross-sectional area of pile
	cyclic loading factor for p-y curves in sand
B	footing half-width
c	undrained shear strength of cohesive soil
C_a	adhesion between base of footing and supporting soil mass
C_1,C_2,C_3	p-y parameters for sands
D	pile diameter
E	Young's modulus of pile
$\underline{e}_j$	j^{th} column of the identity matrix
f	pile shaft friction
f_{ult}	maximum shear resistance of soil beneath footing
$\underline{f}_{PILE}$	vector of pile head forces, in local (battered) coordinates
$\underline{F}^*$	applied pile cap load vector
$\underline{F}_{CAP}$	vector of pile cap reaction forces
$F_{i,j}$	relationship between force component i and deflection component j
$\underline{F}_{PILE}$	vector of pile head forces, in global coordinates
$\underline{F}^O_{PILE}$	vector of forces induced at Point O by forces at the pile head
G	shear modulus of soil
h	depth of representative soil properties
H	depth below the soil surface
I	moment of inertia of pile
J	dimensionless clay parameter
J	Jacobian matrix
$\bar{k}_t$	pile tip stiffness parameter
k	soil modulus of subgrade reaction
K	coefficient of lateral earth pressure
K_o	rotational stiffness of pile head/pile cap connection
L	footing half-length
N_c, N_q, N_γ	dimensionless bearing capacity factors
p	lateral resisting force per unit length of pile

p_o	soil overburden pressure
p_u, p_u'	ultimate lateral resistance per unit length of pile for sands and clays, respectively
P_p	passive pressure resultant
q	unit end bearing pressure
Q	axial resistance of the pile tip
Q_{max}	ultimate axial resistance of the pile tip
q_{ult}	ultimate vertical bearing capacity of soil mass
R	fixity ratio for pile head/pile cap connection
R, R_x, R_y, R_z	equivalent radius for rectangular footing
s	pile perimeter
t	pile cap thickness
t	axial resistance per unit length of pile
t_{max}	ultimate axial resistance of pile shaft per unit length of pile
u, v, w	local coordinate system components of pile head deflection in x-, y-, and z-directions, respectively
U, V, W	global coordinate system components of pile head deflection in x-, y-, and z-directions, respectively
x_p, y_p	pile head location with respect to Point O
$\underline{x}_{PILE}$	pile head displacement in local (battered) coordinates
$\underline{X}_{CAP}$	pile cap displacement
$\underline{X}_{PILE}$	pile head displacement in global coordinates
y	lateral displacement of pile
y_c	reference lateral displacement of pile
z	axial displacement of pile
z_{ref}	reference axial displacement of pile

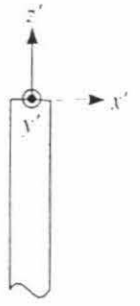

LOCAL COORDINATE SYSTEM

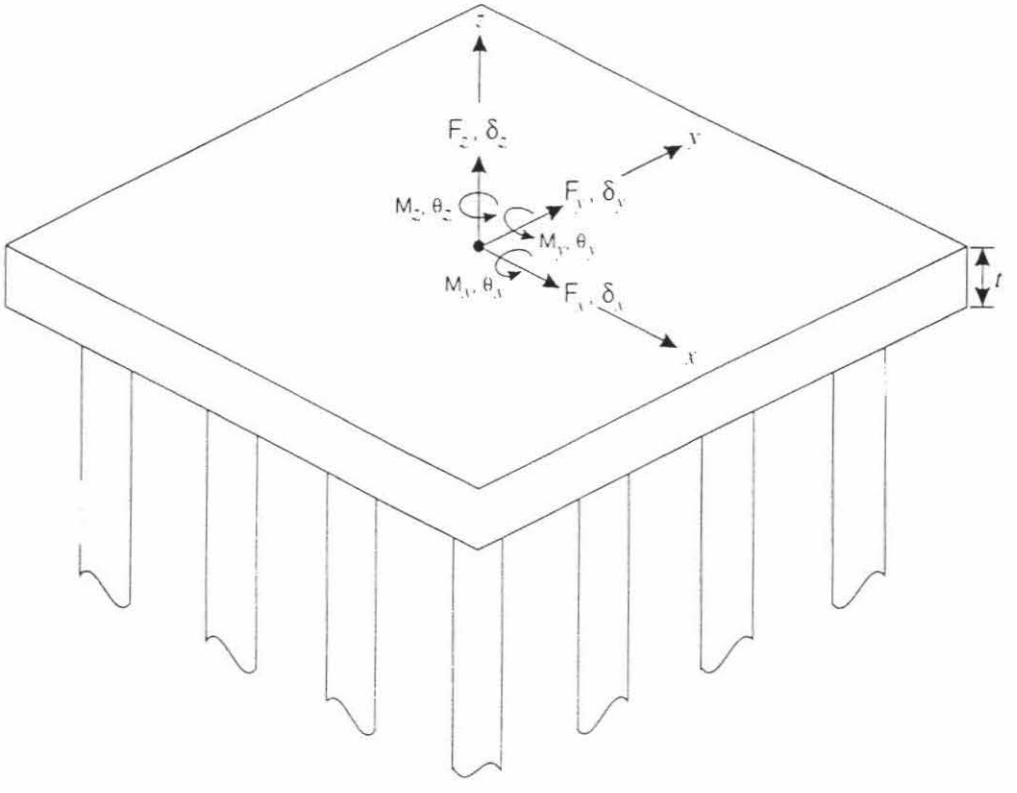

GLOBAL COORDINATE SYSTEM

Figure 1.1

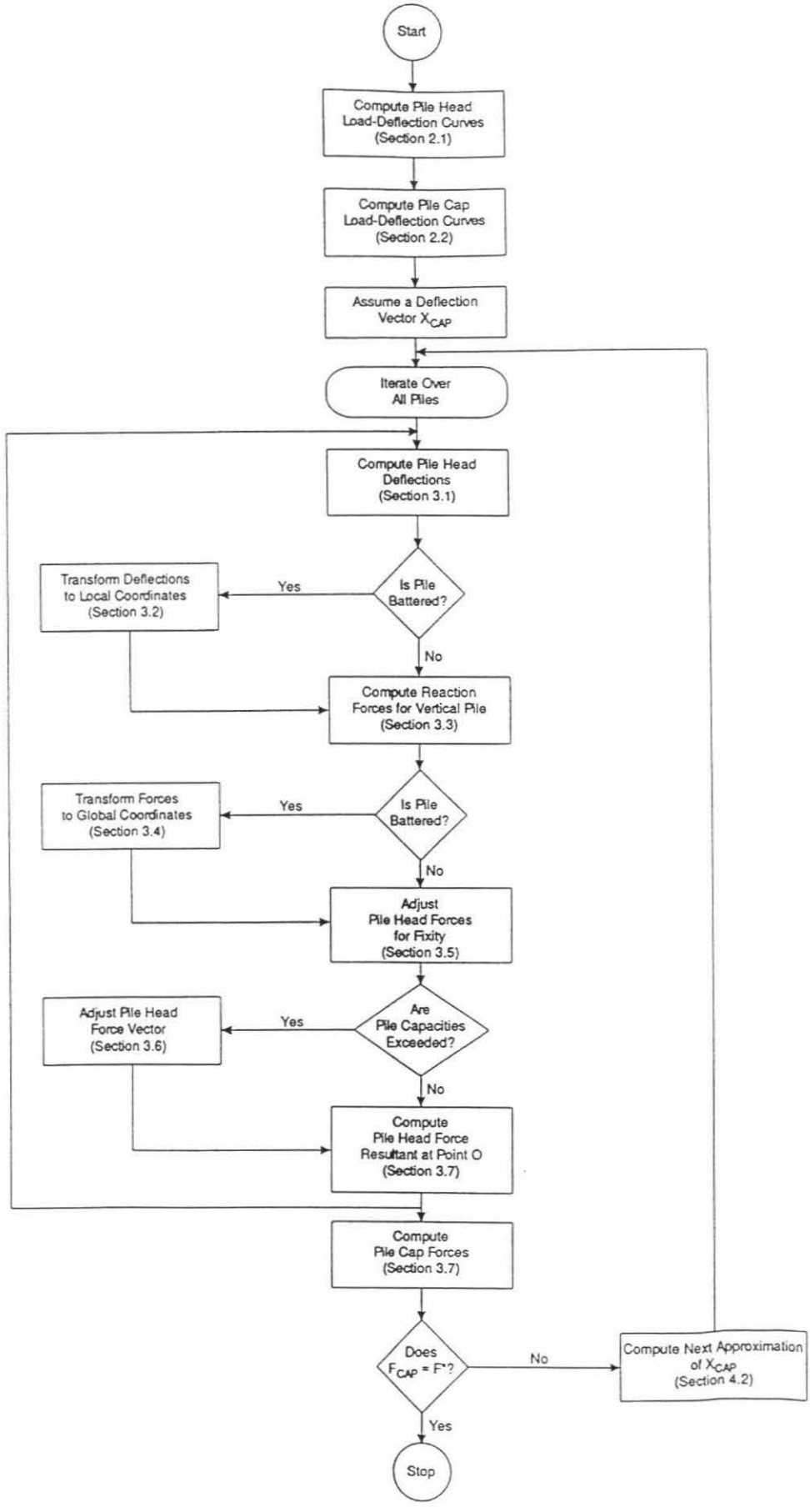
Start
Compute Pile Head Load-Deflection Curves (Section 2.1)
Compute Pile Cap Load-Deflection Curves (Section 2.2)
Assume a Deflection Vector X_{CAP}
Iterate Over All Piles
Compute Pile Head Deflections (Section 3.1)
Is Pile Battered?
Yes
Transform Deflections to Local Coordinates (Section 3.2)
No
Compute Reaction Forces for Vertical Pile (Section 3.3)
Is Pile Battered?
Yes
Transform Forces to Global Coordinates (Section 3.4)
No
Adjust Pile Head Forces for Fixity (Section 3.5)
Are Pile Capacities Exceeded?
Yes
Adjust Pile Head Force Vector (Section 3.6)
No
Compute Pile Head Force Resultant at Point O (Section 3.7)
Compute Pile Cap Forces (Section 3.7)
Does $F_{CAP} = F'$?
No
Compute Next Approximation of X_{CAP} (Section 4.2)
Yes
Stop

Figure 1.2

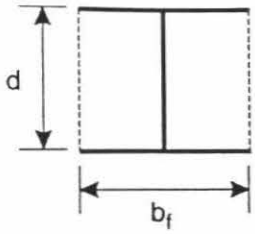

$S = 2(b_f + d)$
$A = b_f d$
$D_1 = b_f$
$D_2 = d$

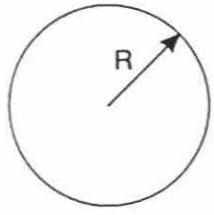

$S = 2\pi R$
$A = \pi R^2$
$D = 2R$

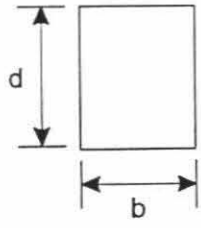

$S = 2(b + d)$
$A = bd$
$D_1 = b$
$D_2 = d$

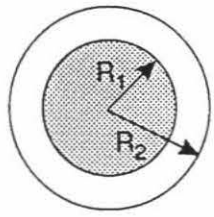

$S = 2\pi R_2$
$A = \pi R^2_2$
$d = 2R_2$

$$(EA)_{PILE} = (EA)_{CONC} + (EA)_{STEEL}$$
$$= E_{CONC}\pi R_1^2 + E_{STEEL}\pi(R_2^2 - R_1^2)$$

Figure 2.1

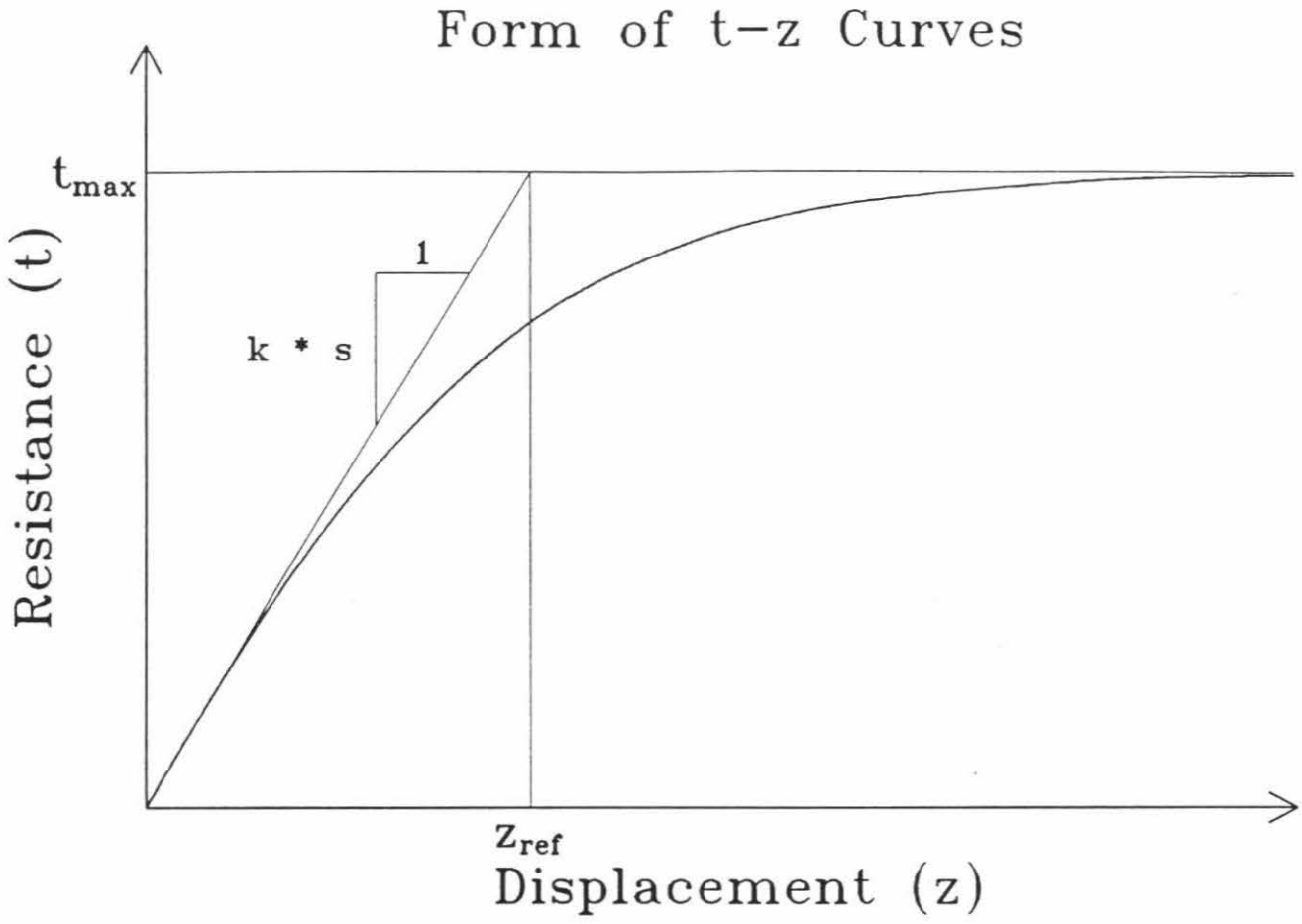

Figure 2.2

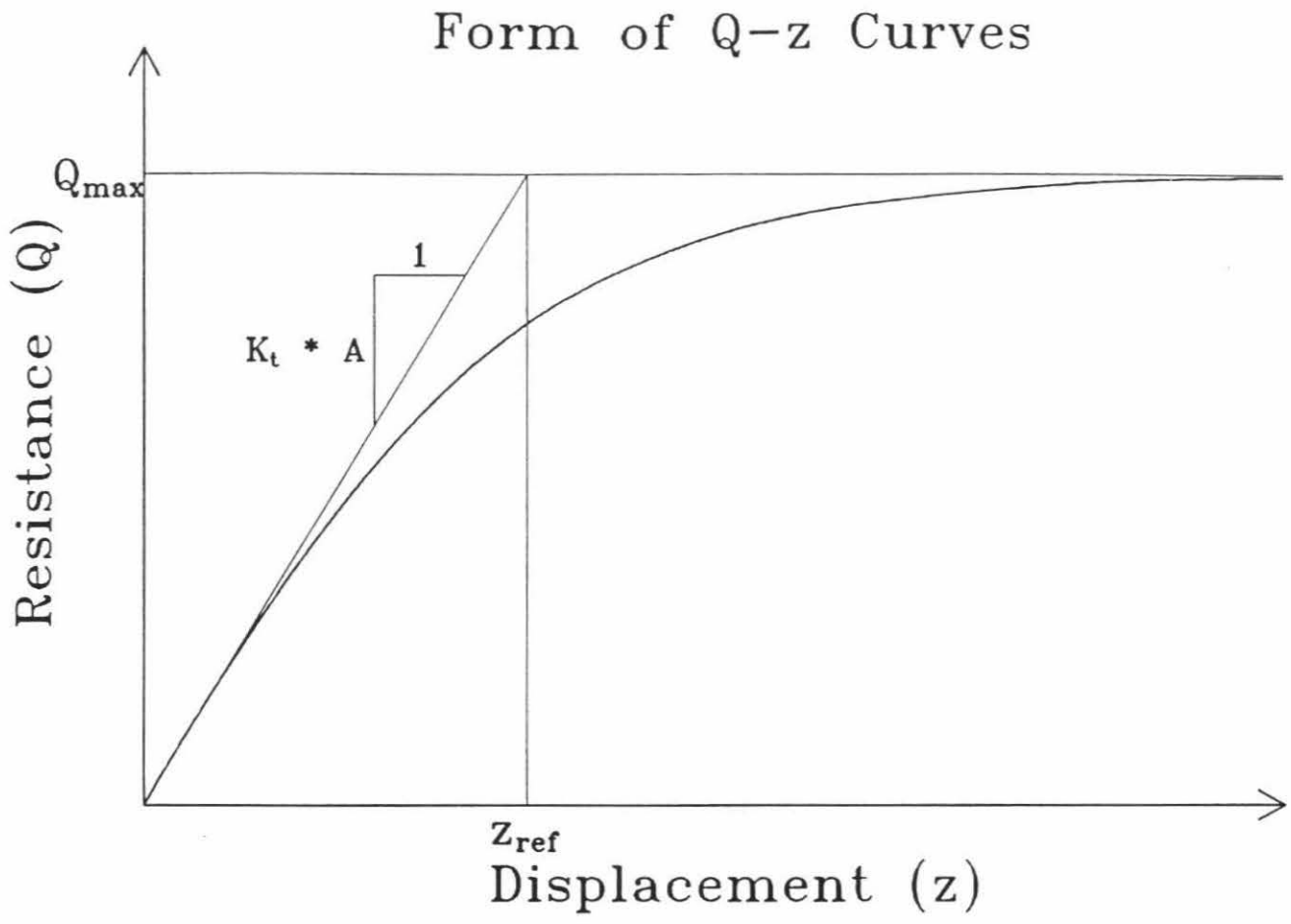
Form of Q-z Curves
Qmax
1
Kt * A
Resistance (Q)
Zref
Displacement (z)

Figure 2.3

Capacity parameters of single pile in granular soils.

BEARING CAPACITY FACTORS - N_q

ϕ* (DEGREES)	26	28	30	31	32	33	34	35	36	37	38	39	40
N_q (DRIVEN PILE DISPLACE-MENT)	10	15	21	24	29	35	42	50	62	77	86	120	145
N_q** (DRILLED PIERS)	5	8	10	12	14	17	21	25	30	38	43	60	72

* LIMIT ϕ TO 28° IF JETTING IS USED

** (A) IN CASE A BAILER OR GRAB BUCKET IS USED BELOW GROUNDWATER TABLE, CALCULATE END BEARING BASED ON ϕ NOT EXCEEDING 28°.

(B) FOR PIERS GREATER THAN 24-INCH DIAMETER, SETTLEMENT RATHER THAN BEARING CAPACITY USUALLY CONTROLS THE DESIGN. FOR ESTIMATING SETTLEMENT, TAKE 50% OF THE SETTLEMENT FOR AN EQUIVALENT FOOTING RESTING ON THE SURFACE OF COMPARABLE GRANULAR SOILS. (CHAPTER 5, DM-7.1).

Ref.: NAVFAC (1986)

Table 2.1

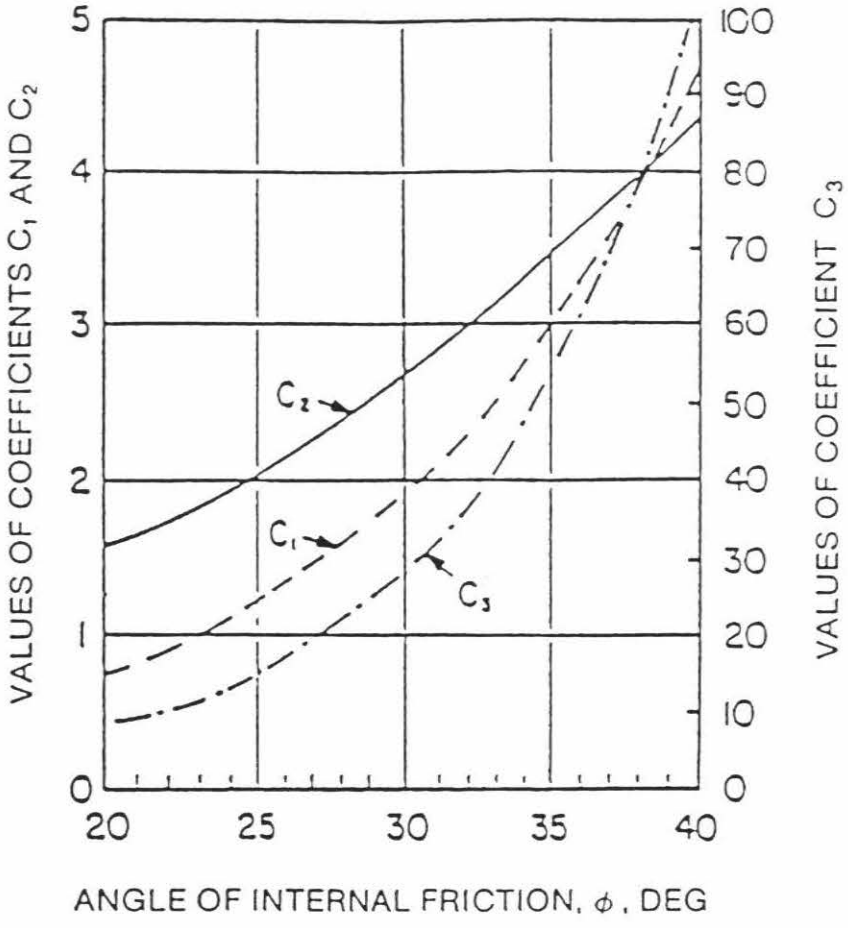

Ref.: API RP2A (1991)

Figure 2.4

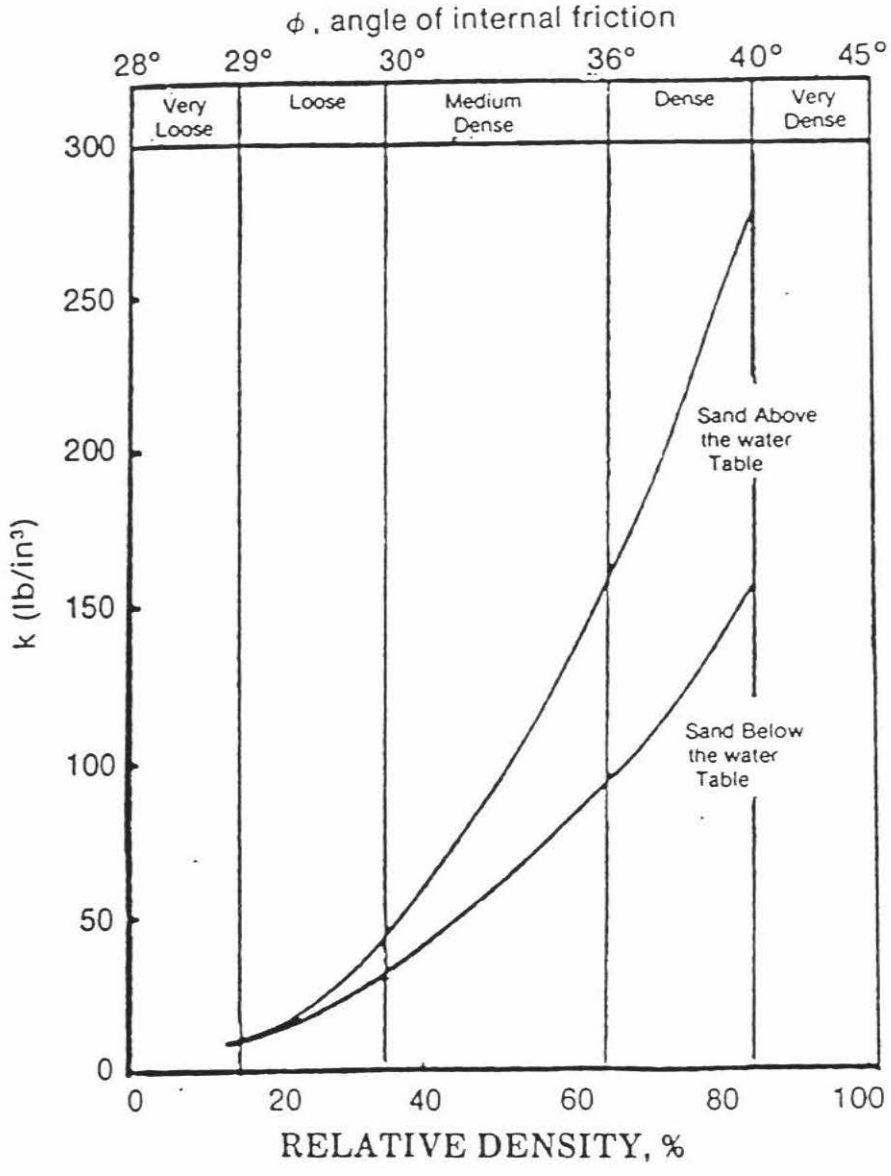

Ref.: API RP2A (1991)

Figure 2.5

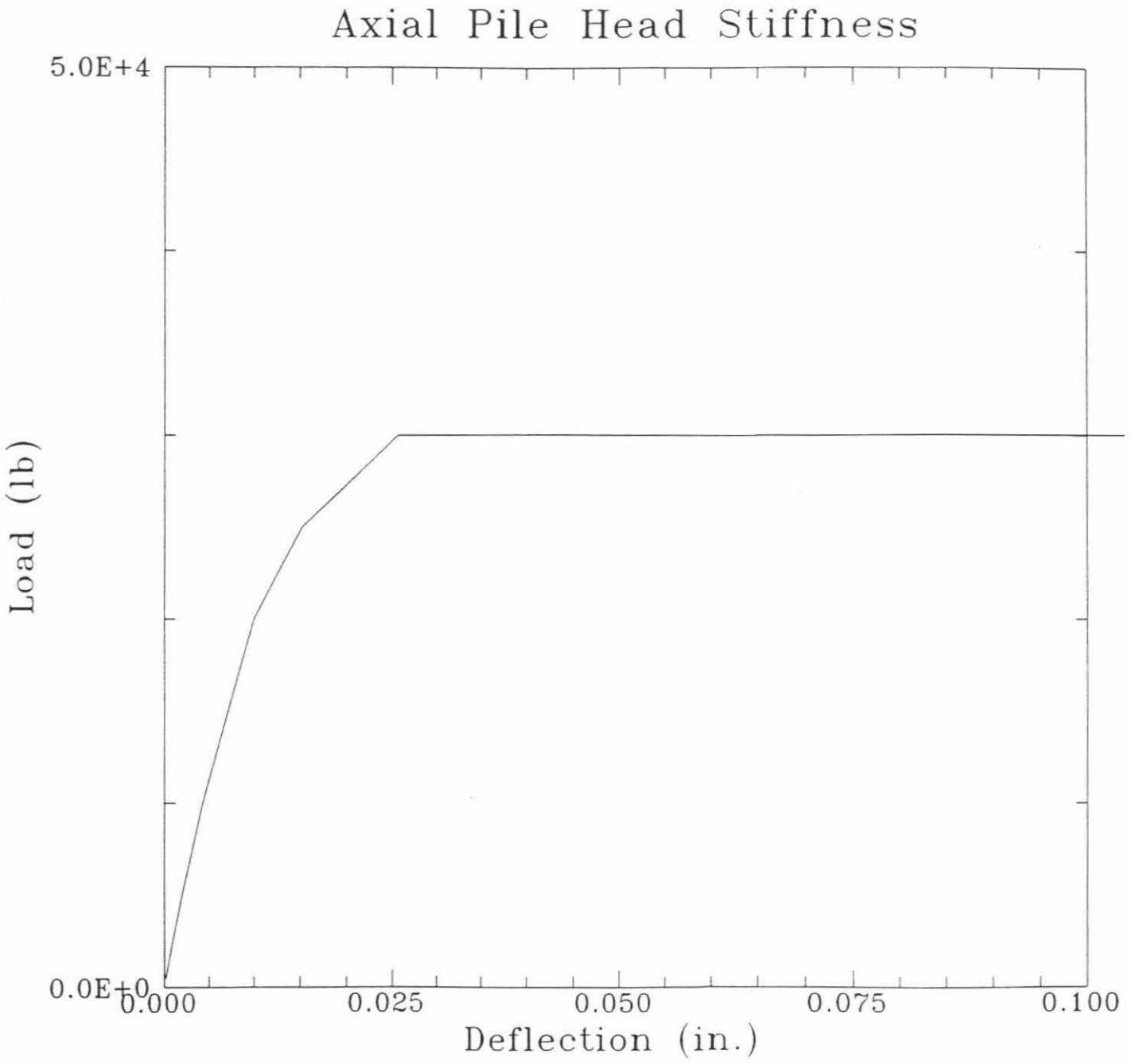
Axial Pile Head Stiffness
5.0E+4
0.0E+0
Load (lb)
0.000
0.025
0.050
0.075
0.100
Deflection (in.)

Figure 2.6

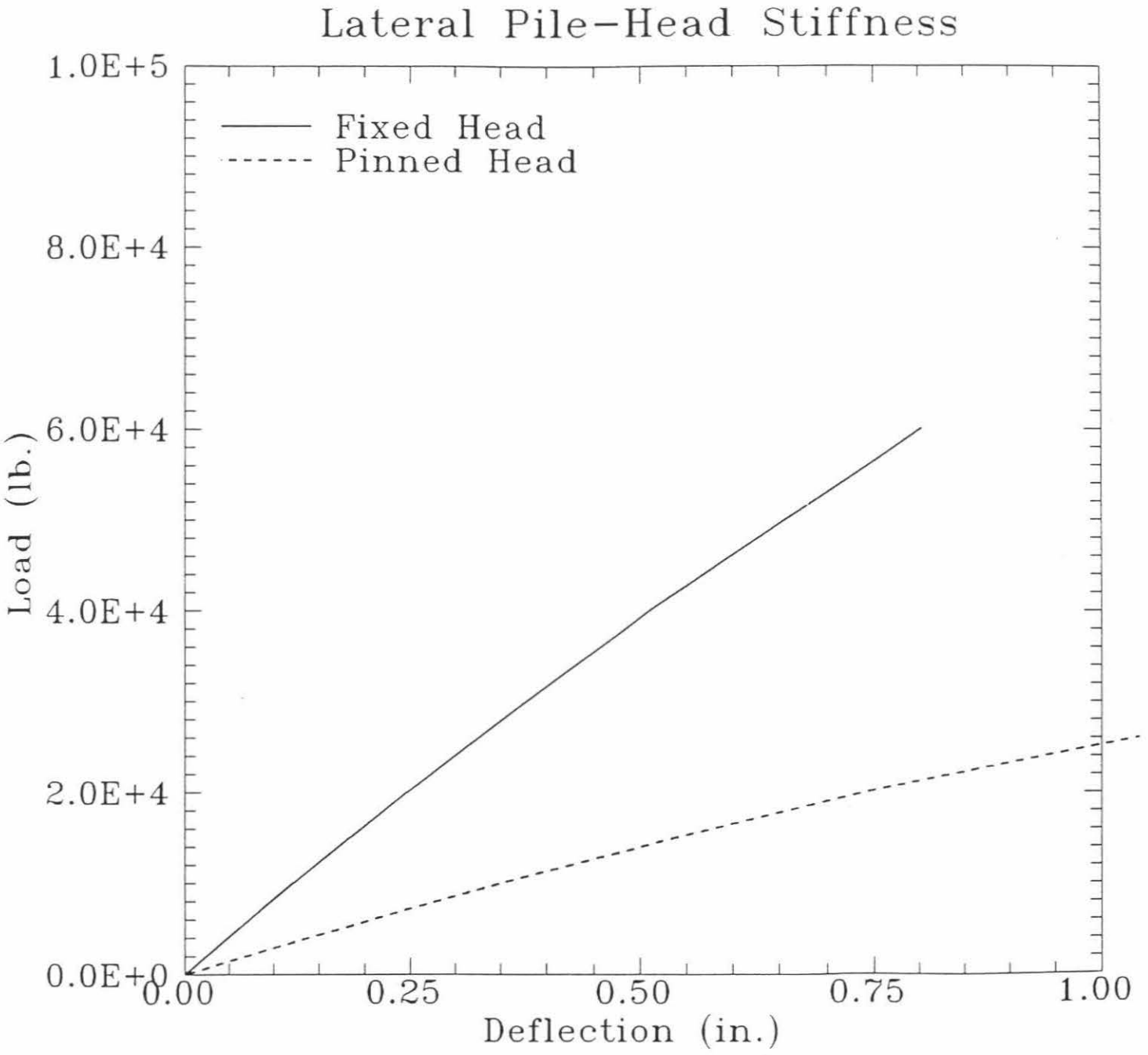
Lateral Pile-Head Stiffness
Fixed Head
Pinned Head
Load (lb.)
1.0E+5
8.0E+4
6.0E+4
4.0E+4
2.0E+4
0.0E+0
0.00
0.25
0.50
0.75
1.00
Deflection (in.)

Figure 2.7

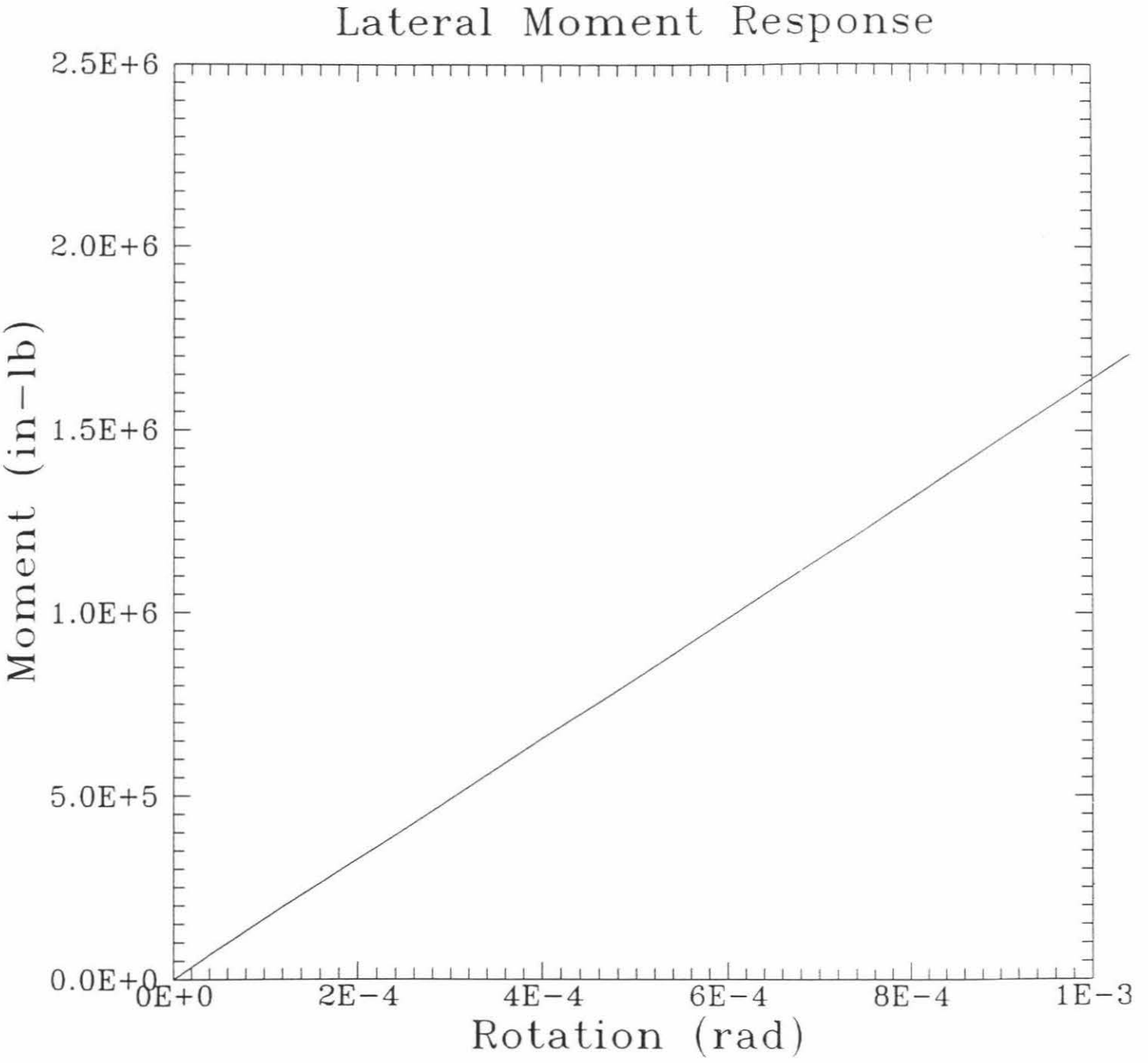
Lateral Moment Response
2.5E+6
2.0E+6
1.5E+6
1.0E+6
5.0E+5
0.0E+0
Moment (in-lb)
0E+0
2E-4
4E-4
6E-4
8E-4
1E-3
Rotation (rad)

Figure 2.8

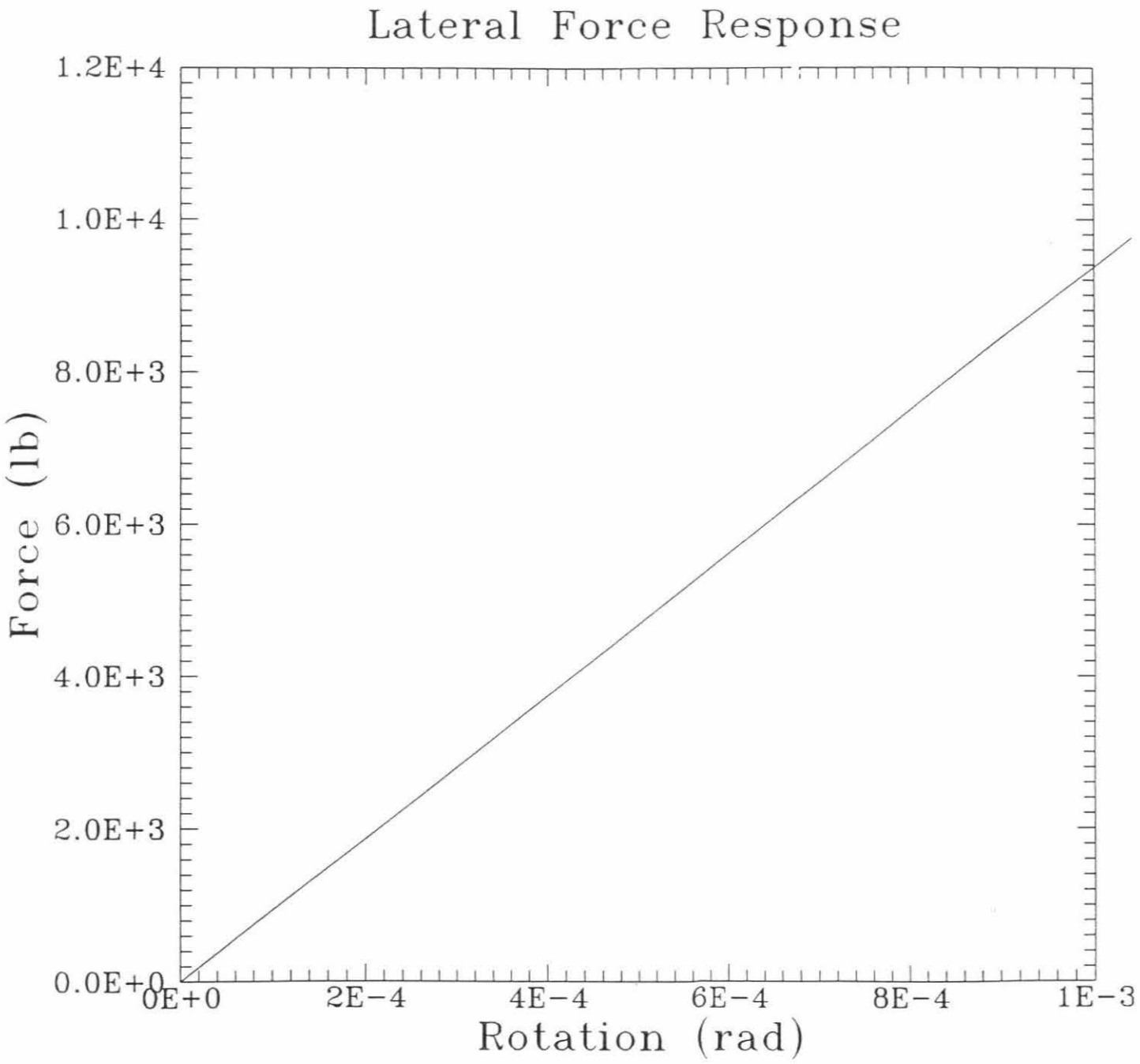
Lateral Force Response
1.2E+4
1.0E+4
8.0E+3
6.0E+3
4.0E+3
2.0E+3
0.0E+0
Force (lb)
0E+0
2E-4
4E-4
6E-4
8E-4
1E-3
Rotation (rad)

Figure 2.9

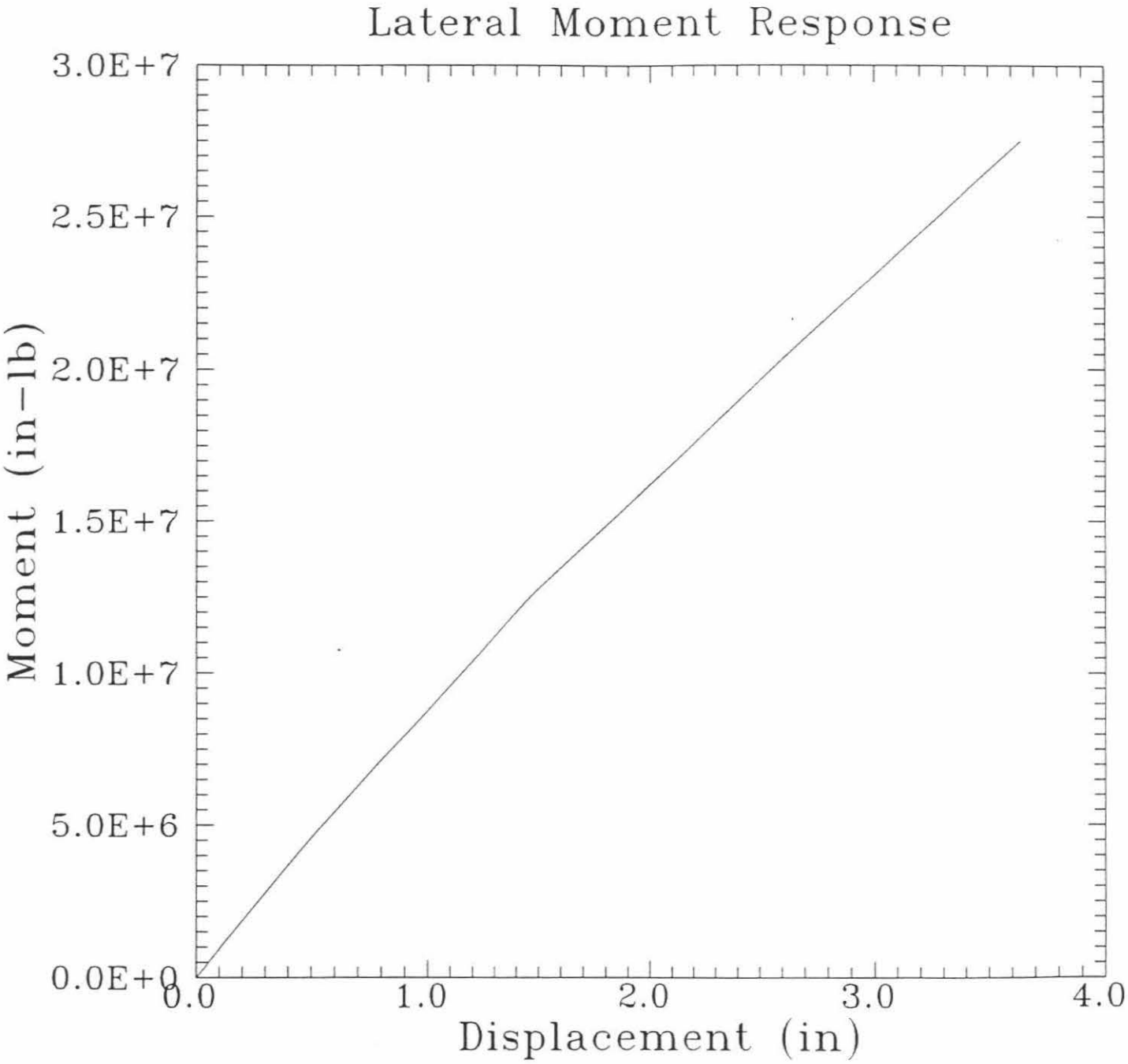
Lateral Moment Response
3.0E+7
2.5E+7
2.0E+7
1.5E+7
1.0E+7
5.0E+6
0.0E+0
Moment (in-lb)
0.0
1.0
2.0
3.0
4.0
Displacement (in)

Figure 2.10

RECTANGULAR FOOTING

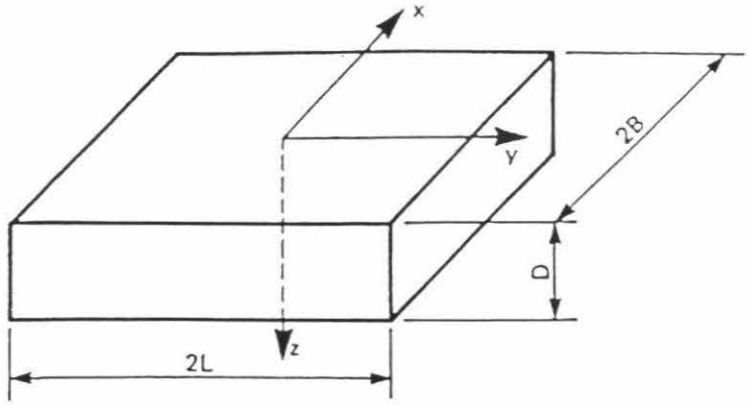

EQUIVALENT CIRCULAR FOOTING

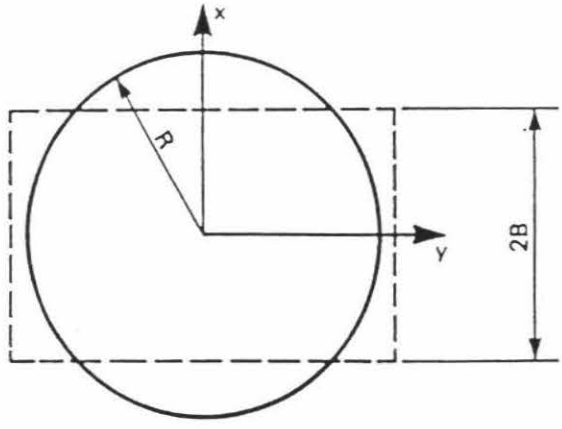

EQUIVALENT RADIUS:

TRANSLATIONAL: $R = \sqrt{\frac{4BL}{\pi}}$

ROTATIONAL: $R = \left[\frac{(2B)(2L)^3}{3\pi}\right]^{1/4}$ .....(x–AXIS ROCKING)

$R = \left[\frac{(2B)^3(2L)}{3\pi}\right]^{1/4}$ .....(y–AXIS ROCKING)

$R = \left[\frac{4BL(4B^2 + 4L^2)}{6\pi}\right]^{1/4}$ .....(z–AXIS TORSION)

Procedure for calculating equivalent radius of a rectangular footing.

Ref.: FHWA (1986)

Figure 2.11

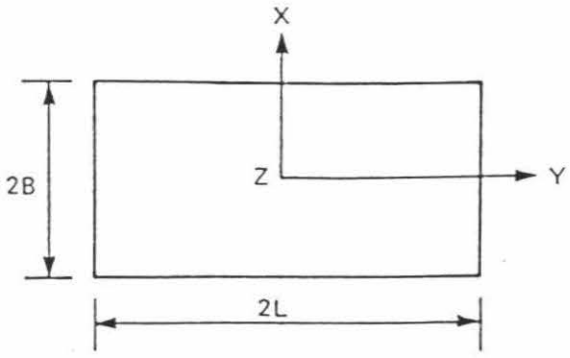

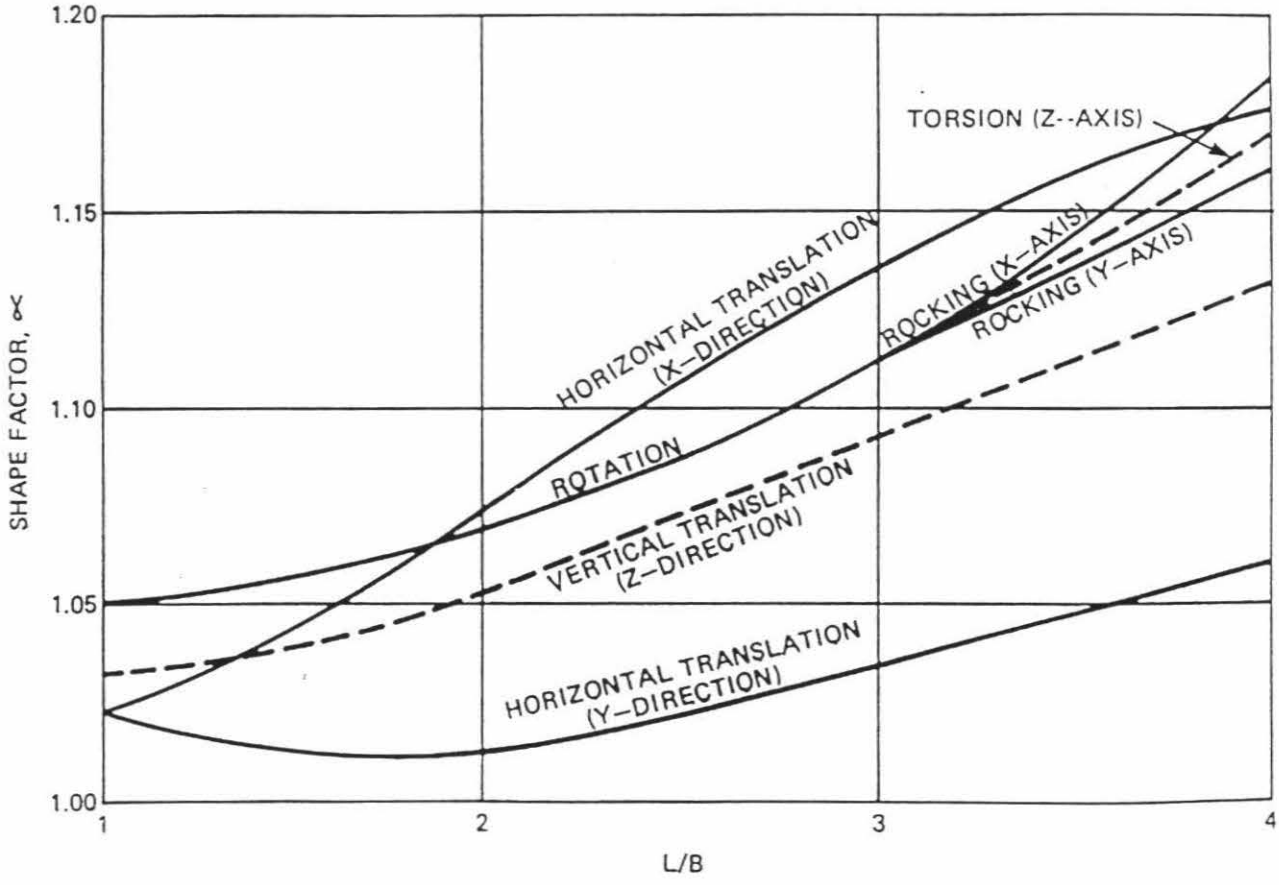

Shape factor for rectangular footings.

Ref.: FHWA (1986)

Figure 2.12

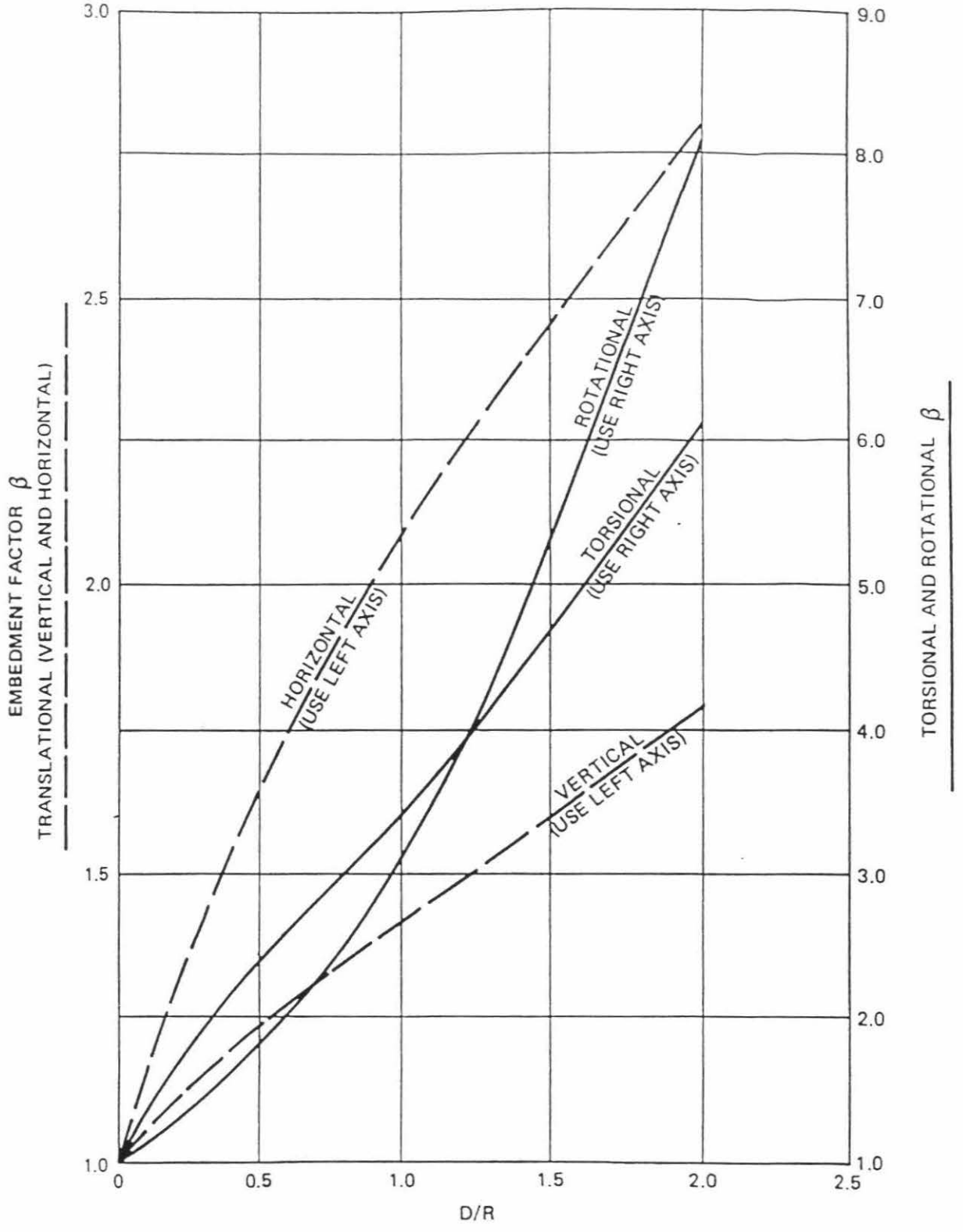

Embedment factor of footings.

Ref.: FHWA (1986)

Figure 2.13

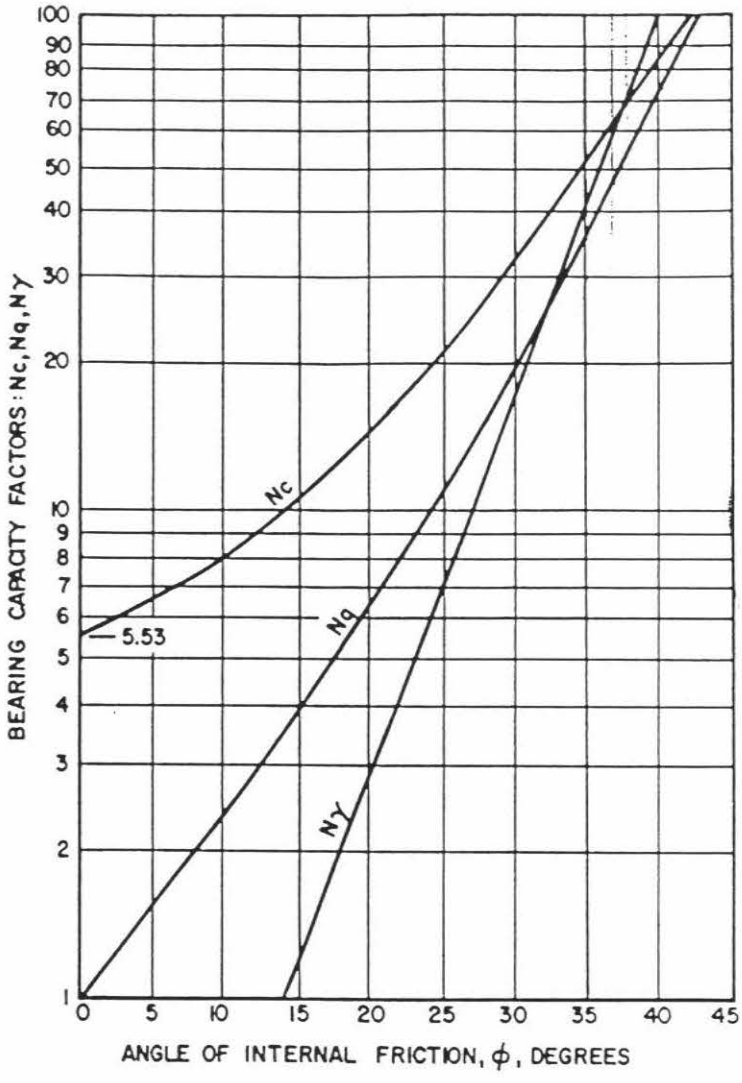
BEARING CAPACITY FACTORS: Nc, Nq, Nγ
100
90
80
70
60
50
40
30
20
10
9
8
7
6
5
4
3
2
1
5.53
Nc
Nq
Nγ
0
5
10
15
20
25
30
35
40
45
ANGLE OF INTERNAL FRICTION, ϕ, DEGREES

Figure 2.14

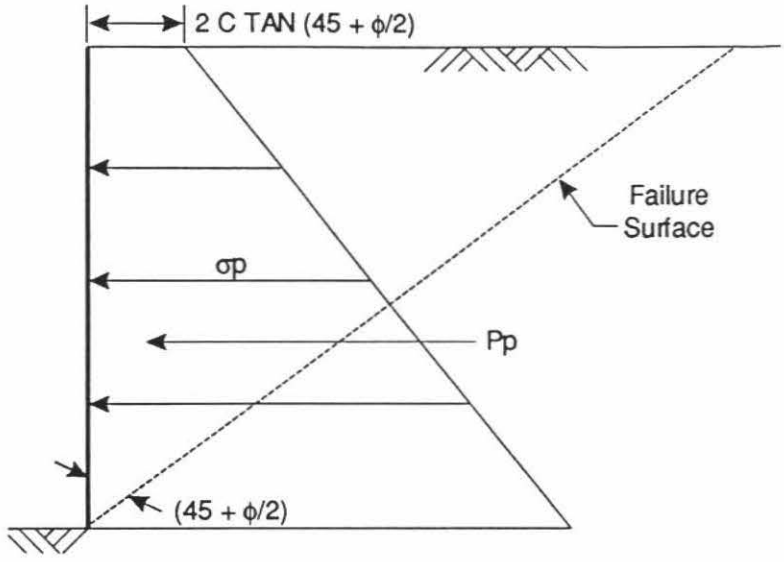

$$\sigma p = \gamma Z \, TAN^2 (45 + \phi/2) + 2 \, C \, TAN (45 + \phi/2)$$

$$Pp = \left(\frac{\gamma H^2}{2}\right) TAN^2 (45 + \phi/2) + 2 \, CH \, TAN (45 + \phi/2)$$

Figure 2.15

Ultimate Friction Factors and Adhesion for Dissimilar Materials

Interface Materials	Friction factor, tan δ	Friction angle, δ degrees
Mass concrete on the following foundation materials:		
Clean sound rock	0.70	35
Clean gravel, gravel-sand mixtures, coarse sand	0.55 to 0.60	29 to 31
Clean fine to medium sand, silty medium to coarse sand, silty or clayey gravel	0.45 to 0.55	24 to 29
Clean fine sand, silty or clayey fine to medium sand	0.35 to 0.45	19 to 24
Fine sandy silt, nonplastic silt	0.30 to 0.35	17 to 19
Very stiff and hard residual or preconsolidated clay	0.40 to 0.50	22 to 26
Medium stiff and stiff clay and silty clay	0.30 to 0.35	17 to 19
(Masonry on foundation materials has same friction factors.)		
Steel sheet piles against the following soils:		
Clean gravel, gravel-sand mixtures, well-graded rock fill with spalls	0.40	22
Clean sand, silty sand-gravel mixture, single size hard rock fill	0.30	17
Silty sand, gravel or sand mixed with silt or clay	0.25	14
Fine sandy silt, nonplastic silt	0.20	11
Formed concrete or concrete sheet piling against the following soils:		
Clean gravel, gravel-sand mixture, well-graded rock fill with spalls	0.40 to 0.50	22 to 26
Clean sand, silty sand-gravel mixture, single size hard rock fill	0.30 to 0.40	17 to 22
Silty sand, gravel or sand mixed with silt or clay	0.30	17
Fine sandy silt, nonplastic silt	0.25	14
Various structural materials:		
Masonry on masonry, igneous and metamorphic rocks:		
Dressed soft rock on dressed soft rock	0.70	35
Dressed hard rock on dressed soft rock	0.65	33
Dressed hard rock on dressed hard rock	0.55	29
Masonry on wood (cross grain)	0.50	26
Steel on steel at sheet pile interlocks	0.30	17

Interface Materials (Cohesion)	Adhesion C_a (psf)
Very soft cohesive soil (0 - 250 psf)	0 - 250
Soft cohesive soil (250 - 500 psf)	250 - 500
Medium stiff cohesive soil (500 - 1000 psf)	500 - 750
Stiff cohesive soil (1000 - 2000 psf)	750 - 950
Very stiff cohesive soil (2000 - 4000 psf)	950 - 1,300

Table 2.3

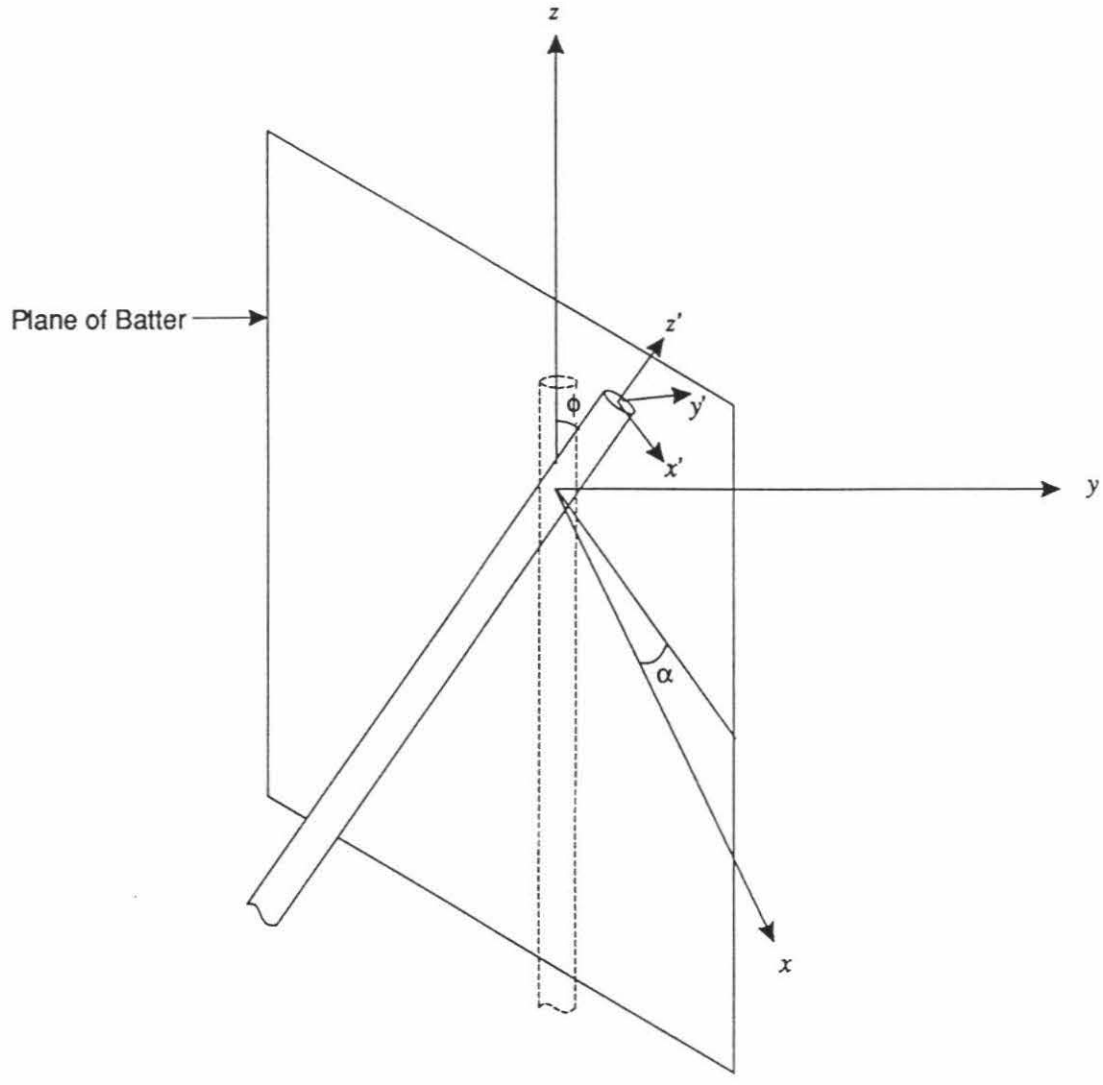

Figure 3.1
Batter Pile Transform

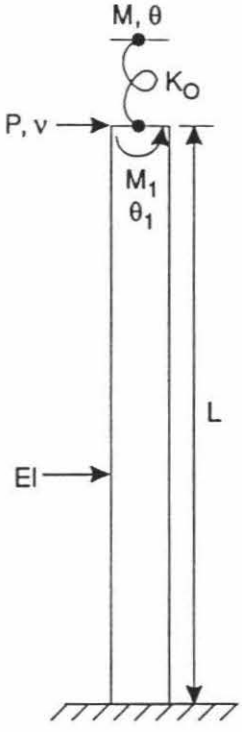

Figure 3.2

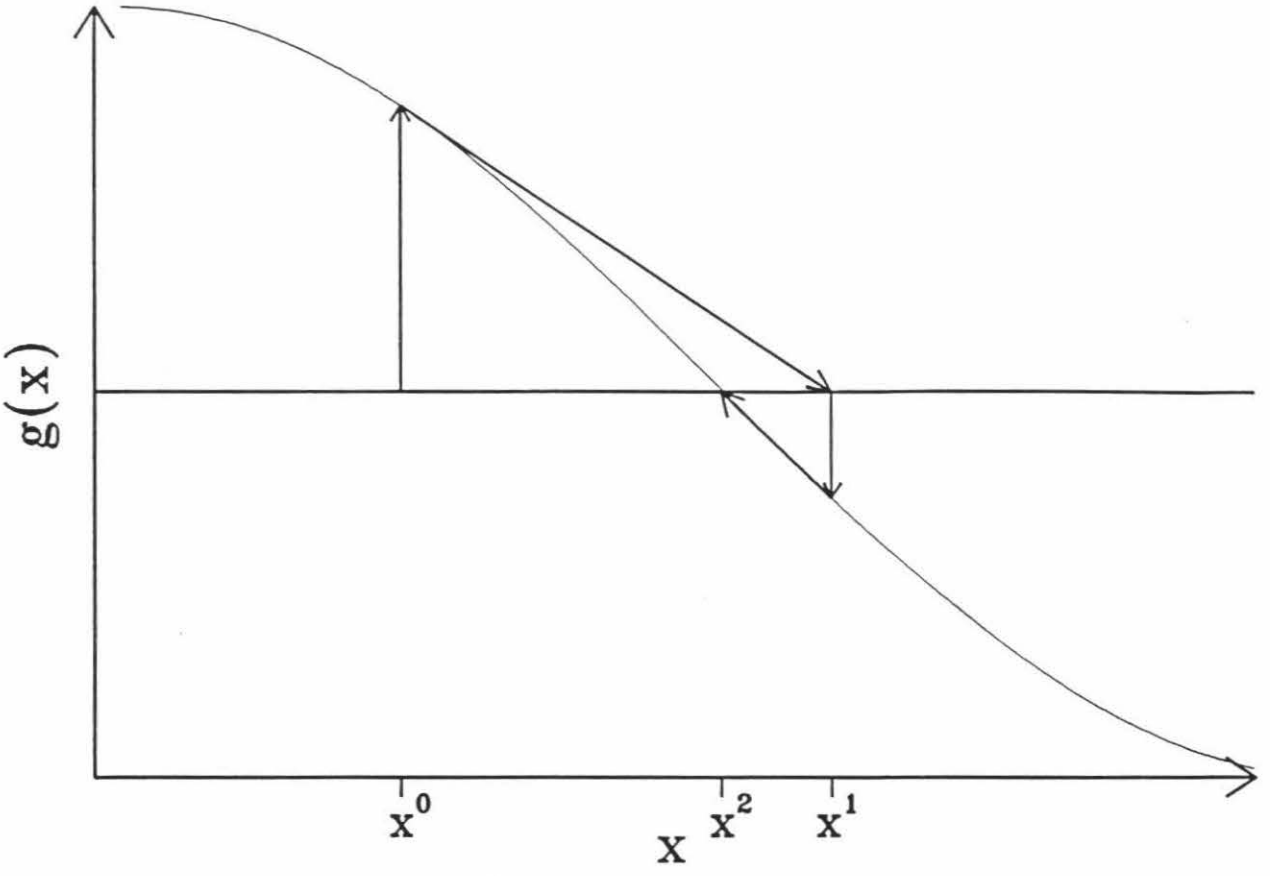

Figure 4.1